Spatial Variation of Magnitude Scaling Factors During the 2010 Darfield and 2011 Christchurch, New Zealand, Earthquakes

By

William Lake Carter

Thesis submitted to the faculty of the Virginia Polytechnic Institute and State University in partial fulfillment of the requirements for the degree of

Master of Science
In
Civil Engineering

Russell A. Green
Adrian Rodriguez-Marek
Joseph E. Dove

February 19, 2016
Blacksburg, VA

Keywords: Liquefaction; Magnitude Scaling Factors; Christchurch; Canterbury Earthquakes

Spatial Variation of Magnitude Scaling Factors During the 2010 Darfield and 2011 Christchurch, New Zealand, Earthquakes

William Lake Carter

ABSTRACT

Magnitude Scaling Factors (MSF) account for the durational effects of strong ground shaking on the inducement of liquefaction within the "simplified" liquefaction evaluation procedure which is the most commonly used approach for assessing liquefaction potential worldwide. Within the context of the simplified procedure, the spatial variation in the seismic demand imposed on the soil traditionally has been assumed to be solely a function of the spatial variation of the peak amplitude of the ground motions and the characteristics of the soil profile. Conversely, MSF have been solely correlated to earthquake magnitude. This assumption fails to appreciate the inverse correlation between the peak amplitude of ground motions and strong ground motion duration, and thus MSF would seemingly vary spatially.

The combination of well-documented liquefaction response during the Darfield and Christchurch, New Zealand, earthquakes, densely-recorded ground motions for the events, and detailed subsurface characterization provides an unprecedented opportunity to investigate the significance of the spatial variation of MSF on the inducement of liquefaction. Towards this end, MSF were computed at 15 strong motion recording station sites across Christchurch and its surroundings using two established approaches. Trends in the site and spatial variation of the MSF computed for both the Darfield and Christchurch earthquakes are scrutinized and their implications on liquefaction evaluations are discussed.

Spatial Variation of Magnitude Scaling Factors During the 2010 Darfield and 2011 Christchurch, New Zealand, Earthquakes

William Lake Carter

PUBLIC ABSTRACT

Earthquakes are notoriously responsible for causing tremendous amounts of damage to buildings, bridges, landforms, and other infrastructure worldwide. Therefore, the ability to better assess or predict earthquake induced damage is precedent. Magnitude Scaling Factors (MSF) are a key component used by engineers to evaluate an earthquake's seismic demand and thereby forecast potential damages. Traditionally, MSF have been solely related to an earthquake's magnitude which may be an over-simplification that could result in less accurate predictions of earthquake induced damage. This study presents that other aspects different from earthquake magnitude, such as distance from the earthquake source, can impact the calculation of seismic demand via MSF. To elucidate this hypothesis, a case study was performed using high quality data collected from the 2010 Darfield and 2011 Christchurch, New Zealand earthquakes. This study revealed that MSF can vary significantly from site to site for the same earthquake event having a specific magnitude. Taking into consideration this spatial variability of MSF may result in more appropriate calculation of earthquake seismic demand and ultimately allow engineers to more accurately predict earthquake induced damage.

Acknowledgements

This research was partially funded by National Science Foundation (NSF) grants CMMI-1030564, CMMI-1306261, CMMI-1435494, and an NSF EAPSI Fellowship OISE-1310886. Dr. Sam Lasley and Mr. Brett Maurer assisted in some of the calculations presented herein. Additionally, Mr. Karim Tarbali and Mr. Varun Joshi assisted with the near-fault ground motion selection process. This support and assistance are gratefully acknowledged. However, any opinions, findings, and conclusions or recommendations expressed in this material are those of the authors and do not necessarily reflect the views of the National Science Foundation.

Table of Contents

List of Tables

List of Figures

Chapter 1: Introduction

1.1 Problem Statement

The objective of this thesis is to use the combination of well-documented liquefaction response during the 2010 Darfield and 2011 Christchurch, New Zealand, earthquakes, densely-recorded ground motions for the events, and detailed subsurface characterization to investigate the significance of the spatial variation of MSF on liquefaction triggering. Liquefaction is a phenomenon that occurs in loose to medium dense saturated cohesionless soil subjected to cyclic loading and can be responsible for tremendous amounts of land damage and adverse effects to buildings and other infrastructure. Magnitude Scaling Factors (MSF) are central to the "simplified" liquefaction evaluation procedure to account for the duration of strong ground shaking on liquefaction triggering. However within the framework of the simplified procedure, MSF have been traditionally correlated to earthquake magnitude and do not explicitly account for variability in site conditions or distance from the source. The corollary to this is that using MSF from conventional approaches, which are site- and source-independent may result in discrepancies between predicted versus observed liquefaction.

1.2 Organization

This thesis is organized into three chapters and four appendices (A-D). The second chapter is a manuscript submitted as a technical paper to the Elsevier journal Soil Dynamics and Earthquake Engineering. Attribution of this manuscript is provided in the subsequent section. The third chapter of this thesis provides a summary of the work performed, the key findings, and recommendations for future work. The back matter of this thesis contains four appendices which provide further detail on the: Christchurch strong motion station (SMS) profiles, selected ground motions for the scenario-based site response analyses, magnitude scaling factors as a function of depth at each SMS site, and spatial variation of MSF across Christchurch.

1.3 Attribution

The manuscript contained in Chapter 2 entitled: "Spatial Variation of Magnitude Scaling Factors During the 2010 Darfield and 2011 Christchurch, New Zealand, Earthquakes," authored by W.L.

Carter et al. has been submitted for consideration as a Technical Paper in the 6ICEGE special issue of the Elsevier journal Soil Dynamics and Earthquake Engineering. The following provides a list of the contributing co-authors and their primary role pertaining to this paper:

Russell A. Green, Ph.D., P.E., Department of Civil and Environmental Engineering, Virginia Tech, Blacksburg, Virginia, U.S.A.

- Research Advisor to the lead author and provided significant oversight and guidance during all phases of this research. Dr. Green is also credited for developing one of the adopted approaches used in this study for computing the number of equivalent cycles and ultimately MSF.

Brendon A. Bradley, Ph.D., Department of Civil and Natural Resources Engineering, University of Canterbury, Christchurch, New Zealand

- New Zealand, EAPSI fellowship sponsor to the lead author and provided significant contribution to the characterization of the ground motions recorded during the 2010 Darfield and 2011 Christchurch earthquakes. In addition, the scenario-based ground motion selection process used in this study was developed by Dr. Bradley.

Liam M. Wotherspoon, Ph.D., Department of Civil and Environmental Engineering, University of Auckland, Auckland, New Zealand

- Took the lead on the soil profile characterization of the Christchurch SMS sites that were used as the basis of the site response analyses performed in this paper.

Misko Cubrinovski, Ph.D., Department of Civil and Natural Resources Engineering, University of Canterbury, Christchurch, New Zealand

- New Zealand, EAPSI fellowship co-sponsor to the lead author and provided expertise on the 2010-2011 Canterbury earthquake sequence and general oversight to the framework of this paper.

Chapter 2: Spatial Variation of Magnitude Scaling Factors During the 2010 Darfield and 2011 Christchurch, New Zealand, Earthquakes

2.1 Abstract

The combination of well-documented liquefaction response during the Darfield and Christchurch, New Zealand, earthquakes, densely-recorded ground motions for the events, and detailed subsurface characterization provides an unprecedented opportunity to investigate the significance of the spatial variation of magnitude scaling factors (MSF) on liquefaction triggering. Towards this end, MSF were computed at 15 SMS sites across Christchurch and its surroundings using two established approaches. Trends in the spatial variation of the MSF computed using number of equivalent cycles (n_{eq}) from both approaches were similar, with the spatial variation being more significant for the Christchurch earthquake than the Darfield earthquake. However, there was no consistent trend for regions with lower computed MSF having experienced more severe or widespread liquefaction. Additionally, there is a general correlation between MSF and a_{max}, but because a_{max} ranges more widely than MSF it has a greater influence on the resulting seismic demand imposed on the soil than MSF does. Nevertheless, the spatial variation of the MSF is deemed significant enough that it warrants being considered for incorporation into future variants of simplified liquefaction evaluation procedures.

2.2 Introduction

The objective of the study presented herein is to assess the significance of the spatial variation of the magnitude scaling factors across Christchurch, New Zealand, and its environs on the assessment of liquefaction triggering during the 2010 Darfield and 2011 Christchurch earthquakes. Liquefaction is a phenomenon that occurs in loose to medium dense saturated cohesionless soil subjected to cyclic loading. It results from the contractive tendency of the soil skeleton during shaking and the consequential transfer of the overburden stress from the soil skeleton to the pore fluid. The "simplified" liquefaction triggering evaluation procedure is the most commonly used approach for assessing liquefaction potential worldwide (Whitman, 1971; Seed and Idriss, 1971). In this procedure, the durational effects of the ground motions are accounted for by magnitude

scaling factors (MSF), which traditionally have only been correlated to earthquake magnitude (e.g., Youd et al., 2001; Cetin et al., 2004; Idriss and Boulanger, 2008). As a result, within the context of the simplified procedure, the spatial variation in the seismic demand imposed on the soil traditionally has been assumed to be solely a function of the spatial variation of the peak amplitude of the ground motions and the characteristics of the soil profile. However, these traditional assumptions fail to appreciate the inverse correlation between the peak amplitude of ground motions and strong ground motion duration. The extreme case of this are motions with forward versus reverse directivity effects, where the former tend to have higher amplitudes and shorter durations and the latter tend to have the opposite trends (Archuleta and Hartzell, 1984; Somerville et al., 1997). Additionally, it is known that ground motion duration varies with site-to-source distance (e.g., Bommer and Martinez-Pereira, 1999; Kempton and Stewart, 2006; Stafford et al., 2009; Lee and Green, 2014), and thus, it would be expected that MSF will also vary with distance from the source.

Christchurch, New Zealand, and its surroundings experienced widespread liquefaction as a result of the 2010-2011 Canterbury Earthquake Sequence (CES) (e.g., Cubrinovski and Green, 2010; Cubrinovski et al., 2011; Green et al., 2014). However, of the 10 events in the CES that are known to have caused liquefaction (Quigley et al., 2013), the 4 September 2010, M_w 7.1 Darfield and 22 February 2011, M_w 6.2 Christchurch earthquakes were the most significant (Figure 2.1). The combination of well-documented liquefaction response during the Darfield and Christchurch earthquakes, densely-recorded ground motions for the events, and detailed subsurface characterization provides an unprecedented opportunity to investigate the significance of the spatial variation of MSF on liquefaction triggering. Of particular relevance to this study is that directivity effects were prevalent in the ground motions recorded during the Darfield earthquake, and to a much lesser extent, during the Christchurch earthquake (e.g., Bradley and Cubrinovski, 2011; Bradley, 2012a,b,c; Shahi and Baker, 2012). The strike slip rupture mechanism of the Darfield earthquake and the orientation of the causative fault relative to Christchurch resulted the manifestation of forward directivity effects throughout much of the city. In contrast, the predominantly reverse rupture mechanism of the Christchurch earthquake and the causative fault orientation only resulted in forward directivity effects in areas south of the city along the Port Hills. This allows a comparison to be made between the spatial variation of MSF across the same region for motions where directivity effects were and were not prominent.

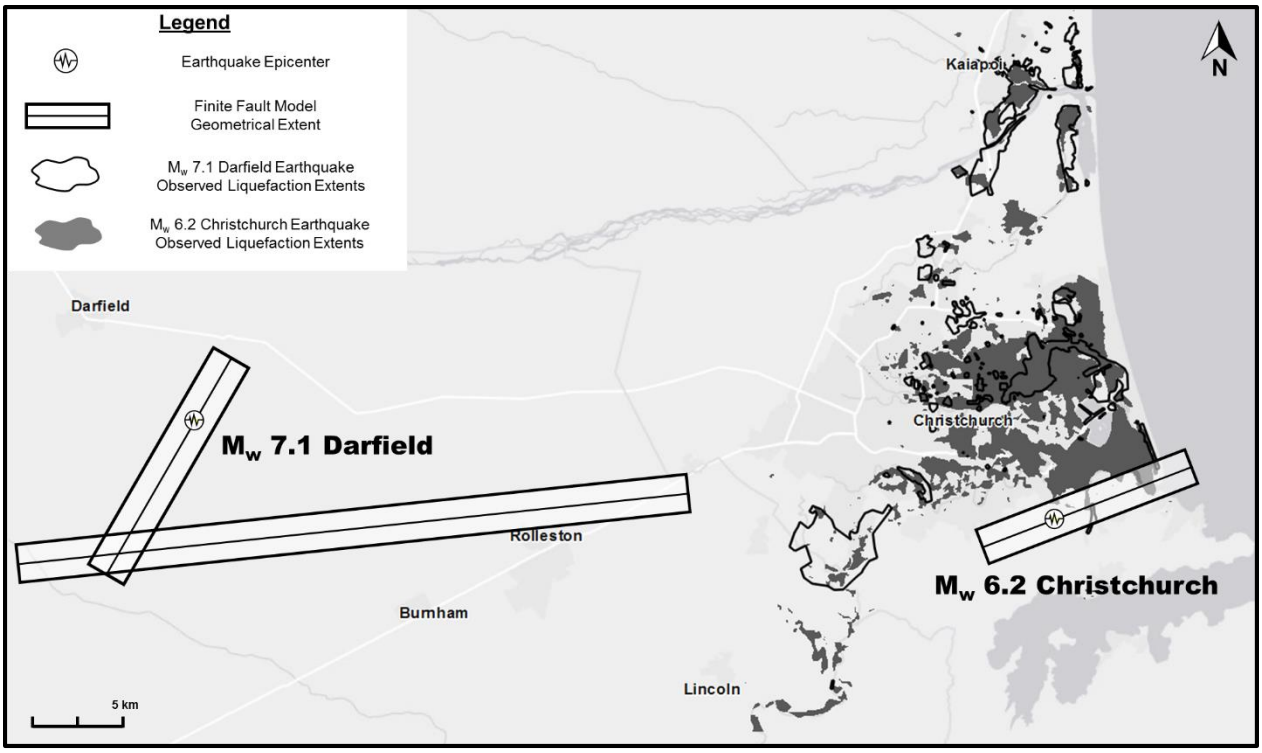

Figure 2.1 Ariel extents of liquefaction observed in Christchurch, NZ following the two largest events in the CES. Areas delineated in black represent liquefaction from the Sept. 4, 2010 Mw 7.1 Darfield earthquake. Areas highlighted in dark gray represent liquefaction from the Feb. 22, 2011 Mw 6.2 Christchurch earthquake. The finite fault model boundaries shown are simplified from Holden et al. (2011) and Beaven et al. (2011) to highlight the rupture portions believed to have contributed the majority of the released energy.

In the following, background information on the geology and geomorphology of the Canterbury region is presented. This is followed by a brief overview of the CES. Next, background information is given on the approaches used to compute MSF. These approaches are then used to compute MSF across the Christchurch region, with the trends in the results discussed.

2.3 Background Information

2.3.1 Geology and Geomorphology of the Christchurch Area

The Canterbury Plains are ~160 km long and up to 60 km wide. The plains are the result of overlapping alluvial fans produced by glacier-fed rivers from the Southern Alps, the main mountain range of the South Island (Forsyth et al., 2008). Uplift of the Southern Alps resulted in rapid deposition during the late Quaternary and inundation of the Canterbury Plains by alluvial and fluvial sediments. The Canterbury Plains are underlain by a deep and complex network of

overlapping fingers of fluvial gravels interbedded with swamp, estuarine, lagoon, and beach deposits of sand, silt, clays, and peat as a result of the glacial and post-glacial movements of the coastline (Brown et al., 1995). Figure 2.2 shows an idealized cross section of the interbedded sedimentary deposits beneath the region. Also shown in this figure is the approximate depth to the uppermost gravel formation (i.e., Riccarton Gravel Formation) for several of the strong motion recording stations (SMSs) located in the Central Business District (CBD) and eastern suburbs of Christchurch (note that the simplified model of the depth to the Riccarton Gravel Formation shown in this figure is in accord with the 3D model of the formation developed by Lee et al. (2015)). The characterization of these SMS sites and several others are discussed later in the paper.

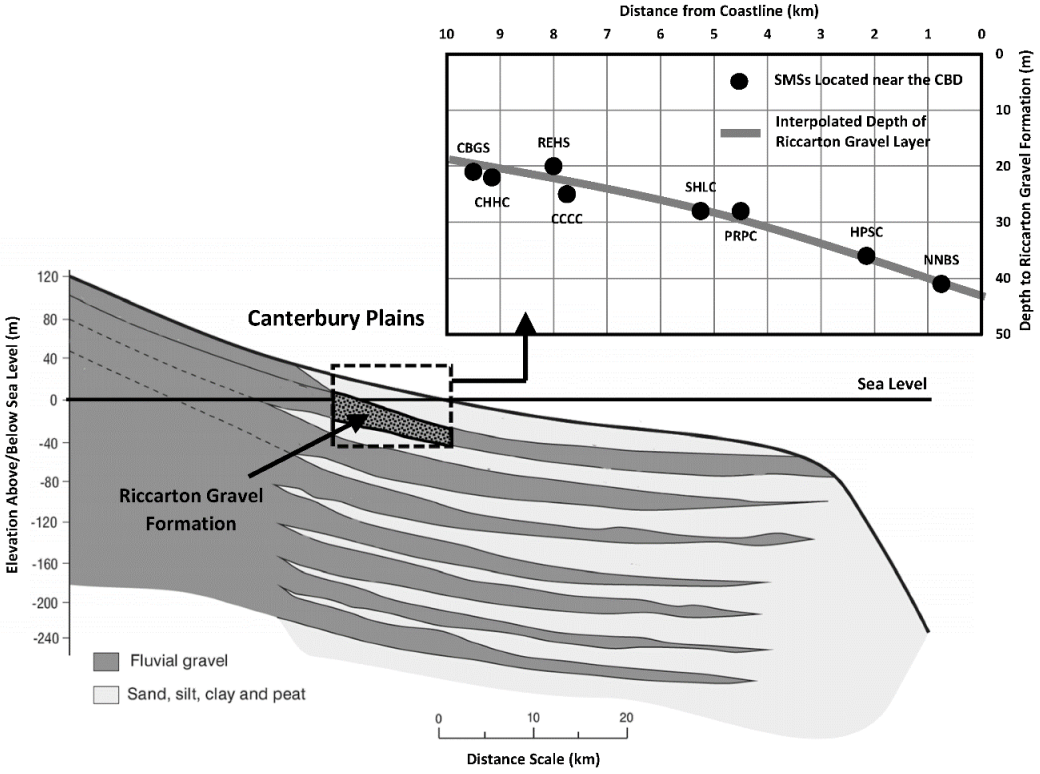

Figure 2.2 Geologic cross section of Christchurch showing the complexity of the interbedded sedimentary deposits and depth to the Riccarton gravel formation for several SMSs (adopted from Forsyth et al., 2008 and Wotherspoon et al., 2015)

In the recent geologic past, most of Christchurch was low-lying floodplains and swamps behind a series of barrier dunes (composed of fine-grained beach/dune sand), estuaries, and lagoons (underlain by fine-grained deposits) of Pegasus Bay. The Waimakariri River regularly flooded Christchurch before levee construction and river realignment, shortly after the city was established

in 1850. The original city center was constructed on slightly higher ground compared to areas to the north and east. Of particular relevance to liquefaction susceptibility of the region are the locations of abandoned paleo-channels of the Waimakariri, Heathcote, and Avon Rivers, and former swamps. These areas are underlain by, and filled with, young loose sandy sediments, with shallow groundwater levels (from 1 to 5 m below ground surface), which are highly susceptible to liquefaction (e.g., Wotherspoon et al., 2012).

2.3.2 Canterbury Earthquake Sequence (CES)

The 2010-2011 CES started at 4:35 am on 4 September 2010 NZ Standard Time (16:35 3 September 2010 UTC), when a previously unmapped fault west of Christchurch ruptured, producing the M_w7.1 Darfield earthquake (Bradley et al., 2014). Although the earthquake caused major damage to the built environment and induced widespread liquefaction, there were no fatalities or major injuries. The CES included twelve other events having $M_w \geq 5.0$ with epicentral locations within 20 km of Christchurch (GeoNet, 2012), and up to ten of these larger events are known to have induced liquefaction (Quigley et al., 2013). However, the M_w6.2, 22 February 2011 Christchurch earthquake was the most damaging event, due to the close proximity of its rupture plane to Christchurch, resulting in 185 fatalities and causing widespread liquefaction (e.g., Cubrinovski et al., 2011; Green et al., 2011; Orense et al., 2011; Cubrinovski et al., 2012; Robinson et al., 2013; Maurer et al., 2014).

The motions from both the Darfield and Christchurch earthquakes were recorded by a dense network of strong ground motion stations (e.g., Cousins and McVerry, 2010; Bradley and Cubrinovski, 2011; Bradley, 2012a,b,c; Bradley et al., 2014). The recordings included a significant number of near-fault motions, many of which show clear evidence of the forward directivity phenomenon (Bradley, 2012c; Bradley and Cubrinovski, 2011; Joshi, 2013). In an effort to better understand site effects in the ground motions recorded across Christchurch, Wotherspoon et al. (2014, 2015a,b) performed a detailed characterization of the shallow (~ 40 m) subsoil conditions at the 15 SMSs shown in Figure 2.3. The profiles obtained by Wotherspoon et al. form the basis of the site response analyses performed herein.

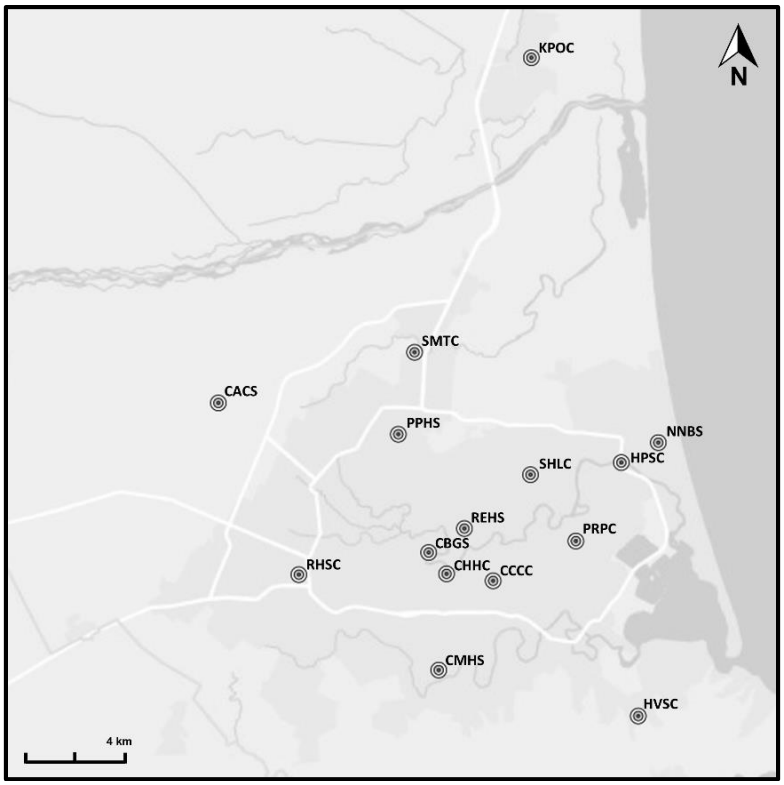

Figure 2.3 Overview of the fifteen SMS sites characterized by Wotherspoon et al. (2014, 2015a,b) and used in this study.

2.3.3 Magnitude Scaling Factors (MSF)

As stated previously, magnitude scaling factors account for the influence of the durational effects of strong ground motion on liquefaction triggering. For historical reasons, MSF are normalized to M_w7.5 events and traditionally have been computed from number of equivalent cycle correlations using the following relationship (e.g., Green, 2001; Boulanger and Idriss, 2015):

$$MSF = \left(\frac{n_{eq\ M7.5}}{n_{eq\ M}}\right)^{b} \qquad \text{Eq. 2.1}$$

where $n_{eqM7.5}$ and n_{eqM} are the number of equivalent cycles for M_w7.5 and M_w events, and *b* is the negative slope of the log(CSR) versus log(N_{liq}) curve for the soil of interest; CSR is cyclic stress ratio (i.e., cyclic shear stress (τ) divided by the initial vertical effective stress(σ'_{vo})), and N_{liq} is the number of cycles required to induce liquefaction in a soil specimen subjected to sinusoidal loading having an amplitude of CSR, typically determined using cyclic triaxial or cyclic simple shear tests.

Alternatively, MSF have been developed directly from the statistical analysis of liquefaction case histories (e.g., Cetin et al., 2004). However, this approach is limited by the relatively narrow variable ranges of the cases in the liquefaction case history databases.

Well-established fatigue theories have been proposed for computing n_{eq} for materials having varying phenomenological behavior; reviews of different approaches for computing n_{eq} are provided in Kaechele (1963), Stallymeyer and Walker (1968), Green and Terri (2005), and Hancock and Bommer (2005), among others. Developed specifically for use in evaluating liquefaction potential, the approaches proposed by Seed et al. (1975) and by Green and Terri (2005) are used herein. These approaches are variants of the Palmgren-Miner (P-M) fatigue theory, with the approach by Green and Terri (2005) better accounting for the non-linear behavior of the soil than the Seed et al. (1975) variant.

Assuming that ground surface accelerations (a) and corresponding shear stresses (τ) in the upper ~6 m (20 ft) of a soil profile are proportional, the Seed et al. (1975) variant of the P-M fatigue theory can be expressed as:

$$n_{eq} = \sum_i 0.5 \cdot \left(\frac{1}{0.65} \cdot \frac{|a_i|}{a_{max}} \right)^{\frac{1}{b}} \qquad \text{Eq. 2.2}$$

where $|a_i|$ is the absolute value of the amplitude of the i^{th} peak (or pulse) in a horizontal acceleration time history recorded at the ground surface, and a_{max} is the peak ground acceleration for the same acceleration time history; b is as defined for Eq. 2.1. Inherent to the Seed et al. (1975) procedure, the ratio of acceleration and peak ground acceleration (a/a_{max}) is assumed equal to τ/τ_{max}, where τ_{max} is the maximum shear stress induced in the soil profile at the depth of interest.

There are several different "peak counting" methods (ASTM, 2011) that are used in fatigue analyses. Seed et al. (1975) used a version of the mean crossing peak counting (also known as zero-crossing) method wherein the amplitude of one cycle is taken as the maximum value of the response history between successive zero crossings. Also, Seed et al. (1975) excluded peaks having amplitudes less than approximately $0.3 \cdot a/a_{max}$ in computing n_{eq} because their contribution was considered to be negligible. To calculate the equivalent number of cycles from two mutually

perpendicular horizontal components of motion, Seed et al. suggested two ways without giving a clear preference for one or the other: (1) Normalize each component of motion by its own a_{max}; and (2) Normalize both components of motion by the larger a_{max} of the two motions. Although Seed et al. do not state a preference for one approach over the other, approach (1) has been widely used in subsequent studies. Using this approach, Seed et al. (1975) computed $n_{eqM7.5} = 15$ from a suite of ~60 motions from earthquakes in the western US and South America.

In the Green and Terri (2005) approach, dissipated energy is explicitly used as the damage metric. n_{eq} is determined by equating the energy dissipated in a soil element subjected to an earthquake motion to the energy dissipated in the same soil element subjected to a sinusoidal motion of a given amplitude and a duration of n_{eq}. Dissipated energy was selected as the damage metric because it has been shown to correlate with excess pore pressure generation in saturated cohessionless soil samples subjected to undrained cyclic loading (e.g., Green et al., 2000; Polito et al., 2008). Furthermore, from a microscopic perspective, energy is thought to be predominantly dissipated by the friction between sand grains as they move relative to each other as the soil skeleton breaks down, which is requisite for the inducement of liquefaction.

Conceptually, the Green and Terri (2005) approach for computing n_{eq} is shown in Figure 2.4 Stress and strain time histories at various depths in the soil profile are obtained from a numerical site response analysis. By integrating the variation of shear stress over shear strain, the cumulative dissipated energy per unit volume of soil can be computed (i.e., the cumulative area bounded by the stress-strain hysteresis loops). n_{eq} is then determined by dividing the cumulative dissipated energy for the entire earthquake motion by the energy dissipated in one equivalent cycle. For historical reasons, the shear stress amplitude of the equivalent cycle (τ_{avg}) is taken as 0.65 time the maximum induced shear stress (τ_{max}) at the depth of interest, and the dissipated energy associated with the equivalent cycle is determined from the constitutive model used in the site response analysis. Additionally, the *b* value that is needed to relate n_{eq} to MSF per Eq. 1 can also be determined from the constitutive model used in the site response analysis, by assuming that the CSR vs. N_{liq} curve is a contour of constant dissipated energy (Lasley et al., 2016). Finally, from site response analyses performed on 50 soil profiles compiled by Cetin (2000) that are representative of cases in the liquefaction case history database, using 195 pairs of horizontal rock

motions recorded during 47 earthquakes as input motions, Lasely et al. (2016) determined $n_{eqM7.5}$ to be equal to 8.2.

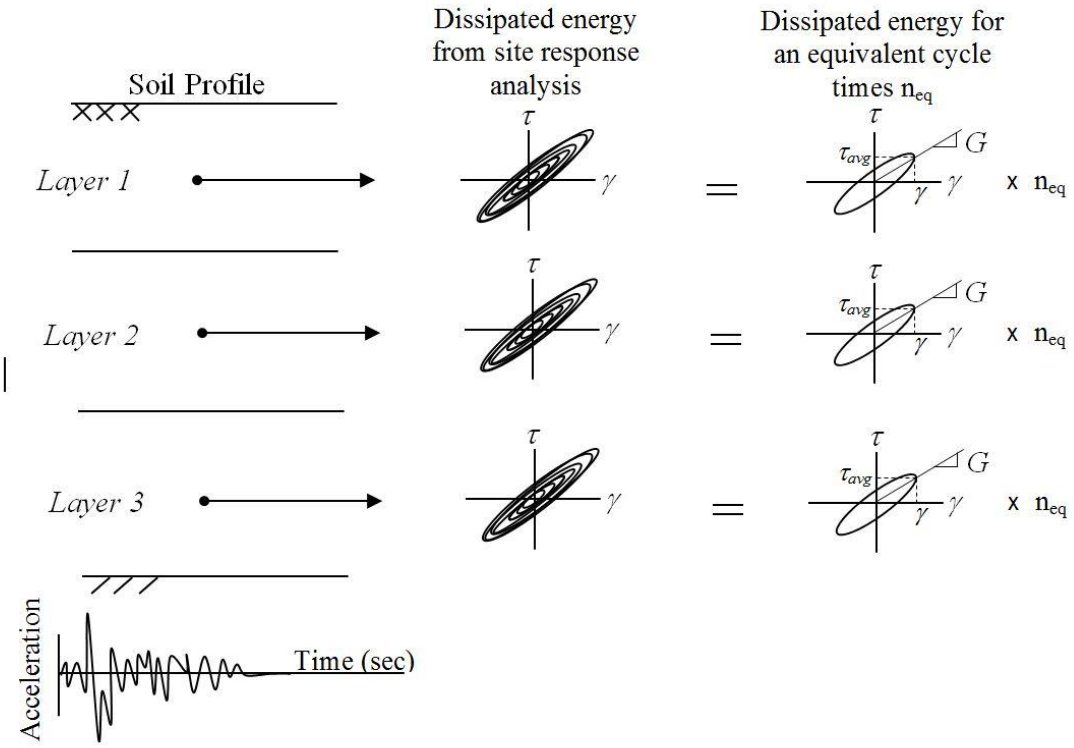

Figure 2.4 Illustration of the Green and Terri (2005) procedure to compute n_{eq} (Green, 2001).

2.4 Computation of MSF for the Darfield and Christchurch Earthquakes

MSF were computed for both the Darfield and Christchurch earthquakes at the 15 SMS sites shown in Figure 2.3 and listed in Table 2.1. These sites were selected because of the detailed site characterization performed at them (Wotherspoon et al., 2014, 2015a,b). As described below, equivalent linear site response analyses were performed to compute n_{eq} as a function of depth at each SMS site per the Green and Terri (2005) procedure and from the computed surface acceleration time histories per the Seed et al. (1975) procedure. Bedrock or the Riccarton Gravel Formation was assumed as the elastic half space in the equivalent linear site response analyses for these sites. For the cases where the Riccarton Gravel Formation was assumed to be the elastic halfspace, this assumption is based on the sharp impedance contrast between the Riccarton Gravel Formation and the looser overlying sediments (Brown and Weeber, 1992). For all the analyses,

the input motions were input as rock-outcrop motions at the depth of the elastic halfspace. Additional information on the SMS site profiles and the selection of the input motions for the site response analyses are given in the following sections.

2.4.1 SMS Profiles

As stated above, detailed site characterization was performed at the 15 SMS sites listed in Table 2.1. Methods used to characterize the site included active and passive-source surface wave testing, standard penetration testing (SPT), cone penetration testing (CPT), and horizontal to vertical spectral ratio (H/V) calculations. The shear wave velocity profiles for the 15 SMS sites used in the site response analyses were developed from the combination of the active and passive-source surface wave techniques, and layering constrained using subsurface investigation data. The idealized soil stratigraphy was inferred for each profile using the collection of CPT soil behavior type indices, and SPT boreholes performed at each site. Because the depth to bedrock at some of the SMS sites is ~500 m, detailed characterization down to bedrock is only possible for HVSC, where the depth to bedrock was only 19 m. Twelve of the other sites were characterized down to the Riccarton Gravel Formation (i.e., CACS, CBGS, CCCC, CHHC, CMHS, KPOC, PPHS, PRPC, REHS, RHSC, SHLC, and SMTC); for all of these sites, the Riccarton Gravel Formation is at a depth less than 30 m. For the remaining two sites (i.e., HPSC and NNBS), the depth to the Riccarton Gravel is greater than 30 m and the sites were only characterized down to ~30 m. For these latter two sites, the small strain shear wave velocity (Vs) profiles were extrapolated to the estimated depth of the Riccarton Gravel Formation using the relationship (Menq, 2003):

$$V_s = A_s \cdot \left(\frac{\sigma'_0}{P_a}\right)^n \qquad \text{Eq. 2.3}$$

where A_s is the small strain shear wave velocity corresponding to an initial effective mean stress equal to 1 atm (P_a), n is a calibrated exponent of normalized effective mean stress, and σ'_0 is the mean effective stress at the depth of the Riccarton Gravel Formation. The values of A_s and n used to model dense gravel were 312 m/s and 0.331, respectively (Menq, 2003). Values of V_s for the Riccarton Gravel Formation at HPSC and NNBS SMS sites were calculated to be 400 and 415

m/s, respectively, which fall in the range of 400-450 m/s measured at the twelve sites noted above and listed in Table 2.1.

Table 2.1 Strong Motion Station (SMS) details

Station Name	Code	Network	Latitude	Longitude	V_s* (m/s)	R_{rup} (km)	
						Dar eqk	Chch eqk
Canterbury Aero Club	CACS	NSMN	-43.48316539	172.5300139	600	11.9	12.9
Christchurch Botanic Gardens	CBGS	NSMN	-43.52933938	172.6198776	400	14.4	4.8
Christchurch Cathedral College	CCCC	CanNet	-43.5380850	172.6474270	400	16.3	2.9
Christchurch Hospital	CHHC	CanNet	-43.53592591	172.6275195	400	14.8	3.9
Cashmere High School	CMHS	NSMN	-43.56561744	172.6241694	400	14.0	1.5
Hulverstone Dr Pumping Station	HPSC	CanNet	-43.50157144	172.7021909	400	21.7	4.1
Heathcote Valley School	HVSC	CanNet	-43.57977835	172.7094230	760	20.8	3.9
Kaipoi North School	KPOC	CanNet	-43.37646016	172.6637603	450	27.7	17.5
North New Brighton School	NNBS	NSMN	-43.49541878	172.7179969	415	23.2	4.0
Papanui High School	PPHS	NSMN	-43.49284238	172.6069135	400	15.4	8.8
Pages Rd Pumping Station	PRPC	CanNet	-43.52580347	172.6827633	400	19.4	2.6
Christchurch Resthaven	REHS	NSMN	-43.52194513	172.6351501	400	15.9	4.9
Riccarton High School	RHSC	CanNet	-43.5361720	172.5644040	450	10.0	6.6
Shirley Library	SHLC	CanNet	-43.50533475	172.6633938	400	18.7	5.3
Styx Mill Transfer Station	SMTC	CanNet	-43.46752930	172.6138611	400	17.6	10.9

*The listed Vs are for the elastic halfspace assumed in the equivalent linear site response analyses, which corresponded to the Riccarton Gravel Formation of all sites except HVSC, where the listed value is for the Banks Peninsula volcanic rock.

Figure 2.5 shows the profile for the North New Brighton School (NNBS) SMS site used in the equivalent linear site response analyses, performed using ShakeVT2 (Lasley et al., 2014). The profiles for all 15 SMS sites are shown in Appendix A. The non-linear behavior of the soil was assumed to follow the Darendeli and Stokoe (2001) shear modulus and damping degradation curves.

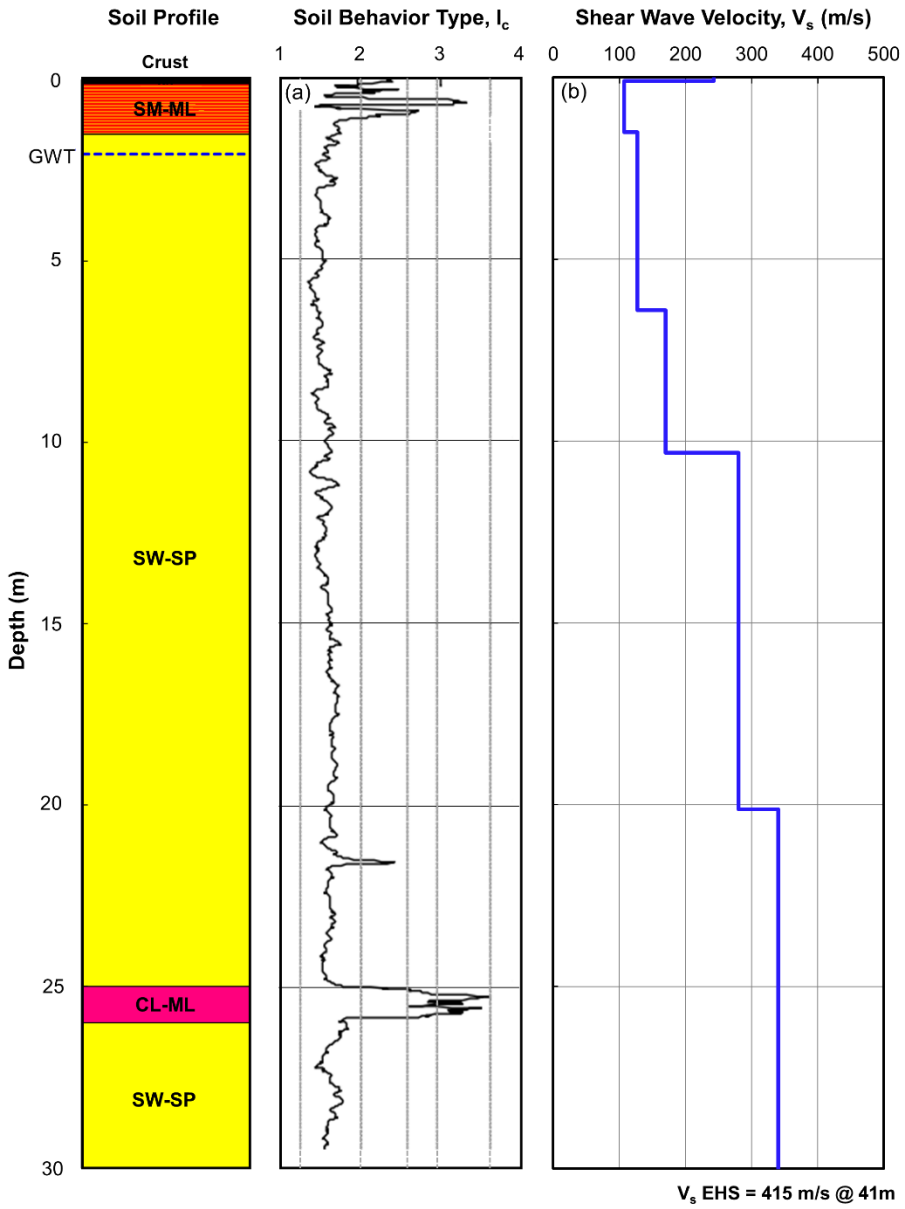

Figure 2.5 North New Brighton (NNBS) SMS soil profile along with profiles of: (a) CPT soil behavior type index, and (b) shear wave velocity obtained by Wotherspoon et al.

2.4.2 Input Ground Motions

An ensemble of site- and event-specific motion sets were selected for use in the site response analyses. Towards this end, 15 sets of horizontal motions were selected for each SMS-earthquake scenario using the generalized conditional intensity measure (GCIM) approach (Bradley 2010a, 2012d). The GCIM-based ground motion selection process for a given scenario can be broken down into two main steps. The first step entails the selection of motions that fall within a range of target causal parameters (e.g., M_w, R_{rup}, V_{s30}, source mechanism, etc.). For this study, the following causal parameters and ranges were used: $M_w \pm 0.75$ magnitude units (i.e., Mw: 6.35-7.85 and 5.45-6.95 for the Darfield and Christchurch earthquakes, respectively), $R_{rup} < 75$ km, and $V_{s30} > 150$ m/s. Additionally, to ensure the selected motions were from shallow crustal events in active tectonic regions, analogous to the tectonic settings of the Darfield and Christchurch events, motions were only selected from the NGA West ground motion database (Chiou et al., 2008), supplemented with "pulse-like" motions from the NGA West2 database (Seyhan et al., 2014) to ensure an adequate number of candidate motions with directivity effects.

The second step in the GCIM-based ground motion selection process entails the use of target distributions of intensity measures generated from ground motion predictive equations (GMPEs). To capture ground motion severity for a specific SMS-earthquake scenario, a multivariate distribution of intensity measures (e.g., spectral acceleration, cumulative absolute velocity, Arias intensity, significant duration, etc.) computed from GMPEs is used as the target. Each of the chosen intensity measures can be weighted according to their deemed significance, and to optimize the fit of candidate motions to the target distributions, scale factors can be applied to the amplitude of the motions.

For this study, spectral acceleration (SA), cumulative absolute velocity (CAV), Arias intensity (I_a), and 5-75% and 5-95% significant durations (D_{s575} and D_{s595}, respectively) were chosen as the target intensity measures. These intensity measures were chosen because each is considered to influence liquefaction triggering. Listings of the GMPEs used to compute the respective target distributions of intensity measures and the weights assigned to each intensity measure are given in Table 2.2 (Tarbali and Bradley, 2014). The target distributions of the intensity measures were computed for each SMS site using the small strain shear wave velocity for the assumed elastic half space, listed

in Table 2.1. The target SA for a damping ratio of 5% was defined at 21 oscillator periods: T = 0.05, 0.075, 0.1, 0.15, 0.2, 0.25, 0.3, 0.4, 0.5, 0.75, 1.0, 1.5, 2.0, 2.5, 3.0, 3.5, 4.0, 4.5, 5.0, 7.5, and 10.0 s. For the scenarios where forward directivity was considered (Joshi, 2013), the spectral accelerations were amplified at the pulse period (T_p) determined from the actual recorded motions at the site using the Shahi and Baker (2011) narrowband model. Scale factors ranging from 0.5 to 2 were applied to the amplitude of the motions to optimize the fit of the motions to the target distributions. In total, 15 sets of horizontal motions were selected for each SMS-earthquake pair, resulting in a total of 900 motions selected (2 motions per horizontal set × 15 sets of motions per SMS-earthquake scenario × 15 SMS × 2 earthquakes = 900 motions). The sets of ground motions selected for the NNBS SMS site for both the Darfield and Christchurch earthquakes using the GCIM-based process are discussed in the following.

Table 2.2 Summary of intensity measures and weighting scheme used in GCIM ground motion selection process

Intensity Measure	GMPE	Weight
Spectral Acceleration (SA)	Bradley (2013b)	60%*
Cumulative Absolute Velocity (CAV)	Campbell and Bozorgnia (2010)	10%
Arias Intensity (I_a)	Campbell and Bozorgnia (2012)	10%
5-75% Significant Duration (D_{s575})	Bommer et al. (2009)	10%
5-95% Significant Duration (D_{s595})	Bommer et al. (2009)	10%

*Evenly distributed to 21 SA ordinates (i.e. 60%/21 ≈ 2.86% per SA ordinate)

Figure 2.6 shows the M_w vs. R_{rup} distributions of selected ground motions for the NNBS SMS site for both the Darfield and Christchurch earthquakes. As expected, based on the adopted causal parameter bounds, it can be seen that the selected ground motions have magnitude and distance values that are relatively consistent with the 'target' values for the considered events (albeit the source-to-site distances for the Christchurch earthquake scenario are larger than the target due to the paucity of as-recorded motions for <5km distances). Figure 2.7 shows the median and the 16th and 84th percentiles of the 5% damped target response spectrum. For comparison, the response spectra for the selected motions are also shown, along with the median and the 16th and 84th percentiles for the selected motions. As may be observed, the distributions of SA fit the target distributions reasonably well for both earthquakes, albeit more so for the Christchurch earthquake

which does not include the pronounced long-period forward directivity spectral peak. Figure 2.8 shows the target distributions for the other intensity measures chosen, along with those for the selected motions. For these other intensity measures, the selected motions appropriately represent the target distribution. Appendix B provides ground motion selection plots (e.g. Figures 2.6-8) for all 15 SMS sites.

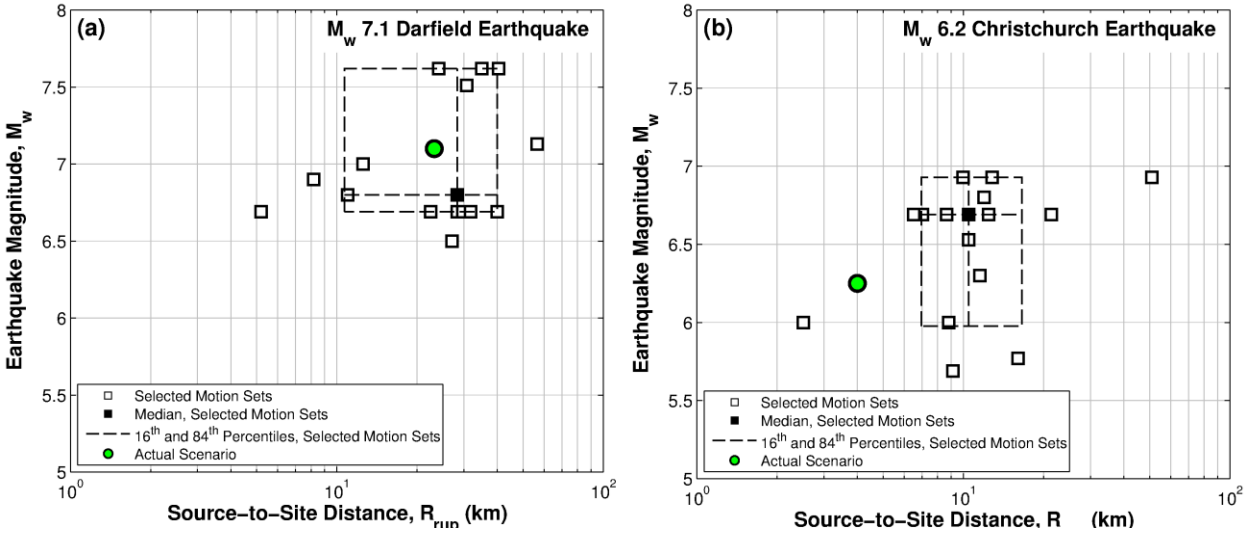

Figure 2.6 Distributions of causal parameters, M_w and R_{rup}, for the selected motion sets for both the: (a) Darfield earthquake, and (b) Christchurch earthquake scenarios at the NNBS SMS site.

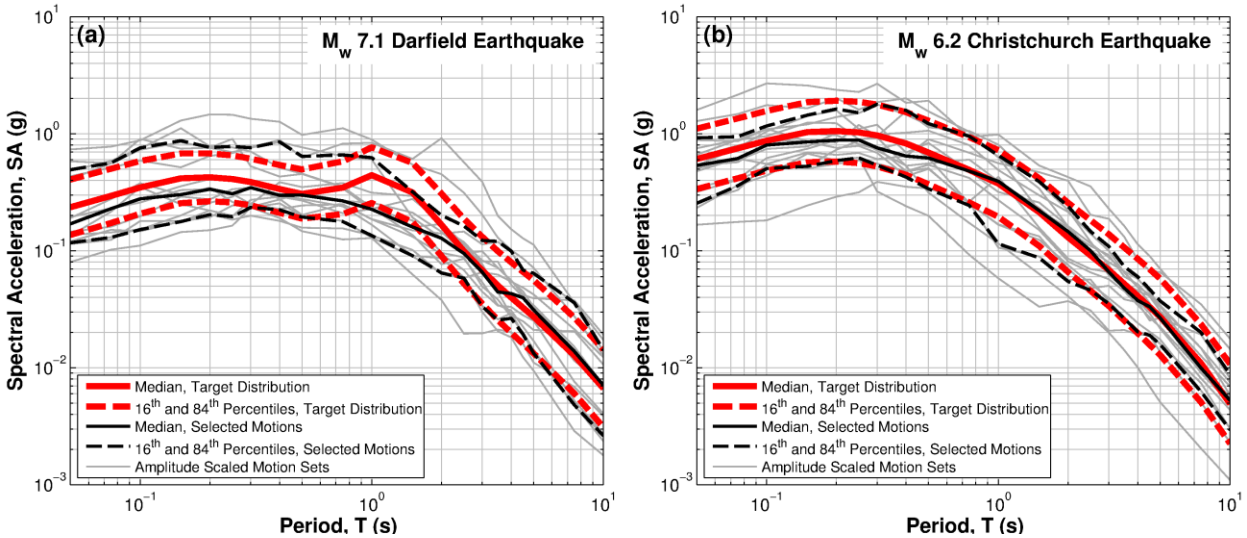

Figure 2.7 5% damped response spectra of the target motions and selected motion for the NNBS SMS site for the: (a) Darfield earthquake, and (b) Christchurch earthquake.

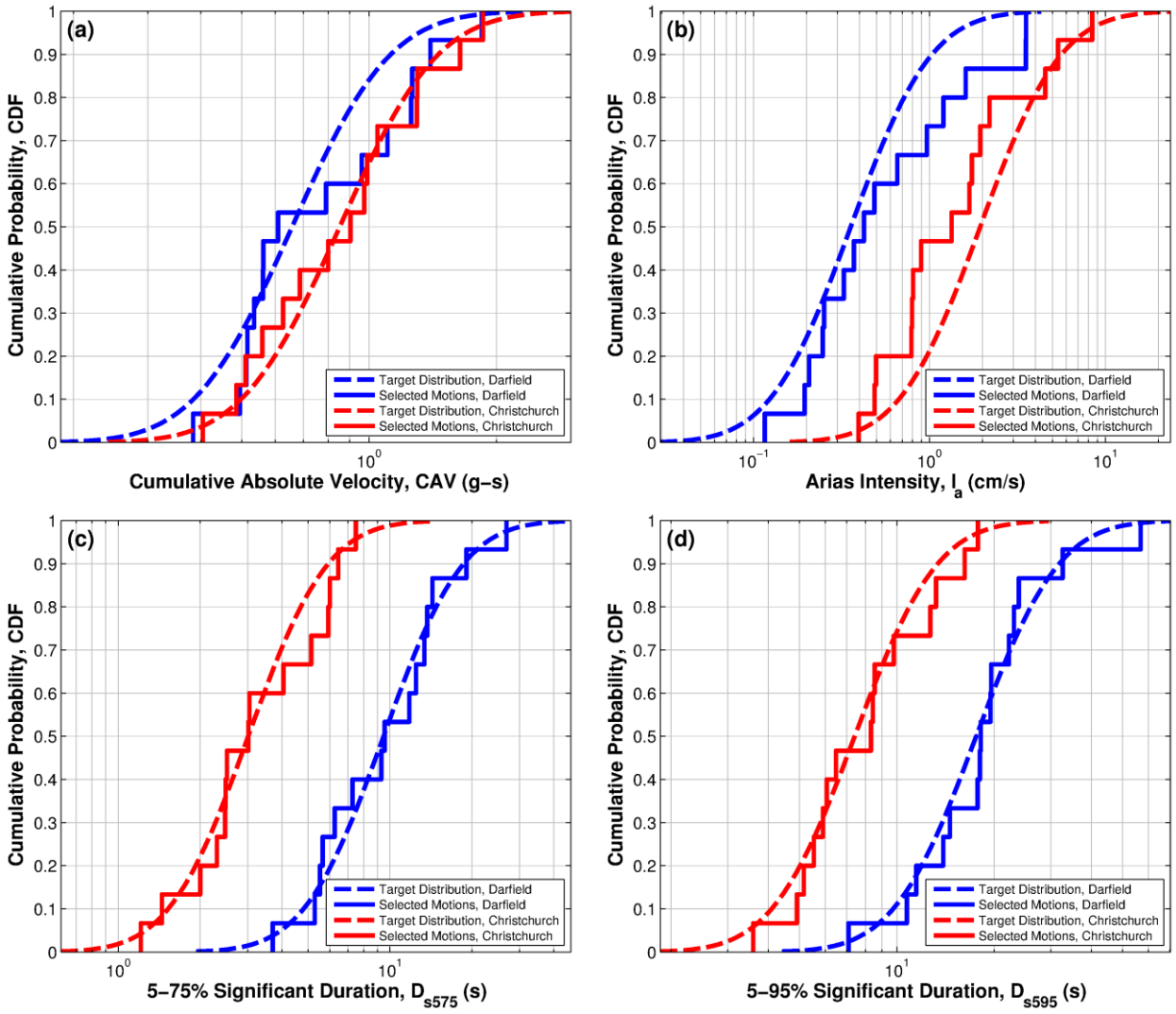

Figure 2.8 Cumulative distributions of the target and selected motions for the NNBS SMS site for both the Darfield and Christchurch earthquakes: (a) CAV; (b) I_a; (c) D_{s575} ; and (d) D_{s595}.

2.5 Results and Discussion

Using the Seed et al. (1975) and Green and Terri (2005) approaches for computing n_{eqM} in conjunction with the results from the site response analyses performed as described above, MSF were computed per Eq. 2.1 for each of the 15 SMS sites for both the Darfield and Christchurch earthquakes. In computing n_{eqM} per the Seed et al. (1975) procedure (i.e., per Eq. 2.2) and in computing the MSF for using the n_{eqM} from both the Seed et al. (1975) and Green and Terri (2005) (i.e., per Eq. 2.1), *b* was assumed to equal 0.34. As shown in Lasley et al. (2016), this value is consistent with the Darendeli and Stokoe (2001) shear modulus and damping degradation curves for a range of densities and effective confining stresses, based on the assumption that a CSR vs.

N_{liq} curve is a contour of constant dissipated energy. This assumption has been shown to be reasonably in accord with laboratory data (e.g., Kokusho and Kaneko, 2014; Polito et al., 2013). Additionally, b = 0.34 is consistent with laboratory curves developed from high-quality undisturbed samples obtained by freezing (Yoshimi et al., 1984).

The MSFs for the NNBS SMS site are shown in Figure 2.9 and those for all 15 SMS sites are shown in Appendix C. A few trends may be observed from this figure. First, the MSF for the Darfield earthquake are generally less than those for the Christchurch earthquake, which is expected because the magnitude for the Darfield earthquake is larger than that for the Christchurch earthquake (i.e., M_w7.1 vs. M_w6.2). Second, the MSF computed using the n_{eqM} from the Green and Terri (2005) approach is relatively constant with depth, although the standard deviation decreases slightly with depth; this trend was also identified by Lasley et al. (2016) (Note that the MSF computed using the n_{eqM} from the Seed et al. (1975) approach are computed using surface ground motions; hence, the corresponding MSFs and standard deviations are assumed constant with depth). Third, the MSFs computed using the n_{eqM} from the Seed et al. (1975) approach are larger than those computed using the n_{eqM} computed using the Green and Terri (2005) approach. This actually has more to do with the values used for $n_{eqM7.5}$ (i.e., 15 for the Seed et al. approach versus 8.2 for the Green and Terri approach) rather than with the computed values for n_{eqM}, which were very similar for both approaches. However, the focus of this study is on the spatial variation of MSF during the Darfield and Christchurch earthquakes, not on the absolute values of the MSF at any given site. Similarly, it should be noted that the MSF computed herein (either those computed using the n_{eqM} from the Seed et al. (1975) or the Green and Terri (2005) approaches) should not be used in conjunction with any of the existing simplified liquefaction evaluation procedures. Rather, the MSF recommended by a given procedure should be used with that procedure.

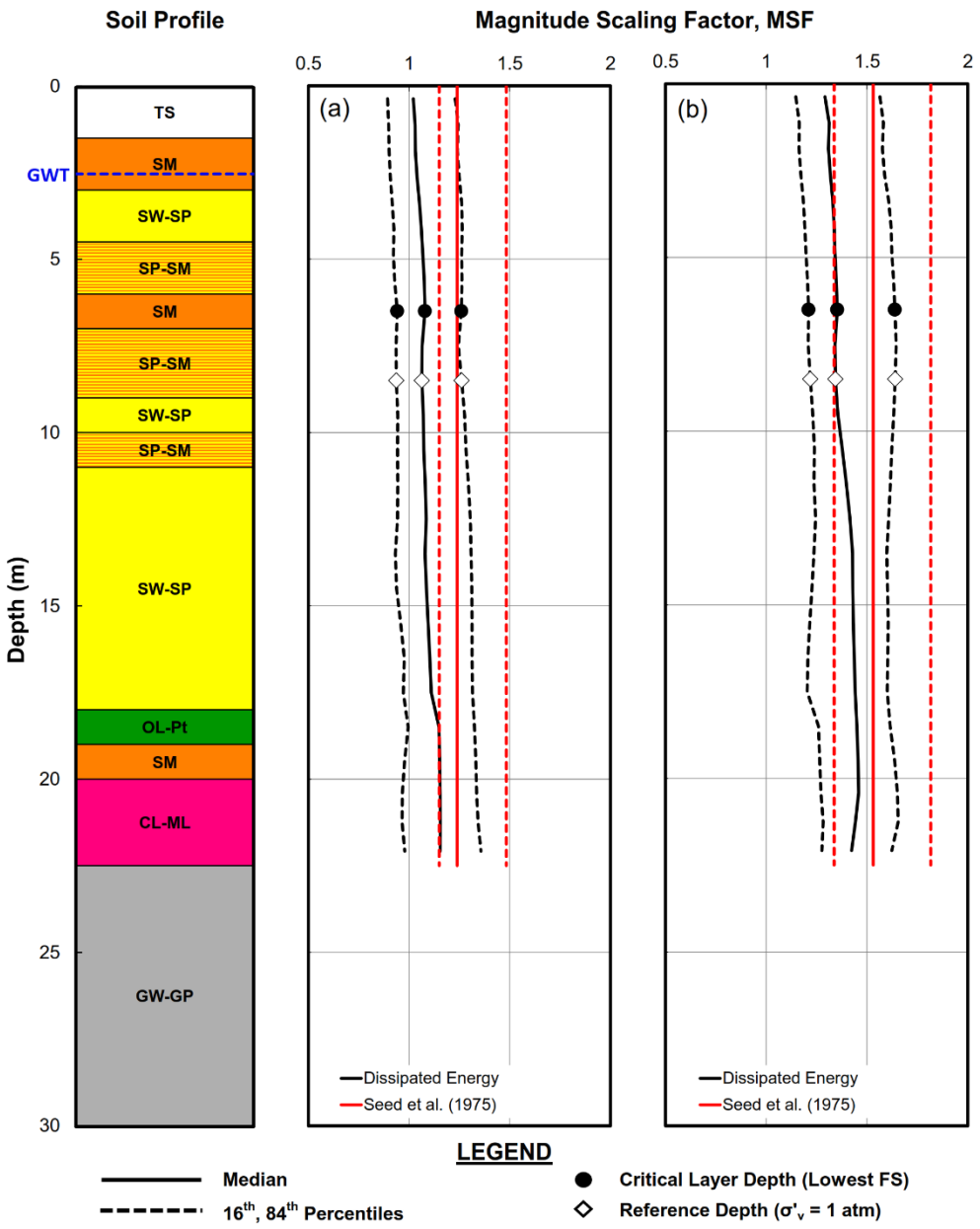

Figure 2.9 MSF computed for NNBS SMS site using the Green and Terri (2005) and Seed et al. (1975) approaches for computing number of equivalent cycles for: (a) Darfield earthquake, and (b) Christchurch earthquake.

Contour plots of MSF computed using the n_{eqM} from the Green and Terri (2005) approach for both the Darfield and Christchurch earthquakes are shown in Figure 2.10; similar plots for MSF computed using n_{eqM} from the Seed et al. (1975) approach are shown in Appendix D. As may be observed, similar trends are shown in contour plots of the MSF computed using the Green and Terri (2005) and the Seed et al. (1975) approaches. These contours are superimposed on maps of

the Christchurch region, with areas that experienced liquefaction also shown. Because the MSF computed using the n_{eqM} from the Green and Terri (2005) approach vary to some extent with depth, the contour plots are developed from the MSF computed at the "critical" depths for each of the SMSs, where critical depth is assumed herein to be that to the layer most susceptible to liquefaction (i.e., depth to the layer having the lowest computed factor of safety against liquefaction). For SMSs sites where no layers were deemed susceptible to liquefaction, the critical depth was taken as ~4.75 m which corresponds to the median critical depth of compiled liquefaction case histories (e.g., Cetin et al., 2004; Boulanger and Idriss, 2014). Both the depths to the layer having the lowest factor of safety against liquefaction and to an initial vertical effective stress of 1 atm are identified in Figure 2.9 for the NNBS SMS site and are tabulated in Table 2.3 for all sites. The median a_{max} values computed at the SMS sites are also summarized in Table 2.3 with similar contour plots provided in Figure 2.11 to elucidate any correlation between MSF and a_{max} for both earthquake scenarios.

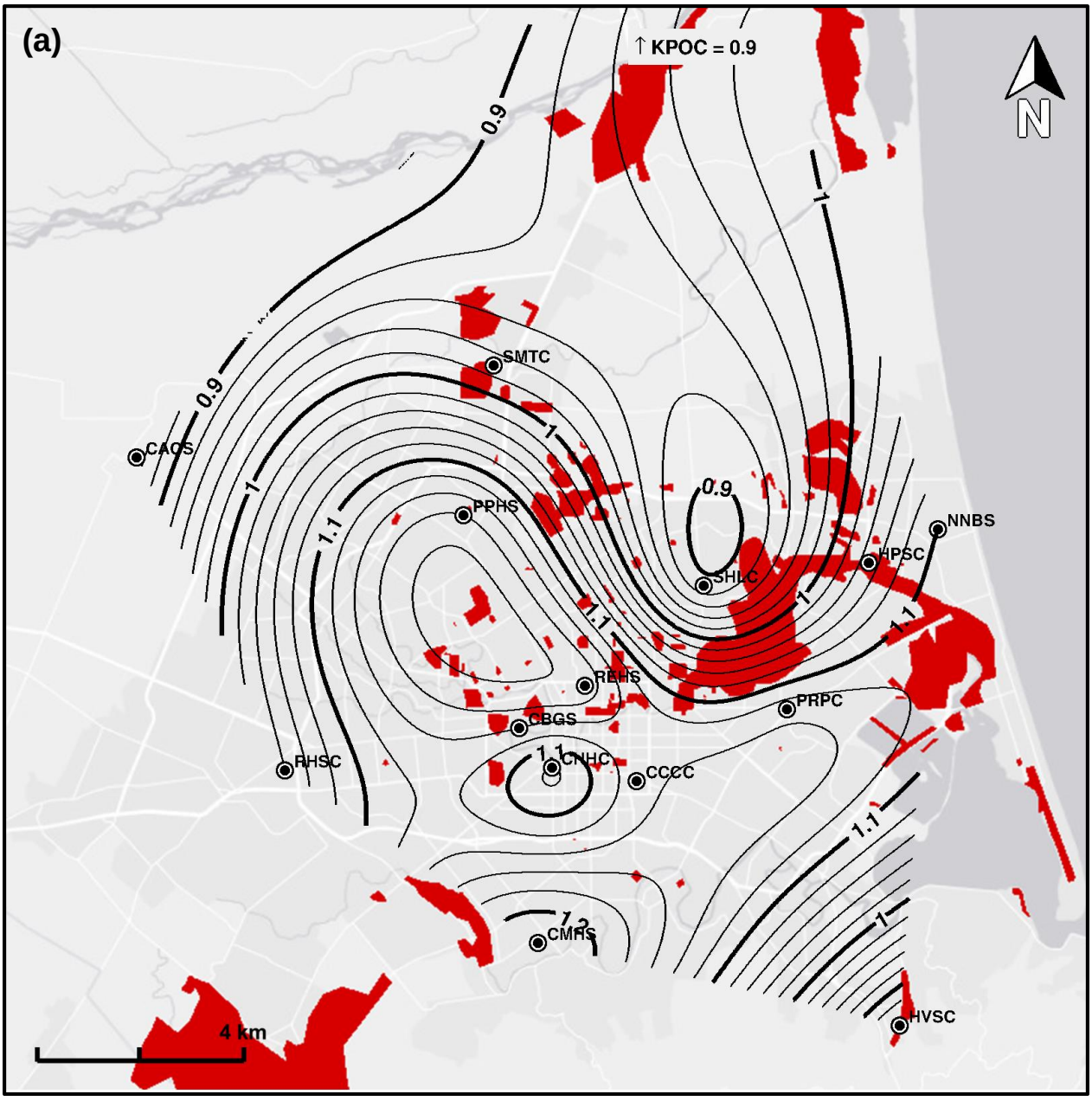
(a)
↑ KPOC = 0.9
N
0.9
1
1.1
1.2
SMTC
CAOS
PPHS
SHLC
HPSC
NNBS
RELHS
PRPC
CBGS
CNHC
CCCC
RHSC
CMHS
HVSC
4 km

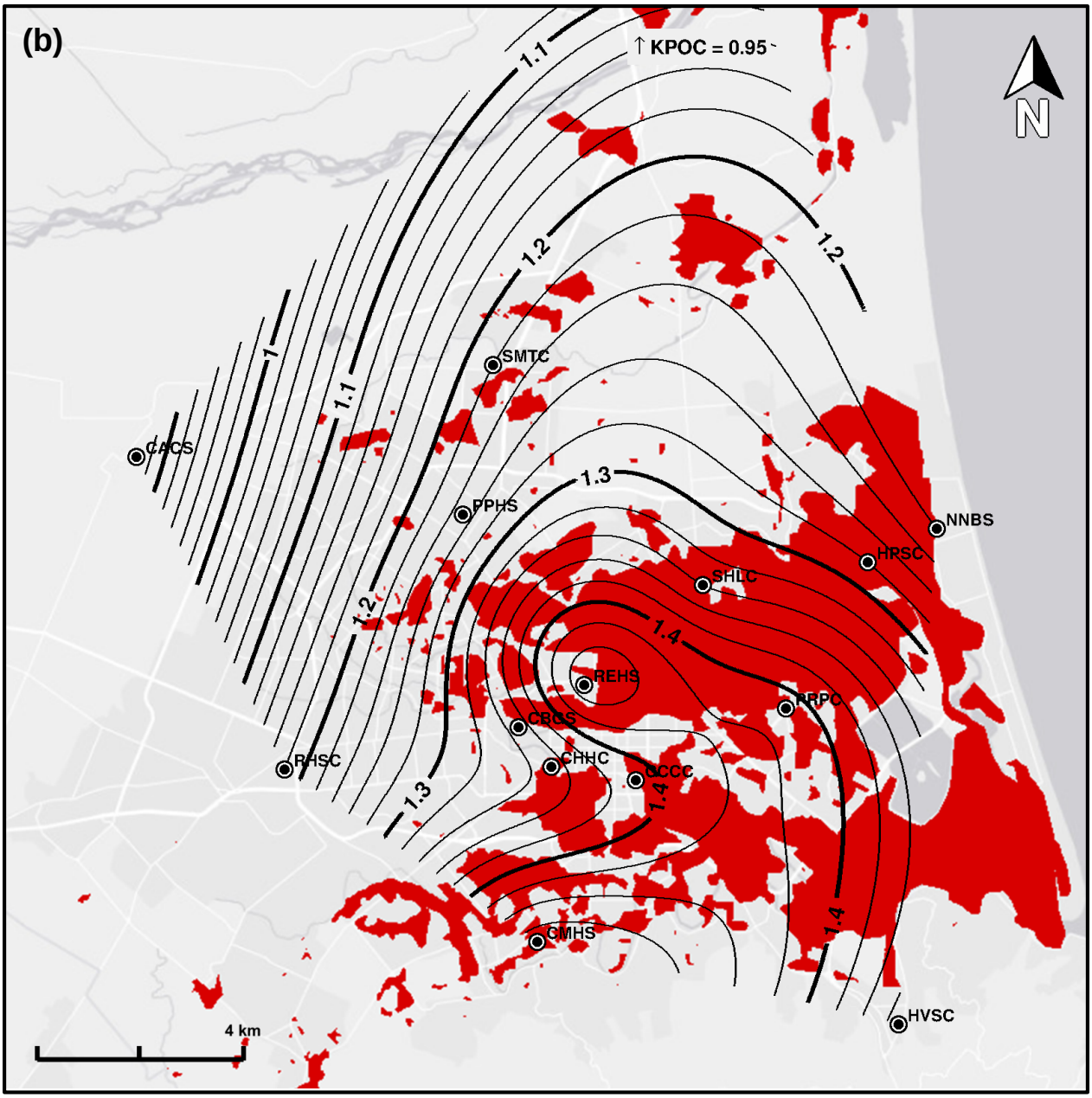

Figure 2.10 Contour plots of MSF computed using neqM from the Green and Terri (2005) approach for the: (a) Darfield earthquake, and (b) Christchurch earthquake.

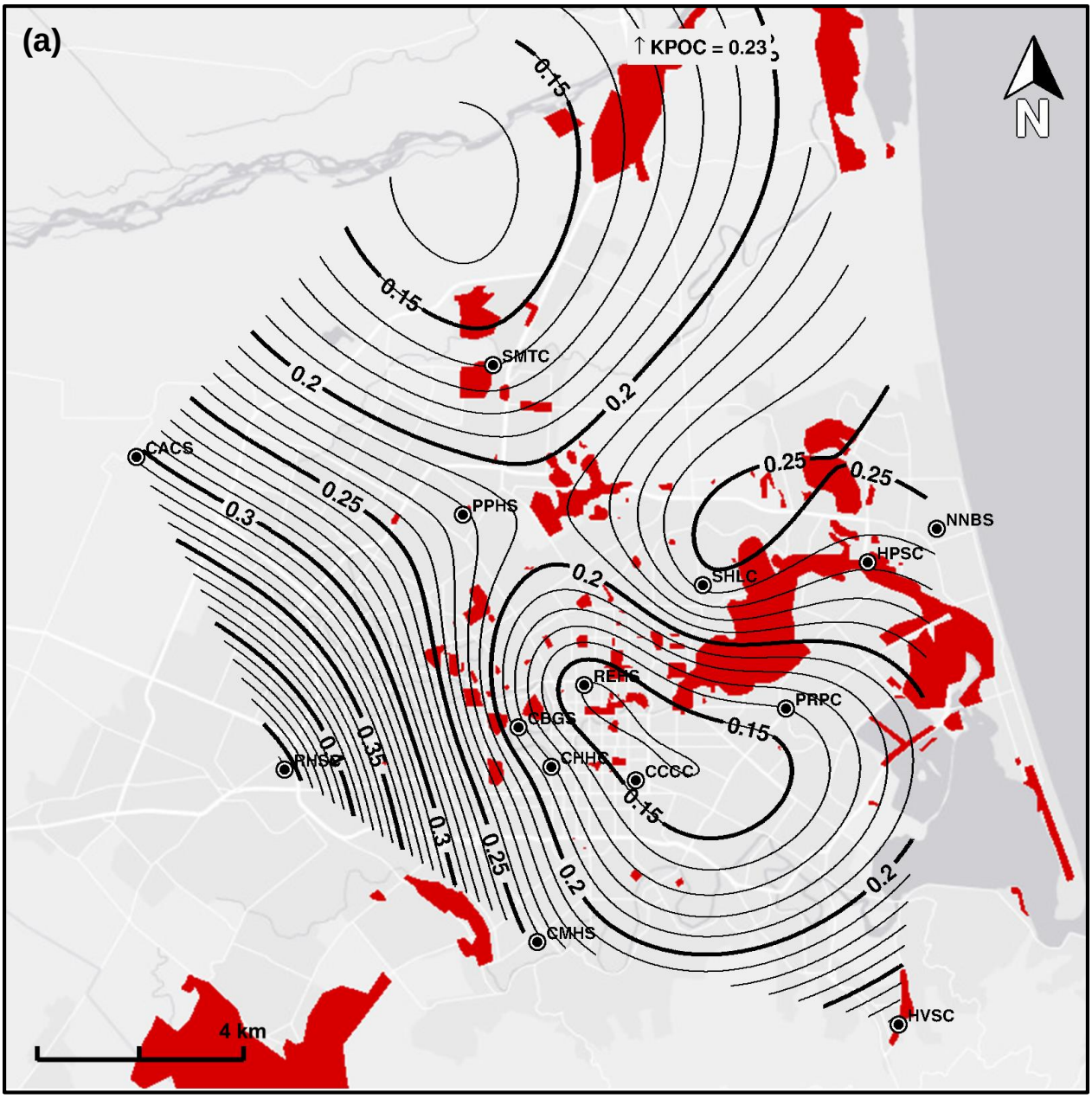
(a)
KPOC = 0.23
N
SMTC
CACS
PPHS
NNBS
HPSC
SHLC
RELC
PRPC
CBGS
CHHS
CCCC
PHSC
CMHS
HVSC
0.15
0.2
0.25
0.3
0.35
4 km

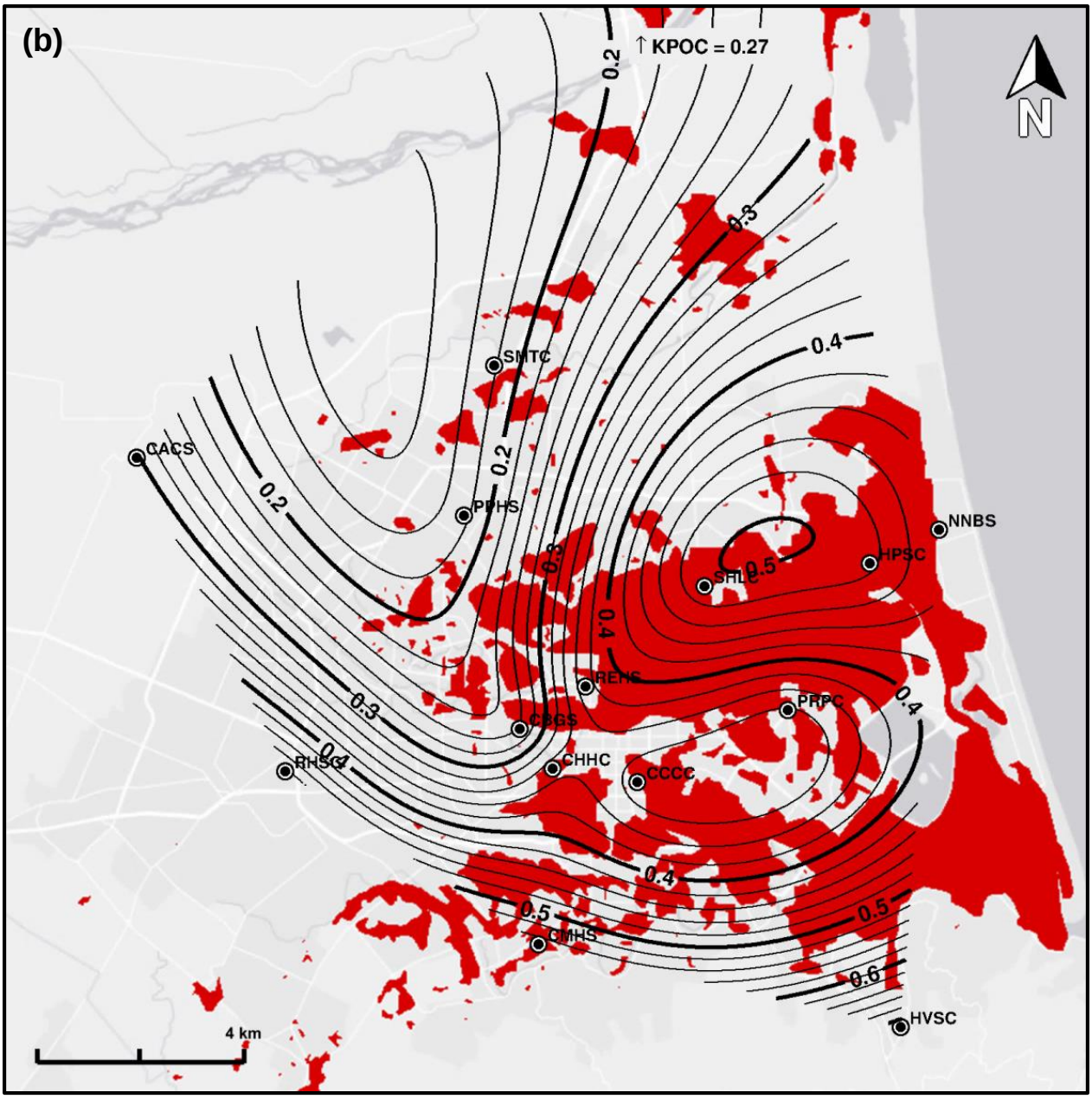

Figure 2.11 Contour plots of median a_{max} computed at the ground surface from the site response analyses for the: (a) Darfield earthquake, and (b) Christchurch earthquake.

Table 2.3 a_{max} and MSF computed for the SMS sites.

Station	a_{max} (g) (Surface)		σ'_{vo} = 1 atm Depth (m)	MSF (Reference Depth)				Critical Depth (m)	MSF (Critical Depth)			
	Dar Eqk	Chch Eqk		Dar Eqk		Chch Eqk			Dar Eqk		Chch Eqk	
				Sea75[1]	GT05[2]	Sea75	GT05		Sea75	GT05	Sea75	GT05
CACS	0.31	0.30	4.5	1.11	0.85	1.07	0.86	4.5	1.11	0.85	1.07	0.86
CBGS	0.19	0.26	6.5	1.28	1.08	1.48	1.26	13.5	1.28	1.14	1.48	1.35
CCCC	0.15	0.33	9.4	1.35	1.13	1.56	1.39	5.8	1.35	1.13	1.56	1.39
CHHC	0.18	0.35	8.5	1.24	1.06	1.53	1.34	6.5	1.24	1.08	1.53	1.35
CMHS	0.24	0.55	7.4	1.43	1.20	1.56	1.47	8.2	1.43	1.22	1.56	1.47
HPSC	0.23	0.48	9.5	1.33	1.05	1.53	1.29	2.4	1.33	1.05	1.53	1.28
HVSC	0.29	0.71	9.5	1.02	0.86	1.57	1.20	4.5	1.02	0.85	1.57	1.33
KPOC	0.23	0.27	8.9	1.11	0.92	1.13	0.90	4.3	1.11	0.90	1.13	0.95
NNBS	0.25	0.44	8.9	1.35	1.10	1.58	1.22	9.8	1.35	1.10	1.58	1.22
PPHS	0.22	0.18	9.2	1.37	1.23	1.43	1.25	3.3	1.37	1.16	1.43	1.25
PRPC	0.16	0.34	8.5	1.37	1.17	1.55	1.41	4.5	1.37	1.13	1.55	1.41
REHS	0.14	0.37	10.5	1.41	1.07	1.66	1.38	2.6	1.41	1.17	1.66	1.45
RHSC	0.46	0.49	6.3	1.19	1.05	1.30	1.21	4.8	1.19	1.04	1.30	1.18
SHLC	0.24	0.49	7.5	1.15	0.91	1.60	1.32	4.5	1.15	0.91	1.60	1.34
SMTC	0.16	0.18	9.8	1.19	0.95	1.40	1.20	11.5	1.19	0.97	1.40	1.22

[1] Sea75 are MSF based on n_{eqM} computed using the Seed et al. (1975) approach

[2] GT05 are MSF based on n_{eqM} computed using the Green and Terri (2005) approach

As may be observed from Figure 2.10, the MSF for the Darfield and Christchurch earthquakes range from approximately 0.9 to 1.2 and from approximately 0.95 to 1.46, respectively, with a general trend of MSF being higher in the southern part of the Christchurch and increasing in a northerly direction. However, despite these ranges in MSF being relatively significant, particularly for the Christchurch earthquake, there does not appear to be a consistent correlation between lower computed MSF and observed liquefaction. For example, widespread liquefaction was observed in Kaiapoi during the Darfield earthquake, which is an area having a relatively low MSF (~0.9). However, Kaiapoi did not experience as severe or as widespread liquefaction during the Christchurch earthquake, but the MSF for this area for this event are also relatively low (~0.95). More significantly, portions of the CBD and eastern Christchurch experienced severe and widespread liquefaction during the Christchurch earthquake, yet relatively high MSF are computed for these regions for this event. However, it should be realized that the seismic demand imposed on the soil is both a function of the amplitude and the duration of the motions, where the former is proportional to a_{max}. Additionally, the capacity of the soil to resist liquefaction varies spatially, which inherently influenced the liquefaction response observed during the Darfield and Christchurch earthquakes.

In comparing contour maps of the median a_{max} values from the site response analyses (Figure 2.11) with the contour maps for MSFs (Figure 2.10), it is observed that there is a general correlation between MSF and a_{max} (i.e., regions having higher a_{max} values also have higher MSFs). This results in opposing effects on the seismic demand imposed in the soil (i.e., higher a_{max} induces higher seismic demand in the soil, while a higher MSF results in a lower seismic demand). However, of the two parameters, a_{max} ranges more widely than MSF and thus has a greater influence on the resulting seismic demand imposed on the soil. Nevertheless, the spatial variation of the MSF is significant enough that it could potentially contribute to discrepancies between predicted versus observed liquefaction.

2.6 Conclusions

MSF accounts for the durational effects of strong ground shaking on liquefaction triggering within the simplified liquefaction evaluation procedure, and it has traditionally been assumed that they are only a function of earthquake magnitude. However, this assumption fails to appreciate the inverse correlation between the peak amplitude of ground motions and strong ground motion duration, and thus would seemingly vary spatially (e.g., distance from source). The combination of well-documented liquefaction response during the Darfield and Christchurch, New Zealand, earthquakes, densely-recorded ground motions for the events, and detailed subsurface characterization provides an unprecedented opportunity to investigate the significance of the spatial variation of MSF on liquefaction triggering. Towards this end, MSF were computed at 15 SMS sites across Christchurch and its environs using n_{eqM} computed using the approaches proposed by Seed et al. (1975) and by Green and Terri (2005). Trends in the spatial variation of the MSF computed using n_{eqM} from both approaches were similar, and the MSF computed using the n_{eqM} from the Green and Terri (2005) approach ranged from 0.9 to 1.2 and from 0.95 to 1.46 across Christchurch for the Darfield and Christchurch earthquakes, respectively. However, there was no consistent trend for regions with lower computed MSF having experienced more severe or widespread liquefaction. Additionally, it was observed that there is a general correlation between MSF and a_{max} (i.e., regions having higher a_{max} values also have higher MSFs), but a_{max} ranges more widely than MSF and thus has a greater influence on the resulting seismic demand imposed on the soil. Regardless, the spatial variation of the MSF is deemed significant enough that it could result in discrepancies between predicted versus observed liquefaction and thus warrants to be accounted for in future variants of simplified liquefaction evaluation procedures.

2.7 References

Archuleta, R.J. and Hartzell, S.H. (1981). "Effects of fault finiteness on near-source ground motion." *Bulletin of the Seismological Society of America*, 71, 939-957.

ASTM (2011). "Practices for Cycle Counting in Fatigue Analysis." ASTM Standard E1049, 1985, *ASTM International*, West Conshohocken, PA, www.astm.org

Beavan, J., Fielding,, E., Motagh, M., Samsonov, S. and Donnelly, N. (2011). Fault Location and Slip Distribution of the 22 February 2011 Mw 6.2 Christchurch, New Zealand, Earthquake from Geodetic Data. *Seismological Research Letters. 82*, 86(6), 789-799.

Bommer, J.J., and Martinez-Pereira, A. (1999). "The effective duration of earthquake strong motion." Journal of Earthquake Engineering, 3(2), 127–172.

Bommer, J.J., Stafford, P.J., and Alarcón, J.E. (2009). "Empirical equations for the prediction of the significant, bracketed, and uniform duration of earthquake ground motion." *Bulletin of the Seismological Society of America*, 99(6), 3217-3233.

Boulanger, R.W., and Idriss, I.M. (2014). "CPT and SPT based liquefaction triggering procedures." Report No. UCD/CGM-14/01, Center for Geotechnical Modeling, Department of Civil and Environmental Engineering, University of California, Davis, CA, 134 pp.

Boulanger, R.W. and Idriss, I.M. (2015). "Magnitude scaling factors in liquefaction triggering procedures." *Soil Dynamics and Earthquake Engineering*, 79(Part B), 296-303.

Bradley, B.A. (2010a). "A generalized conditional intensity measure approach and holistic ground-motion selection." *Earthquake Engineering and Structural Dynamics*, 39(12), 1321-1342.

Bradley, B.A. (2010b). "Site-specific and spatially distributed ground-motion prediction of acceleration spectrum intensity." *Bulletin of the Seismological Society of America*, 100(2), 792-801.

Bradley, B.A. and Cubrinovski, M. (2011). "Near-Source Strong Ground Motions Observed in the 22 February 2011 Christchurch Earthquake." *Bulletin of the New Zealand Society for Earthquake Engineering*, 44(4):181–194.

Bradley, B.A. (2012a). "A ground motion selection algorithm based on the generalized conditional intensity measure approach." *Soil Dynamics and Earthquake Engineering*, 40, 48-61.

Bradley, B.A. (2012b). "Observed Ground Motions in the 4 September 2010 Darfield and 22 February 2011 Christchurch Earthquakes." Proc. 2012 NZSEE Conference, 13-15 Apr 2012, Paper 037.

Bradley, B.A. (2012c) Ground motions observed in the Darfield and Christchurch earthquakes and the importance of local site response effects. *New Zealand Journal of Geology and Geophysics* 55(3): 279-286

Bradley, B.A. (2012d). "Strong ground motion characteristics observed in the 4 September 2010 Darfield, New Zealand earthquake." *Soil Dynamics and Earthquake Engineering*, 42, 32–46.

Bradley, B.A. (2013a). Ground motion selection for seismic risk analysis of civil infrastructures. Handbook of seismic risk analysis and management of civil infrastructure systems. S. Tasfamariam and K. Goda, *Woodhead Publishing Ltd.*

Bradley, B.A. (2013b). "A New Zealand-Specific Pseudospectral Acceleration Ground-Motion Prediction Equation for Active Shallow Crustal Earthquakes Based on Foreign Models." *Bulletin of the Seismological Society of America*, 103(3), 1801-1822.

Bradley, B.A., Quigley, M.C., Van Dissen, R.J., and Litchfield, N.J. (2014). "Ground motion and seismic source aspects of the Canterbury earthquake sequence." *Earthquake Spectra*, 30(1), 1-15.

Brown, L.J., Beetham, R.D., Paterson, B.R., and Weeber, J.H. (1995). "Geology of Christchurch, New Zealand," *Environmental & Engineering Geoscience*, 1(4), 427-488.

Brown, L.J. and Weeber, J.H. (1992). "Geology of the Christchurch urban area." Geological and Nuclear Sciences, 110pp.

Campbell, K.W. and Bozorgnia, Y. (2010). "A ground motion prediction equation for the horizontal component of cumulative absolute velocity (CAV) based on the PEER NGA strong motion database." *Earthquake Spectra*, 26(3), 635-650.

Campbell, K.W. and Bozorgnia, Y. (2012). "A comparison of ground motion prediction equations for Arias intensity and cumulative absolute velocity developed using a consistent database and functional form." *Earthquake Spectra*, 28(3), 931-941.

Cetin, K.O. (2000). "Reliability-based assessment of seismic soil liquefaction initiation hazard." Ph.D. Thesis, University of California at Berkeley, Berkeley, CA.

Cetin, K.O., Seed, R.B., Der Kiureghian, A., Tokimatsu, K., Harder, Jr., L.F., Kayen, R.E., and Moss, R.E.S. (2004). "Standard Penetration Test-Based Probabilistic and Deterministic Assessment of Seismic Soil Liquefaction Potential," *Journal of Geotechnical and Geoenvironmental Engineering*, 130(12), 1314-1340.

Chiou, B., Darragh, R., Gregor, N., and Silva, W. (2008). "NGA Project Strong-Motion Database." *Earthquake Spectra*, 24(1), 23–44.

Cousins, J. and McVerry, G.H. (2010). "Overview of strong motion data from the Darfield earthquake." *Bulletin of the New Zealand Society for Earthquake Engineering*, 43(4), 222-227.

Cubrinovski, M. and Green, R.A., eds., (2010). Geotechnical Reconnaissance of the 2010 Darfield (Canterbury) Earthquake, (contributing authors in alphabetical order: J. Allen, S. Ashford, E. Bowman, B. Bradley, B. Cox, M. Cubrinovski, R. Green, T. Hutchinson, E. Kavazanjian, R. Orense, M. Pender, M. Quigley, and L. Wotherspoon), *Bulletin of the New Zealand Society for Earthquake Engineering*, 43(4), 243-320.

Cubrinovski, M., Bradley, B., Wotherspoon, L., Green, R., Bray, J., Woods, C., Pender, M., Allen, J., Bradshaw, A., Rix, G., Taylor, M., Robinson, K., Henderson, D., Giorgini, S., Ma, K., Winkley, A., Zupan, J., O'Rourke, T., DePascale, G., and Wells, D. (2011). Geotechnical aspects of the 22 February 2011 Christchurch earthquake, *Bulletin of the New Zealand Society for Earthquake Engineering*, 43(4), 205-226.

Darendeli, M.B. and Stokoe II, K.H. (2001). "Development of a new family of normalized modulus reduction and material damping curves." Geotechnical Engineering Report GD01-1, University of Texas at Austin.

Forsyth, P.J., Barrell, D.J.A., and Jongens, R. (compilers) (2008). "Geology of the Christchurch area," *Geological & Nuclear Sciences* 1:250000 Geological Map, 16. Lower Hutt, New Zealand. GNS Science.

Green, R.A. (2001). "Energy-Based Evaluation and Remediation of Liquefiable Soils," Ph.D. Dissertation (J.K. Mitchell, Advisor), Department of Civil and Environmental Engineering, Virginia Polytechnic Institute and State University (Virginia Tech), Blacksburg, VA, 397pp.

Green, R.A., Mitchell, J.K., and Polito, C.P. (2000). "An Energy-Based Excess Pore Pressure Generation Model for Cohesionless Soils," *Proc. The John Booker Memorial Symposium – Developments in Theoretical Geomechanics* (D.W. Smith and J.P. Carter, eds.), A.A. Balkema, Rotterdam, The Neatherlands, 383-390.

Green, R.A. and Terri, G.A. (2005). "Number of Equivalent Cycles Concept for Liquefaction Evaluations – Revisited," *Journal of Geotechnical and Geoenvironmental Engineering*, ASCE, 131(4), 477-488.

Green, R.A., Cubrinovski, M., Cox, B., Wood, C., Wotherspoon, L., Bradley, B., and Maurer, B. (2014). "Select Liquefaction Case Histories from the 2010-2011 Canterbury Earthquake Sequence," *Earthquake Spectra*, 30(1), 131-153.

Hancock, J. and Bommer J.J. (2005). "The effective number of cycles of earthquake ground motion." *Earthquake Engineering and Structural Dynamics*, 34, 637-664.

Holden, C., Beavan, R.J., Fry, B., Reyners, M.E., Ristau, J., Van Dissen, R.J., Villamor, P. and Quigley, M. (2011). Preliminary source model of the Mw 7.1 Darfield earthquake from geological, geodetic and seismic data. paper 164. *Ninth Pacific Conference on Earthquake Engineering: building an earthquake resilient society, April 14-16, 2011, University of Auckland, Auckland, New Zealand*. Auckland, NZ: 9PCEE

Idriss, I.M. and Boulanger, R.W. (2008). *Soil Liquefaction during Earthquakes*, Monograph MNO-12, Earthquake Engineering Research Institute, Oakland, CA, 261 pp.

Joshi VA. (2013). Near-fault forward directivity aspects of strong ground motions in the 2010-11 Canterbury earthquakes. *Master of Engineering Thesis.* November 2013. Christchurch, New Zealand. 354pp.

Kaechele, L. (1963). Review and analysis of cumulative-fatigue-damage theories. Memorandum RM-3650-PR, The Rand Corporation, 1700 Main St., Santa Monica, CA.

Kempton, J.J. and Stewart, J.P. (2006). "Prediction equations for significant duration of earthquake ground motions considering site and near-source effects." *Earthquake Spectra*, 22(4), 985–1013.

Kokusho, T. and Kaneko, Y. (2014). "Dissipated & strain energies in undrained cyclic loading tests for liquefaction potential evaluations." *Proc. 10th U.S. National Conf. on Earthquake Engineering*, Earthquake Engineering Research Institute, Anchorage, AK.

Lasley, S.J., Green, R.A., and Rodriguez-Marek, A. (2014). "Comparison of equivalent-linear site response analysis software." *Proc. 10th U.S. National Conf. on Earthquake Engineering*, Earthquake Engineering Research Institute, Anchorage, AK.

Lasley, S., Green, R.A., and Rodriguez-Marek, A. (2016). "Number of Equivalent Stress Cycles for Liquefaction Evaluations in Active Tectonic and Stable Continental Regimes," *Journal of Geotechnical and Geoenvironmental Engineering*, ASCE. (*in review*).

Lee, R.L., Bradley, B.A., Ghisetti, F., Thomson, E.M., Pettinga, J.R., and Hughes, M.W. (2015). "A geology-based 3D seismic velocity model of Canterbury, New Zealand." *Proc. New Zealand Society for Earthquake Engineering (NZSEE) Annual Conference*, Paper Number O-63.

Lee, J. and Green, R.A. (2014). "An Empirical Significant Duration Relationship for Stable Continental Regions," *Bulletin of Earthquake Engineering*, 12(1), 217-235.

Maurer, B., Green, R., Cubrinovski, M., and Bradley, B.A. (2014). "Evaluation of Liquefaction Potential Index for Assessing Liquefaction Hazard: A Case Study in Christchurch, New Zealand." *Journal of Geotechnical and Geoenvironmental Engineering*, 140(7), 04014032.

Menq, F.-Y. (2003), "Dynamic Properties of Sandy and Gravely Soils," Ph.D. Dissertation, The University of Texas at Austin, 390 pp.

Miner, M.A. (1945). "Cumulative damage in fatigue." *Journal of Applied Mechanics*, 12(3), A159-A164.

Palmgren, A. (1924). "Die lebensdauer von kugellagern (Life length of roller bearings, in German)." *Zeitschrift des Vereins Deutscher Ingenieure*, 68(14), 339-341.

Polito, C., Green, R.A., Dillon, E., and Sohn, C. (2013). "The effect of load shape on the relationship between dissipated energy and residual excess pore pressure generation in cyclic triaxial tests." *Canadian Geotechnical Journal*, 50(9), 1118-1128.

Quigley, M.C., Bastin, S., and Bradley, B.A. (2013) Recurrent liquefaction in Christchurch, New Zealand, during the Canterbury earthquake sequence. *Geology*, 41(4), 419-422.

Robinson, K., Cubrinovski, M., and Bradley, B.A. (2013) *Sensitivity of predicted liquefaction-induced lateral displacements from the 2010 Darfield and 2011 Christchurch earthquakes.* Queenstown, New Zealand: 19th New Zealand Geotechnical Society (NZGS) Symposium, 20-23 Nov 2013.

Seed, H.B. and Idriss, I.M. (1971). "Simplified procedure for evaluating soil liquefaction potential." *Journal of the Soil Mechanics and Foundations Division*, 97(9), 1249–1273.

Seed, H.B., Idriss, I.M., Makdisi, F., and Banerjee, N. (1975). "Representation of irregular stress time histories by equivalent uniform stress series in liquefaction analyses, EERC 75-29." *Earthquake Engineering Research Center*, University of California, Berkeley.

Seyhan, E., Stewart, J.P., Ancheta, T.D., Darragh, R.B., and Graves, R.W. (2014). "NGA-West2 Site Database." *Earthquake Spectra*, 30(3), 1007-1024.

Shahi, S. K. (2013, January). *A probabilistic framework to include the effects of near-fault directivity in seismic hazard assessment*. Stanford University, Stanford.

Shahi, S.K. and Baker, J.W. (2011). "An empirically calibrated framework for including the effects of near-fault directivity in probabilistic seismic hazard analysis." *Bulletin of the Seismological Society of America*, 101(2), 742–755.

Shahi, S.K. and Baker, J. W. (2013). *NGA-West2 Models for Ground-Motion Directionality*. Pacific Earthquake Engineering Research Center.

Somerville, P.G., Smith, N.F., Graves, R.W., and Abrahamson, N.A. (1997). "Modification of empirical strong ground motion attenuation relations to include the amplitude and duration effects of rupture directivity." *Seismological Research Letters*, 68, 199-222.

Stafford, P.J., Alarcon, J.E., and Bommer, J.J. (2009). "Empirical equations for the prediction of the equivalent number of cycles of earthquake ground motion." *Soil Dynamics and Earthquake Engineering*, 29(11-12), 1425-1436.

Stallmeyer, J.E. and Walker, W.H. (1968). "Cumulative damage theories and application." *Journal of the Structural Division*, 94, 2739–2750.

Tarbali, K. and Bradley, B.A. (2014). "Scenario-based ground-motion selection using the generalized conditional intensity measure (GCIM) approach." *Proc. 10th National Conf. Earthquake Engineering, Anchorage, AK*, Earthquake Engineering Research Institute.

Tarbali, K. and Bradley, B.A. (2014). "Representative ground motion ensembles for several major earthquake scenarios in New Zealand." *Bulletin of the New Zealand Society of Earthquake Engineering*, 47(4), 231-252.

Whitman, R.V. (1971). "Resistance of Soil to Liquefaction and Settlement." *Soils and Foundations*, 11(4), 59–68.

Wotherspoon, L.M., Pender, M.J., and Orense, R.P. (2012). "Relationship between observed liquefaction at Kaiapoi following the 2010 Darfield earthquake and former channels of the Waimakariri River." *Engineering Geology*, 125, 45-55.

Wotherspoon, L., Orense, R., Bradley, B.A., Cox, B., Green, R.A., and Wood, C. (2014). "Soil Profile Characterization of Christchurch Strong Motion Stations," *Proc. 10th National Conf. on Earthquake Engineering* (10NCEE), Anchorage, AK, 21-25 July.

Wotherspoon, L.M., Orense, R.P., Bradley, B.A., Cox, B.R., Wood, C.M., and Green, R.A. (2015a). "Soil Profile Characterization of Christchurch Central Business District Strong

Motion Stations," *Bulletin of the New Zealand Society for Earthquake Engineering*, 48(3), 147-157.

Wotherspoon, L., Orense, R., Bradley, B., Cox, B., Wood, C., and Green, R.A. (2015b). "Geotechnical Characterisation of Christchurch Strong Motion Stations," Version 3, Earthquake Commission Report (Project No. 12/629), Earthquake Commission (EQC), Wellington, New Zealand.

Yoshimi, Y., Tokimatsu, K., Kaneko, O., and Makihara, Y. (1984). "Undrained cyclic shear strength of a dense Niigata sand." *Soils and Foundations*, 24(4), 131–145.

Youd, T.L., Idriss, I.M., Andrus, R.D., Arango, I., Castro, G., Christian, J.T., Dobry, R., Finn, W.D.L., Harder, L.F., Hynes, M.E., Ishihara, K., Koester, J.P., Liao, S.S.C., Marcuson III, W.F., Martin, G.R., Mitchell, J.K., Moriwaki, Y., Power, M.S., Robertson, P.K., Seed, R.B., and Stokoe II, K.H. (2001). "Liquefaction Resistance of Soils: Summary Report from the 1996 NCEER and 1998 NCEER/NSF Workshops on Evaluation of Liquefaction Resistance of Soils." *Journal of Geotechnical and Geoenvironmental Engineering*, 127(10), 817–833.

Chapter 3. Thesis Conclusions

3.1 Summary

The objective of this thesis was to use the combination of well-documented liquefaction response during the 2010 Darfield and 2011 Christchurch, New Zealand, earthquakes, densely-recorded ground motions for the events, and detailed subsurface characterization to investigate the significance of spatial variation of MSF on liquefaction triggering. MSF were calculated using two established methods for computing the n_{eqM}; the Seed et al. (1975) and Green and Terri (2005) procedures. The procedure of using the n_{eqM} to calculate MSF is significant because it allows MSF to be computed for specific motions and thus, inherently yielding MSF that are site- and source-dependent. Conversely, traditional methods of computing MSF are correlated solely to M_w and do not explicitly account for spatial variability of ground motion duration. The corollary to this is that using MSF from conventional approaches, which are site- and source-independent may result in discrepancies between predicted versus observed liquefaction. To elucidate the significance of spatial variability, a series of scenario-based site response analyses were performed to compute MSF from n_{eqM} at 15 SMS sites located across Christchurch and its suburbs for both the Darfield and Christchurch earthquake faulting scenarios. The following section highlights the key findings from this work.

3.2 Key Findings

Examination of the results from the scenario-based site response analyses modeled after the 2010 Darfield and 2011 Christchurch earthquakes produced the following key findings:

- Green and Terri (2005) n_{eqM} approach produced slightly lower values of MSF than the Seed et al. 1975 approach.

- MSF varied spatially across Christchurch for both faulting scenarios, more so for the M_w 6.2 Christchurch earthquake (Darfield range = 0.4, Christchurch range = 0.6, where range = MSF_{MAX} –MSF_{MIN}). Trends in the spatial variation of MSF were similar for both n_{eqM} approaches.

- There was no consistent trend between the contours of MSF and the observed liquefaction for either earthquake.

- A general correlation between a_{max} and MSF was observed, where areas with larger a_{max} (higher amplitude) generally had higher MSF (shorter duration). This correlation was more pronounced for the Christchurch earthquake.

3.3 Recommendations for Future Work

Based on this study, the spatial variation of the MSF is deemed significant enough that it could result in discrepancies between predicted versus observed liquefaction and thus warrants further work. Recommendations for extended research include:

- Extend the scope of this study to include the effects of multi-directional shaking.

- Explore other site response analysis approaches (i.e., other than equivalent linear analyses) that better capture soil non-linearity due to large amplitude shaking.

- Investigate the effects of other extreme scenarios (e.g., reverse directivity) on MSF.

- Examine trends in MSF as a function of site-to-source distance and also site stiffness.

- Develop a framework to incorporate spatially variable MSF in future variants of simplified liquefaction evaluation procedures.

Appendix A: Site Response Soil Profiles for the Christchurch SMS Sites

Profiles of soil layering and shear wave velocity for each SMS are presented in Appendix A. The data obtained from Wotherspoon et al. (2014, 2015a,b) was used to generate these profiles which were ultimately used to form the basis of site response analyses.

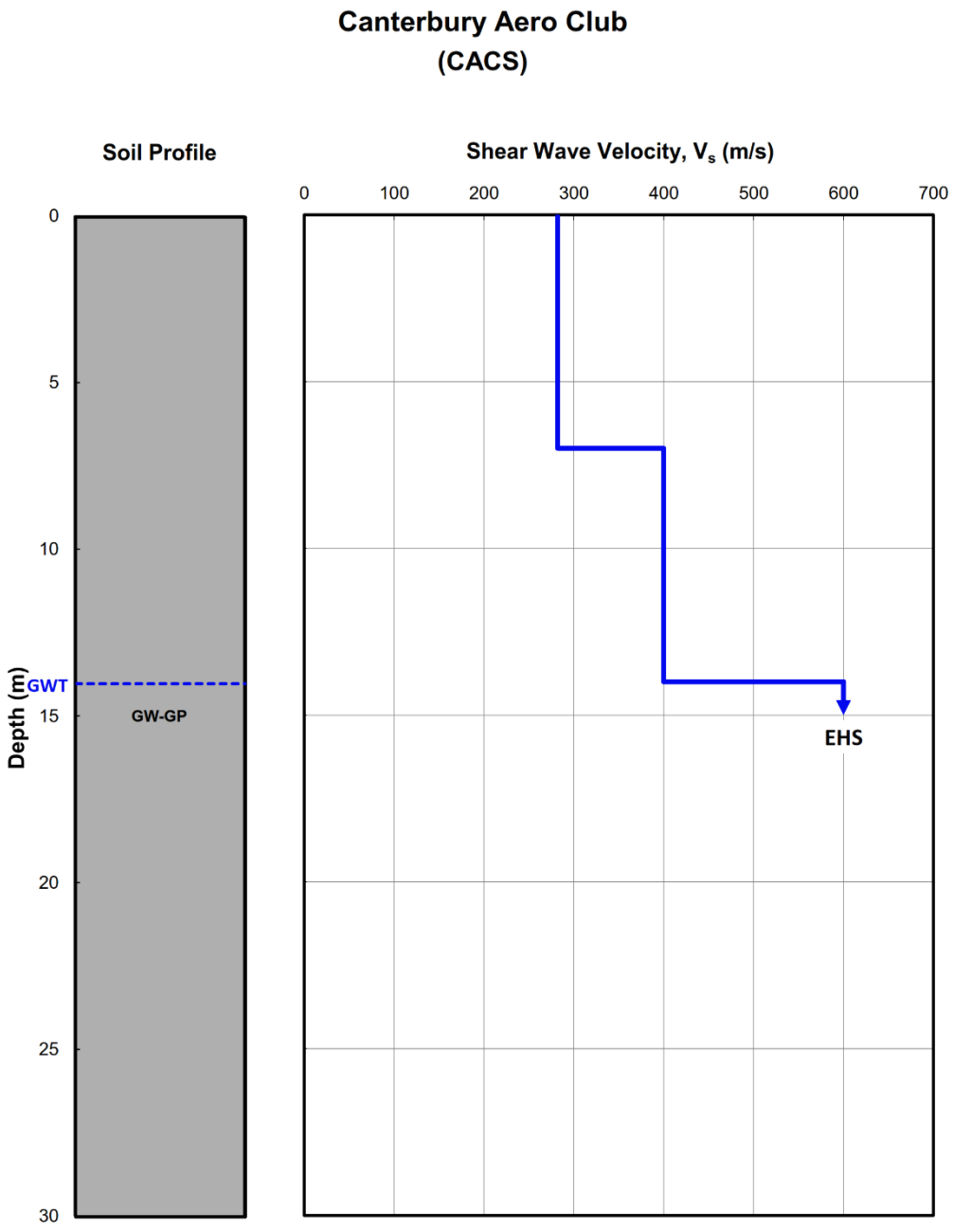

Figure A.1 Canterbury Aero Club (CACS) SMS soil profile and shear wave velocity profile

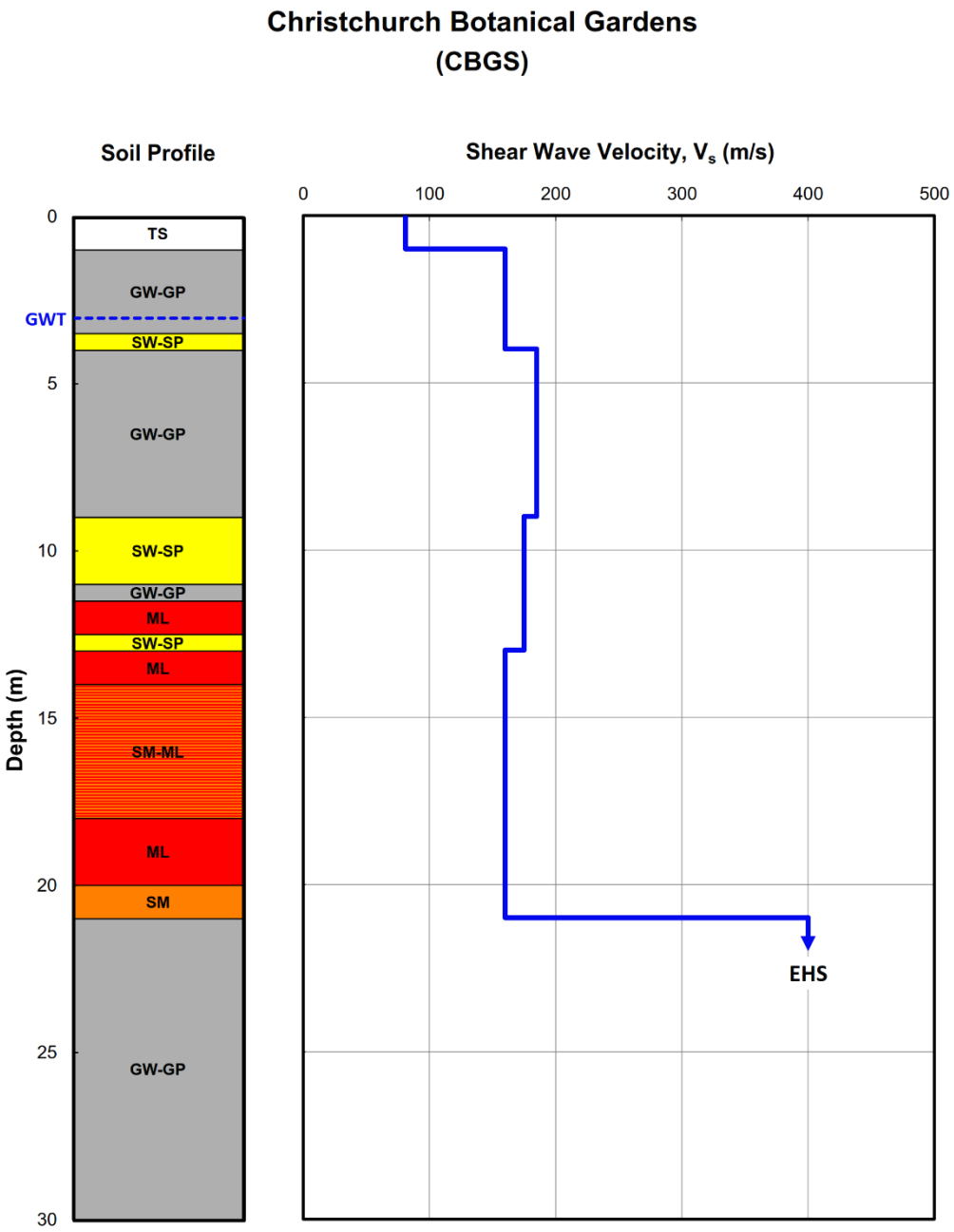

Figure A.2 Christchurch Botanical Gardens (CBGS) SMS soil profile and shear wave velocity profile

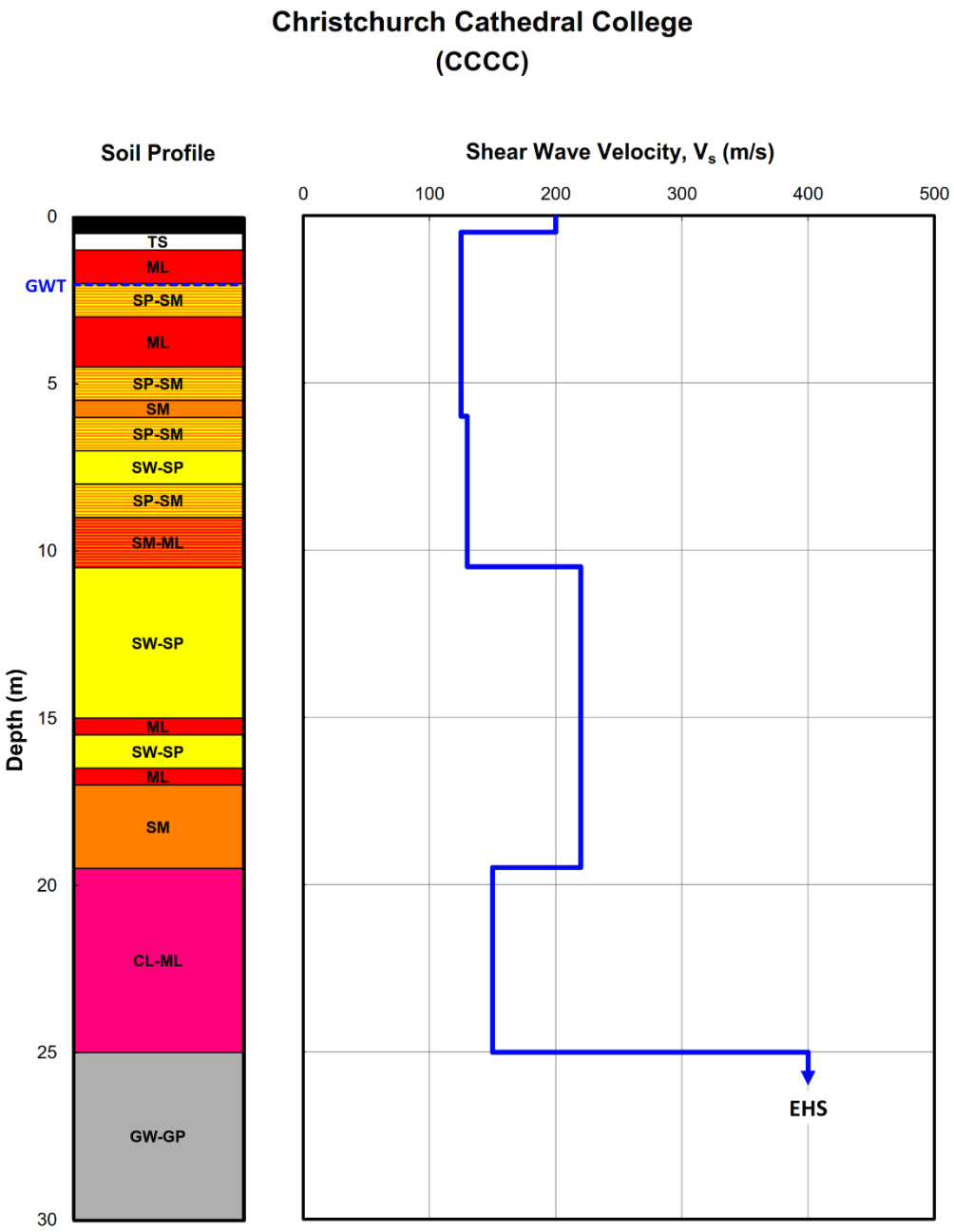

Figure A.3 Christchurch Cathedral College (CCCC) SMS soil profile and shear wave velocity profile

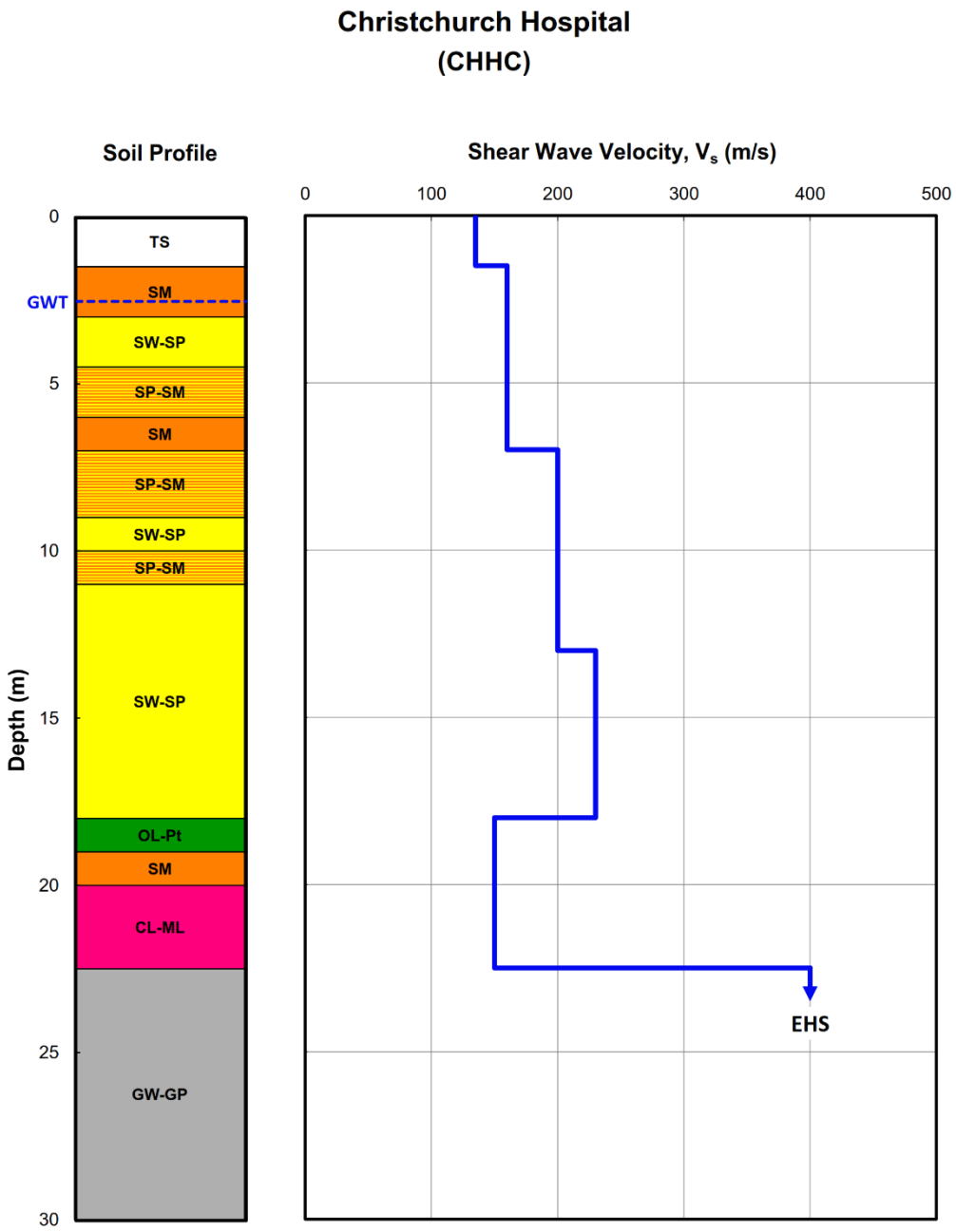

Figure A.4 Christchurch Hospital (CHHC) SMS soil profile and shear wave velocity profile

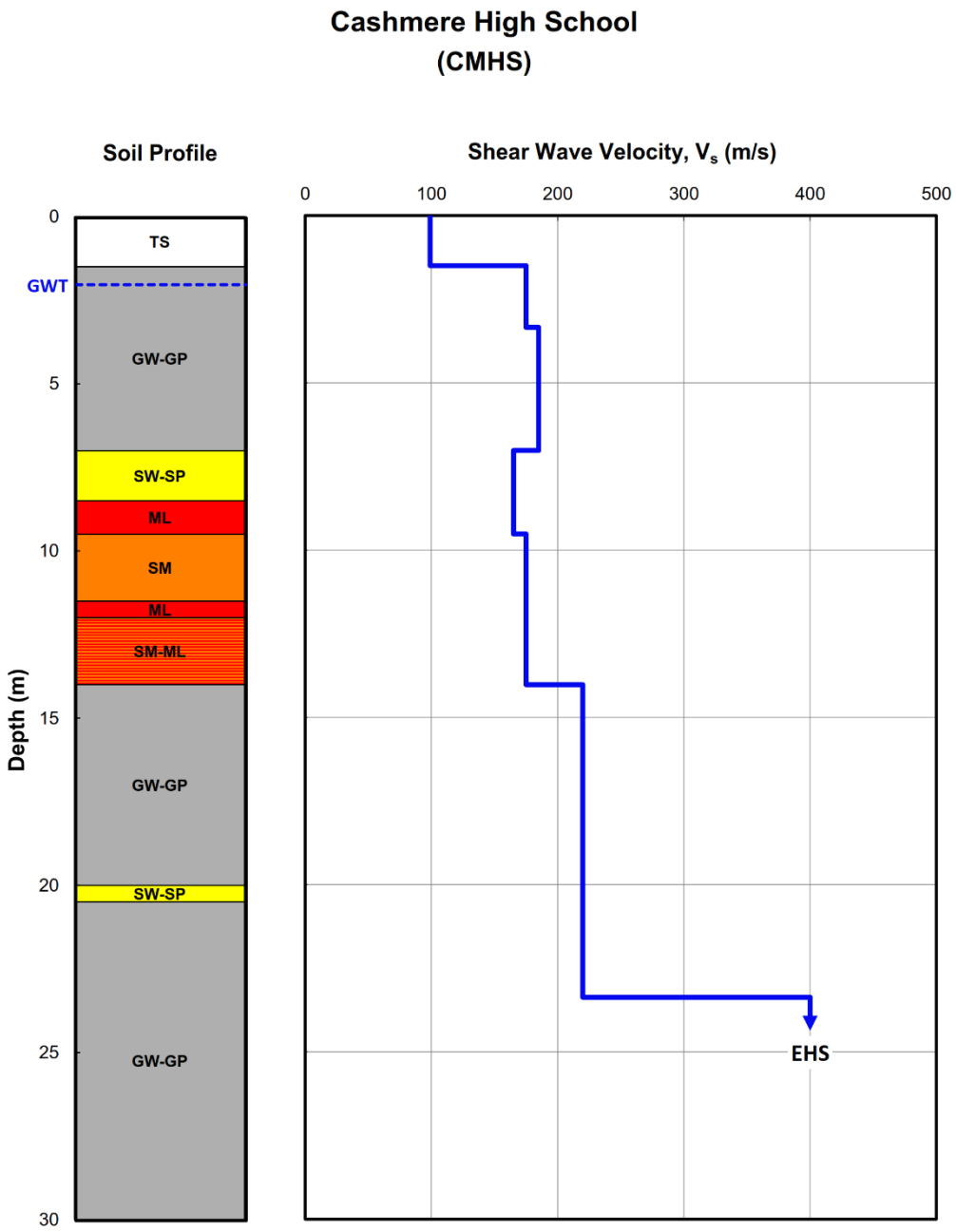

Figure A.5 Cashmere High School (CMHS) SMS soil profile and shear wave velocity profile

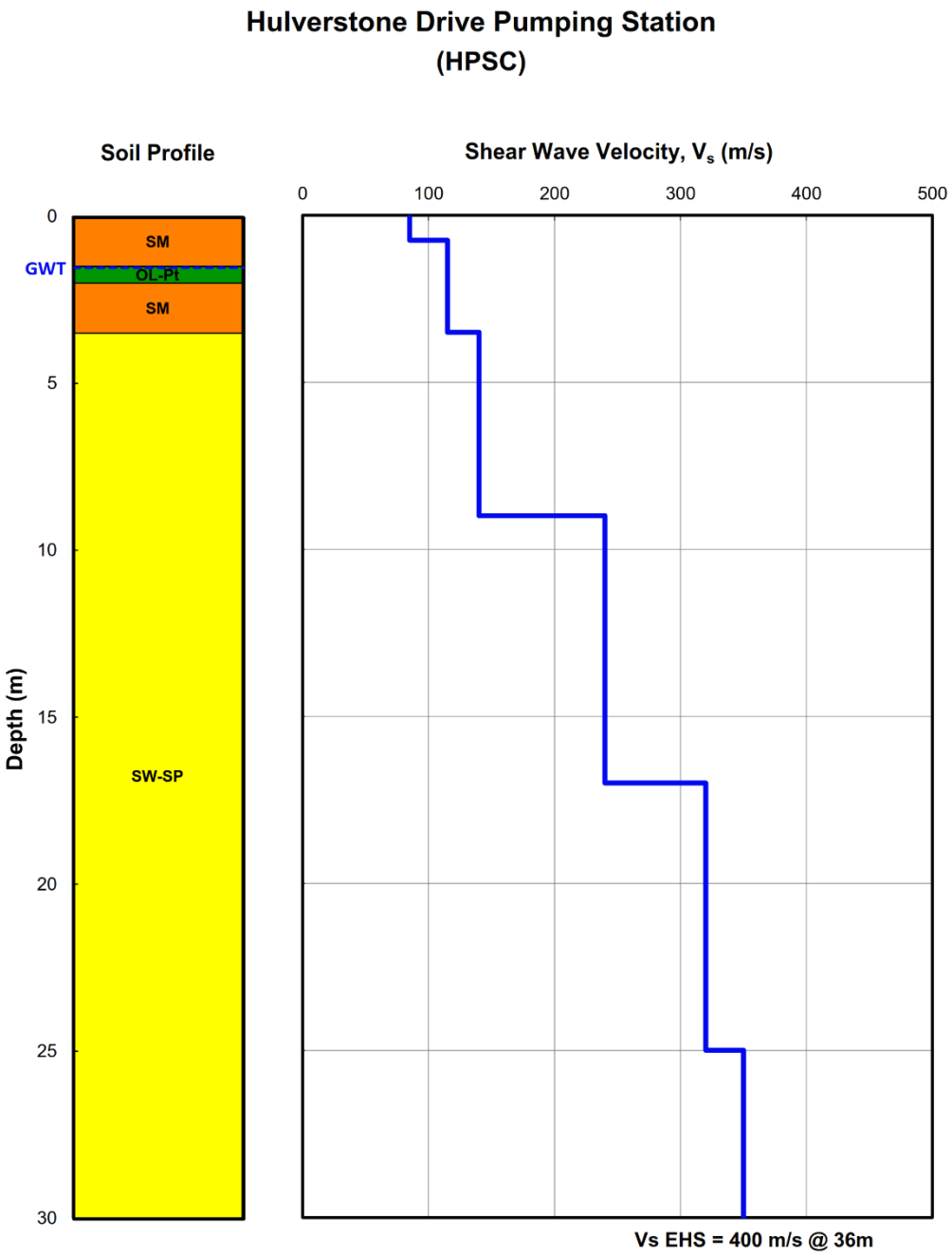

Figure A.6 Hulverstone Drive Pumping Station (HPSC) SMS soil profile and shear wave velocity profile

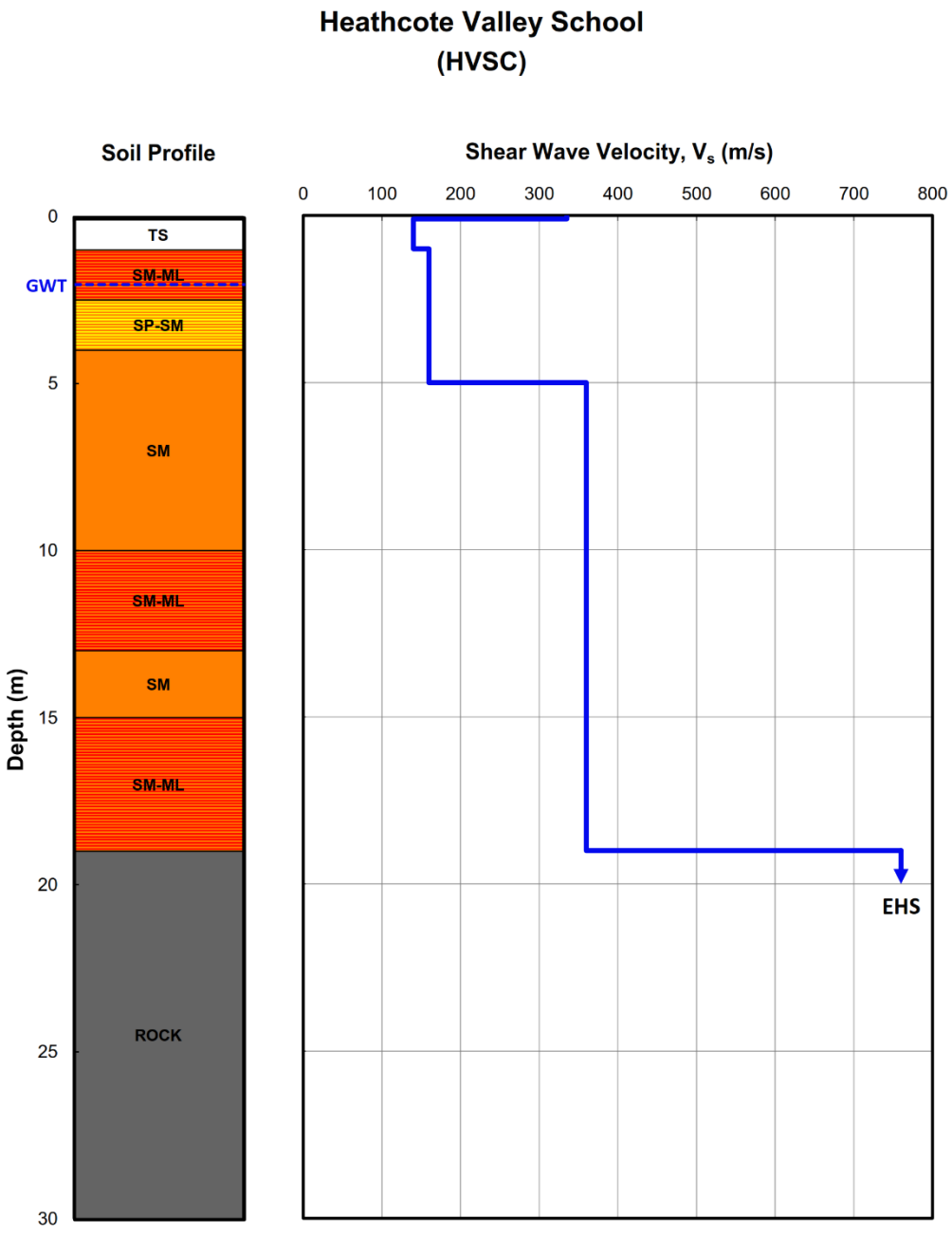

Figure A.7 Heathcote Valley School (HVSC) SMS soil profile and shear wave velocity profile

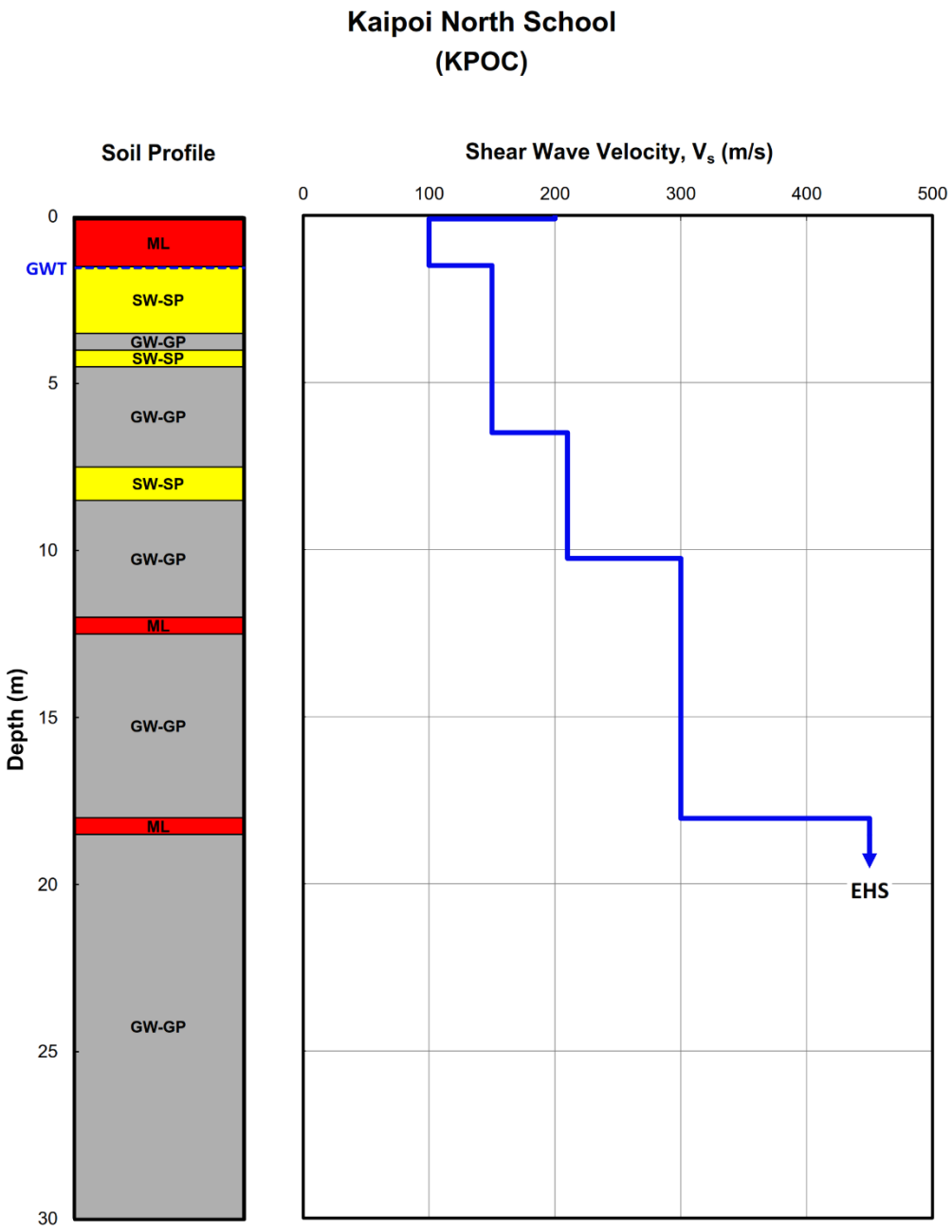

Figure A.8 Kaipoi North School (KPOC) SMS soil profile and shear wave velocity profile

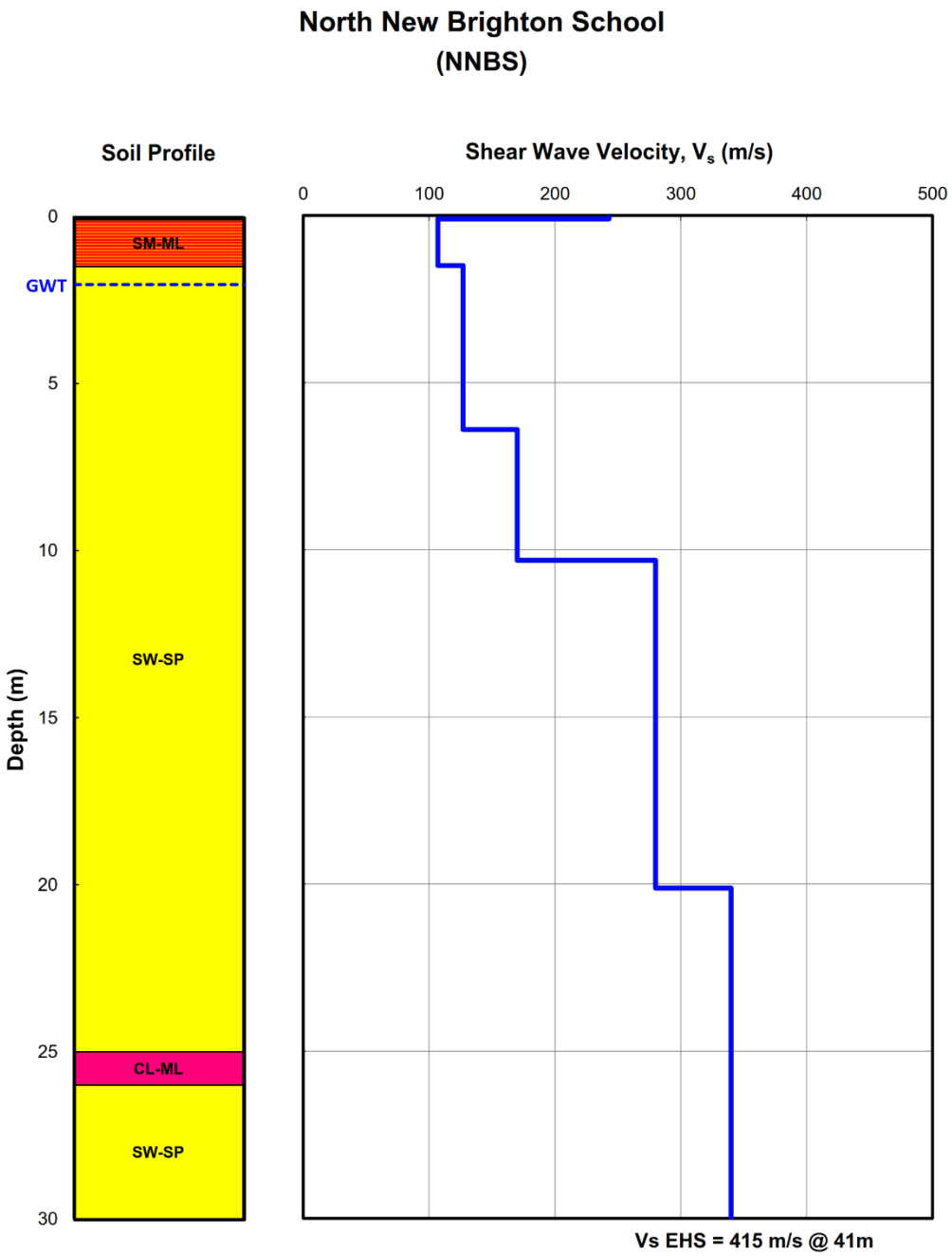

Figure A.9 North New Brighton School (NNBS) SMS soil profile and shear wave velocity profile

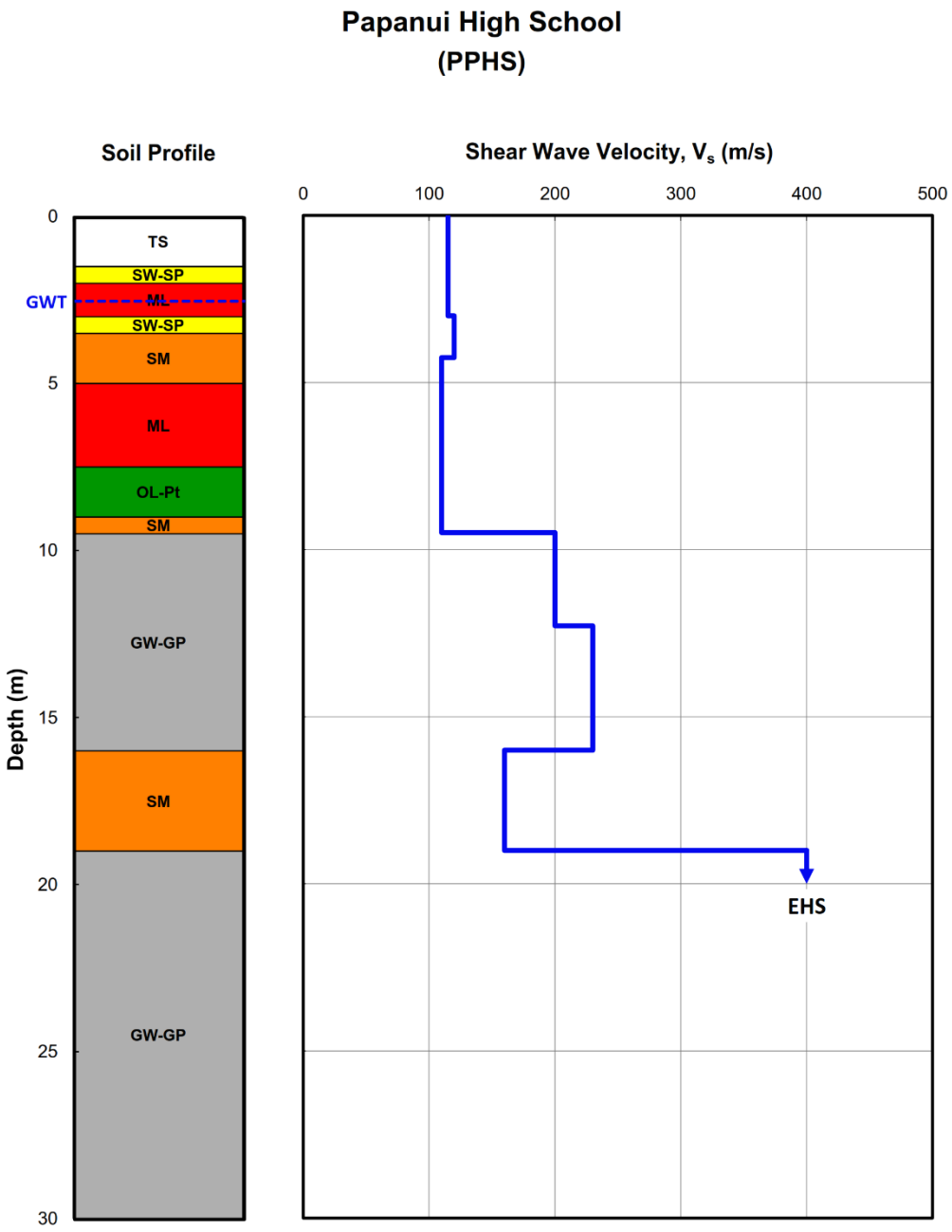

Figure A.10 Papanui High School (PPHS) SMS soil profile and shear wave velocity profile

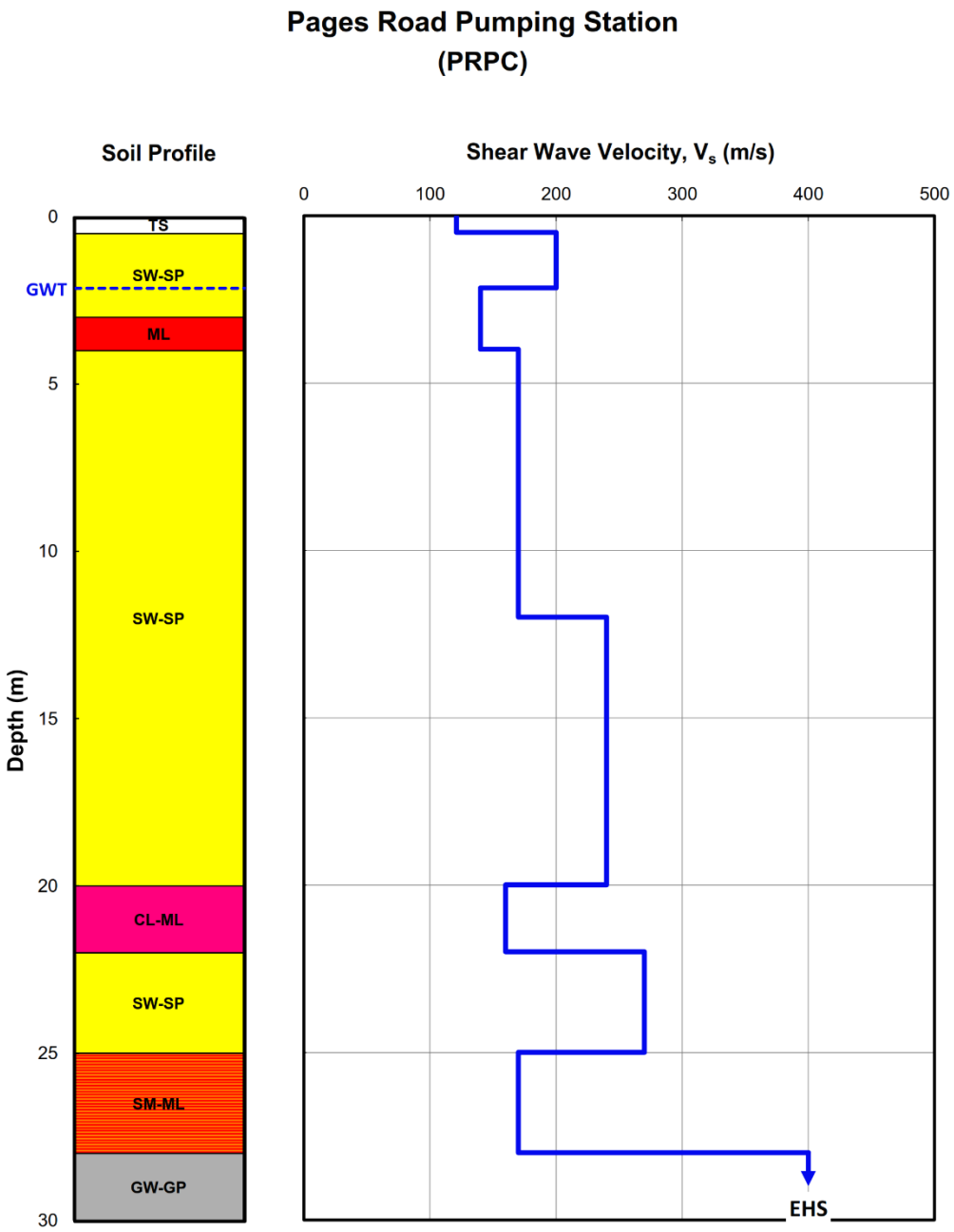

Figure A.11 Pages Road Pumping Station (PRPC) SMS soil profile and shear wave velocity profile

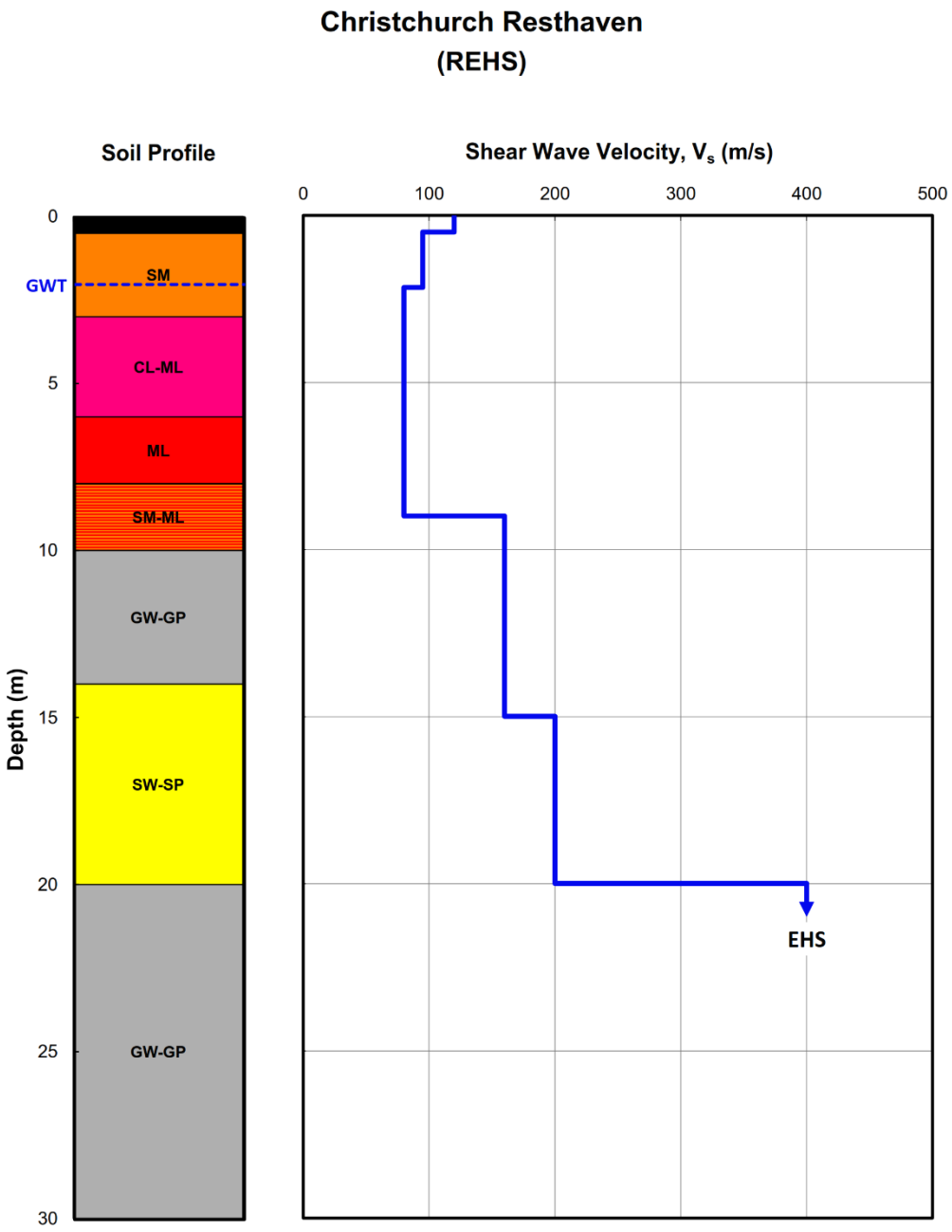

Figure A.12 Christchurch Resthaven (REHS) SMS soil profile and shear wave velocity profile

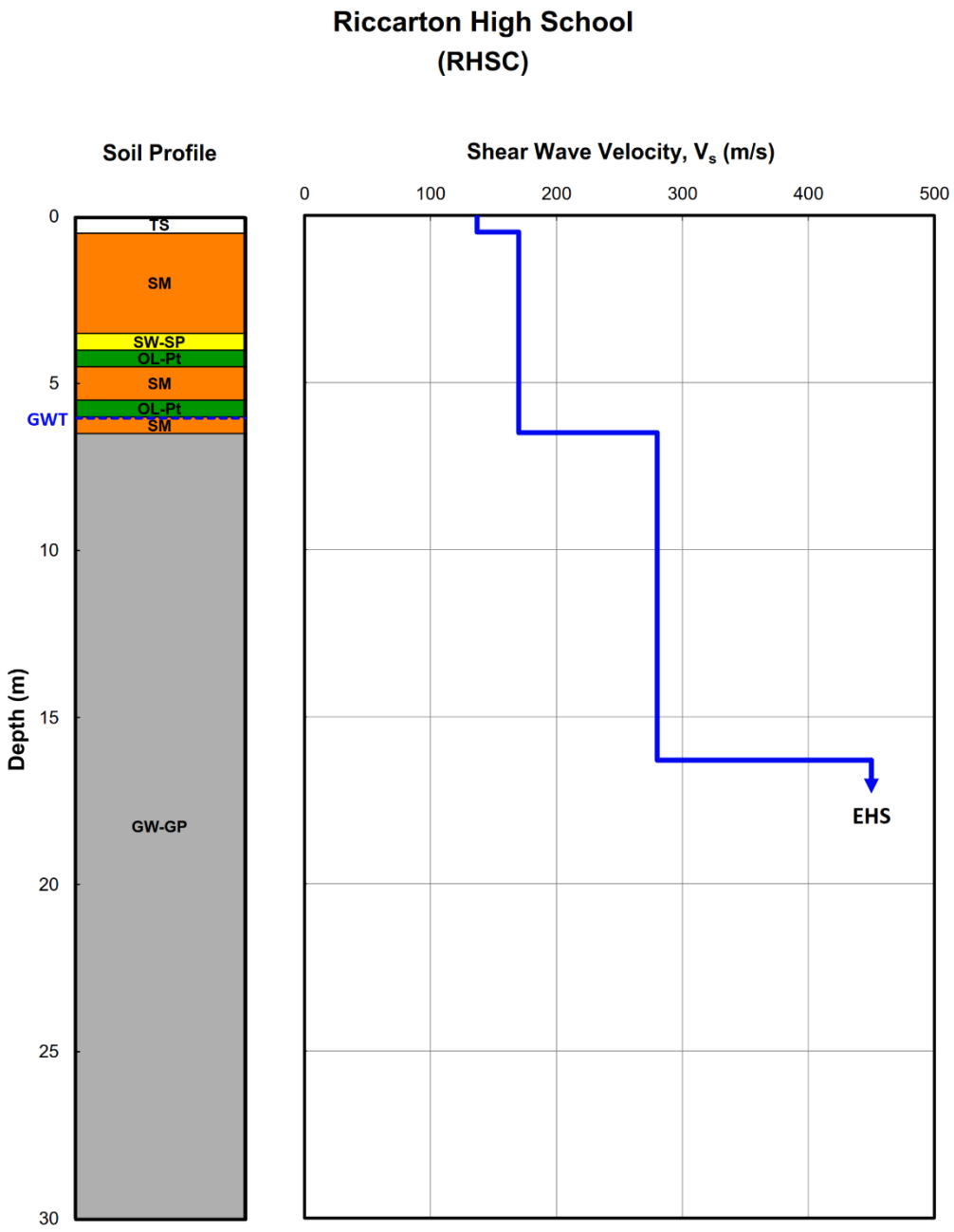

Figure A.13 Riccarton High School (RHSC) SMS soil profile and shear wave velocity profile

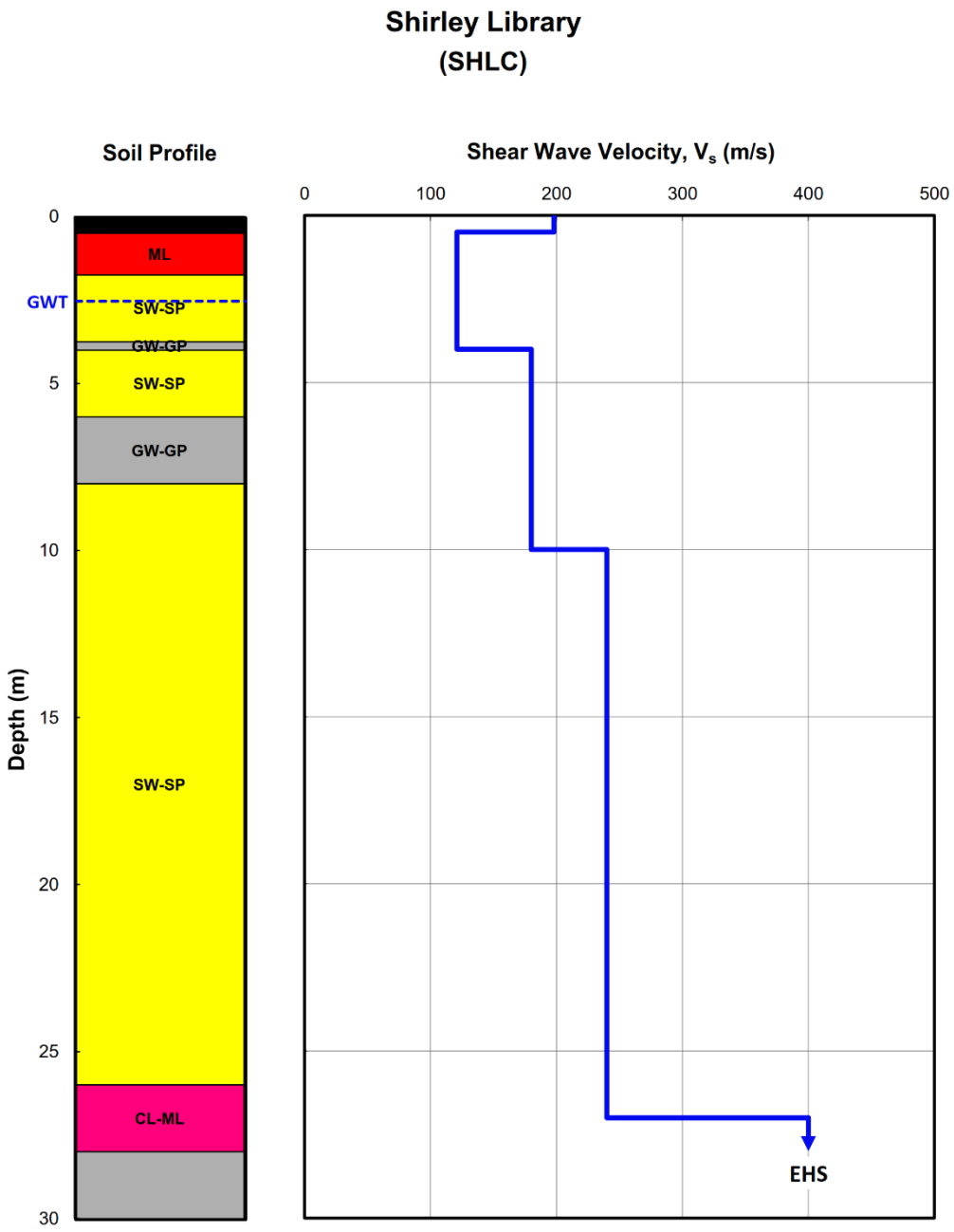

Figure A.14 Shirley Library (SHLC) SMS soil profile and shear wave velocity profile

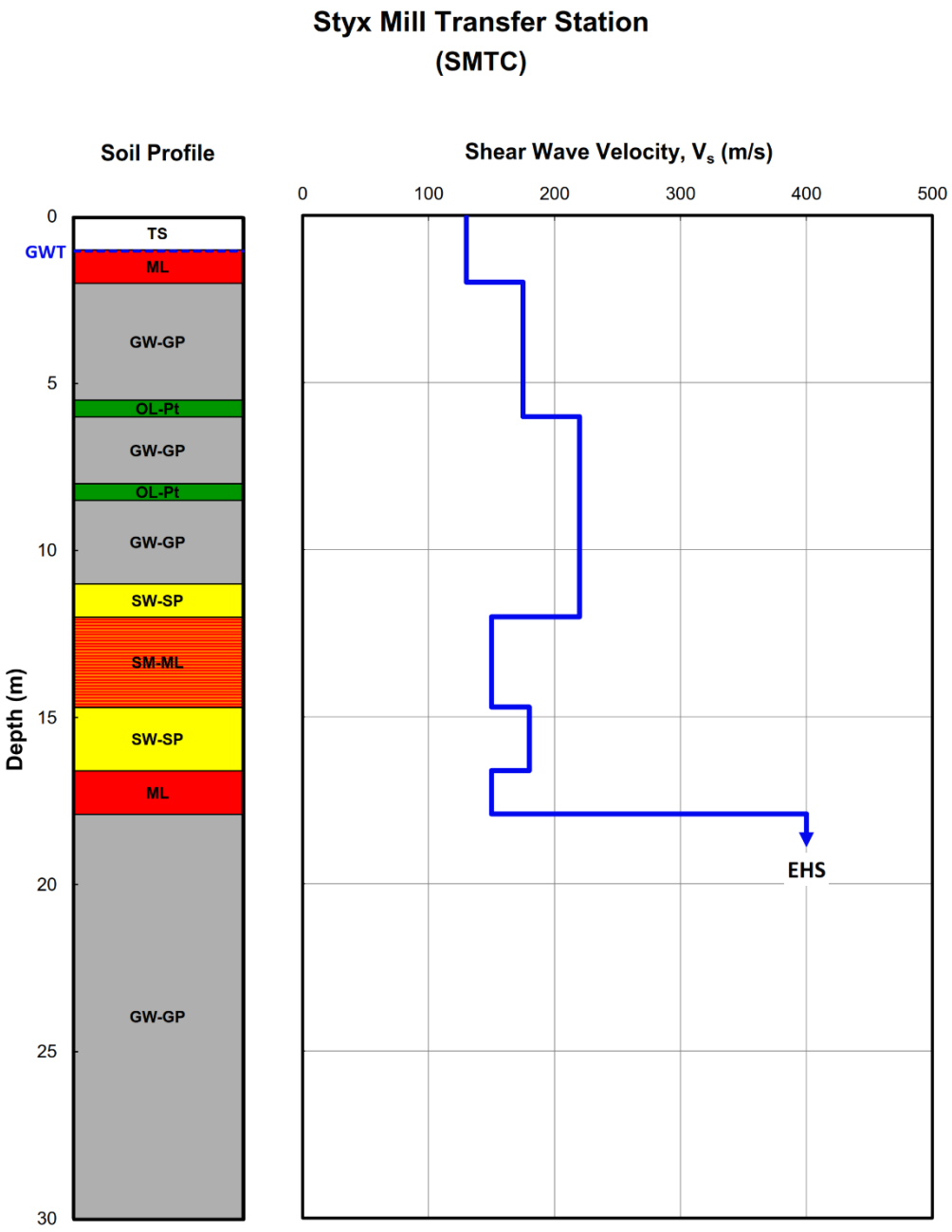

Figure A.15 Styx Mill Transfer Station (SMTC) SMS soil profile and shear wave velocity profile

Appendix B: Ground Motion Selection for the Darfield and Christchurch Rupture Scenarios

Appendix B provides tables and figures showing the inputs and results of the ground motion selection process for the 30 different rupture scenarios (15 SMS sites x 2 earthquakes) examined in this study. 15 sets of horizontal motions were selected for each SMS-earthquake scenario using the generalized conditional intensity measure (GCIM) approach (Bradley 2010a, 2012d). The figures demonstrate the relative fit of the selected motions in relation to the target distributions of intensity measures. The tables document the ground motions selected for each of the different scenarios.

Table B.1 Fault Properties used within the framework of the GCIM methodology for the 2010 Darfield and 2011 Christchurch, NZ earthquakes.

Earthquake Event	M_w	Fault style	Strike	Rake	Dip	Hypocenter Depth (km)
Darfield	7.1	Strike-Slip	85	0	82	10
Christchurch	6.25	Reverse	59	146	69	4

Table B.2 Site Properties used within the framework of the GCIM methodology for the 15 SMS for both the 2010 Darfield and 2011 Christchurch, NZ earthquakes

SMS Code	V_{30}* (m/s)	$Z_{1.0}$ (m)	Sep 4, 2010 - Darfield				Feb 22, 2011 - Christchurch			
			R_{epi} (km)	R_{hyp} (km)	R_{jb} (km)	R_{rup} (km)	R_{epi} (km)	R_{hyp} (km)	R_{jb} (km)	R_{rup} (km)
CACS	600	500	29.0	30.7	9.8	11.9	18.0	18.4	12.9	12.9
CBGS	400	500	36.0	37.4	13.9	14.4	9.0	9.8	4.7	4.8
CCCC	400	500	38.0	39.3	16.0	16.3	6.0	7.2	2.7	2.9
CHHC	400	500	36.0	37.4	14.5	14.8	8.0	8.9	3.8	3.9
CMHS	400	500	36.0	37.4	14.0	14	6.0	7.2	1.1	1.5
HPSC	400	500	43.0	44.1	21.1	21.7	9.0	9.8	3.9	4.1
HVSC	760	500	43.0	44.1	20.8	20.8	1.0	4.1	1.3	3.9
KPOC	450	500	44.0	45.1	25.9	27.7	23.0	23.3	17.5	17.5
NNBS	415	500	44.0	45.1	22.5	23.2	11.0	11.7	3.9	4
PPHS	400	500	35.0	36.4	14.2	15.4	12.0	12.6	8.7	8.8
PRPC	400	500	41.0	42.2	19.0	19.4	6.0	7.2	2.4	2.6
REHS	400	500	37.0	38.3	15.3	15.9	8.0	8.9	4.8	4.9
RHSC	450	500	31.0	32.6	9.4	10	12.0	12.6	6.6	6.6
SHLC	400	500	39.0	40.3	17.9	18.7	9.0	9.8	5.2	5.3
SMTC	400	500	36.0	37.4	16.1	17.6	14.0	14.6	10.9	10.9

*The listed Vs are for the elastic halfspace assumed in the equivalent linear site response analyses, which corresponded to the Riccarton Gravel Formation of all sites except HVSC, where the listed value is for the Banks Peninsula volcanic rock.

Table B.3 Observed pulse period from Joshi (2013) used with the Shahi & Baker (2011) Narrowband Model to account for the forward directivity pulse in the GMPEs

SMS Code	Pulse Period (s)	
	Darfield	Christchurch
CACS	8.3	3.1
CBGS	5.7	3.6
CCCC	3.5	1.6
CHHC	3.7	3.3
CMHS	3	1.7
HPSC	3.8	N/A
HVSC	4.3	0.5
KPOC	N/A	N/A
NNBS	5.4	N/A
PPHS	3.8	3.8
PRPC	3.8	4.6
REHS	4.2	1.4
RHSC	7.1	3.7
SHLC	7.2	1.2
SMTC	8.4	2.9

**Target distributions computed via the GCIM process were modified using the Shahi & Baker 2011 narrowband model for the scenarios where a forward directivity pulse was identified.

Canterbury Aero Club

(CACS)

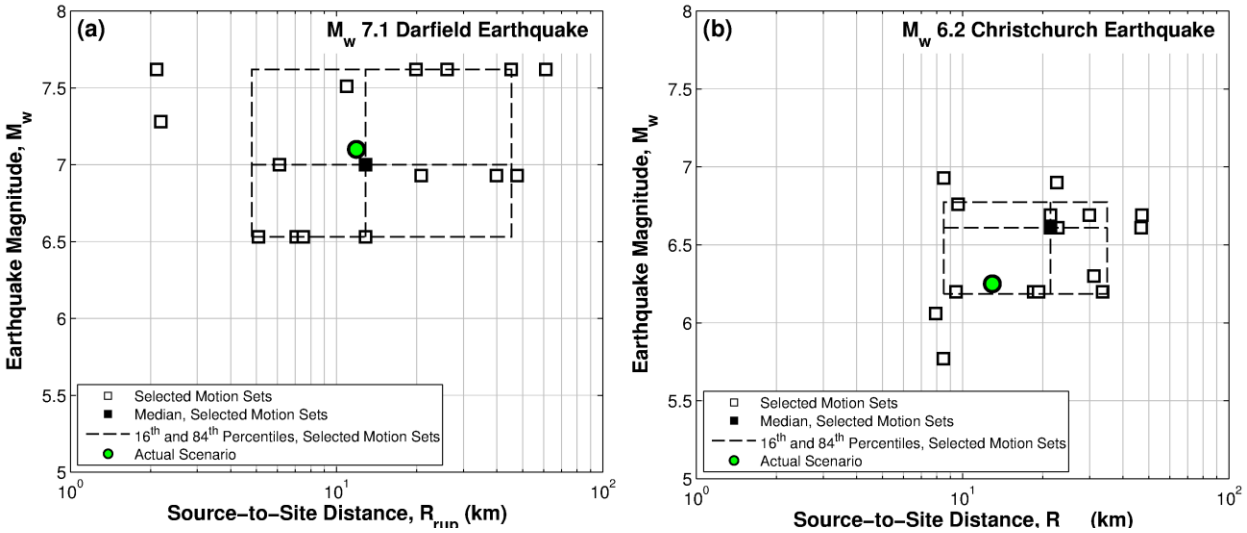

Figure B.1 Distributions of causal parameters, M_w and R_{rup}, for the selected motion sets for both the: (a) Darfield earthquake, and (b) Christchurch earthquake scenarios at the CACS SMS site.

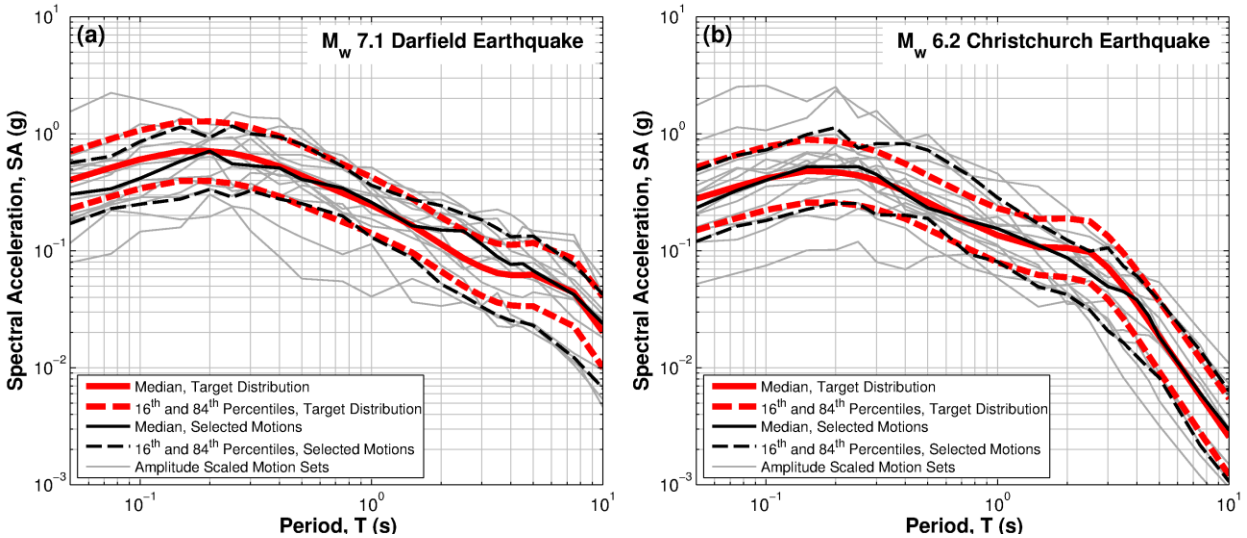

Figure B.2 5% damped response spectra of the target motions and selected motion for the CACS SMS site for the: (a) Darfield earthquake, and (b) Christchurch earthquake.

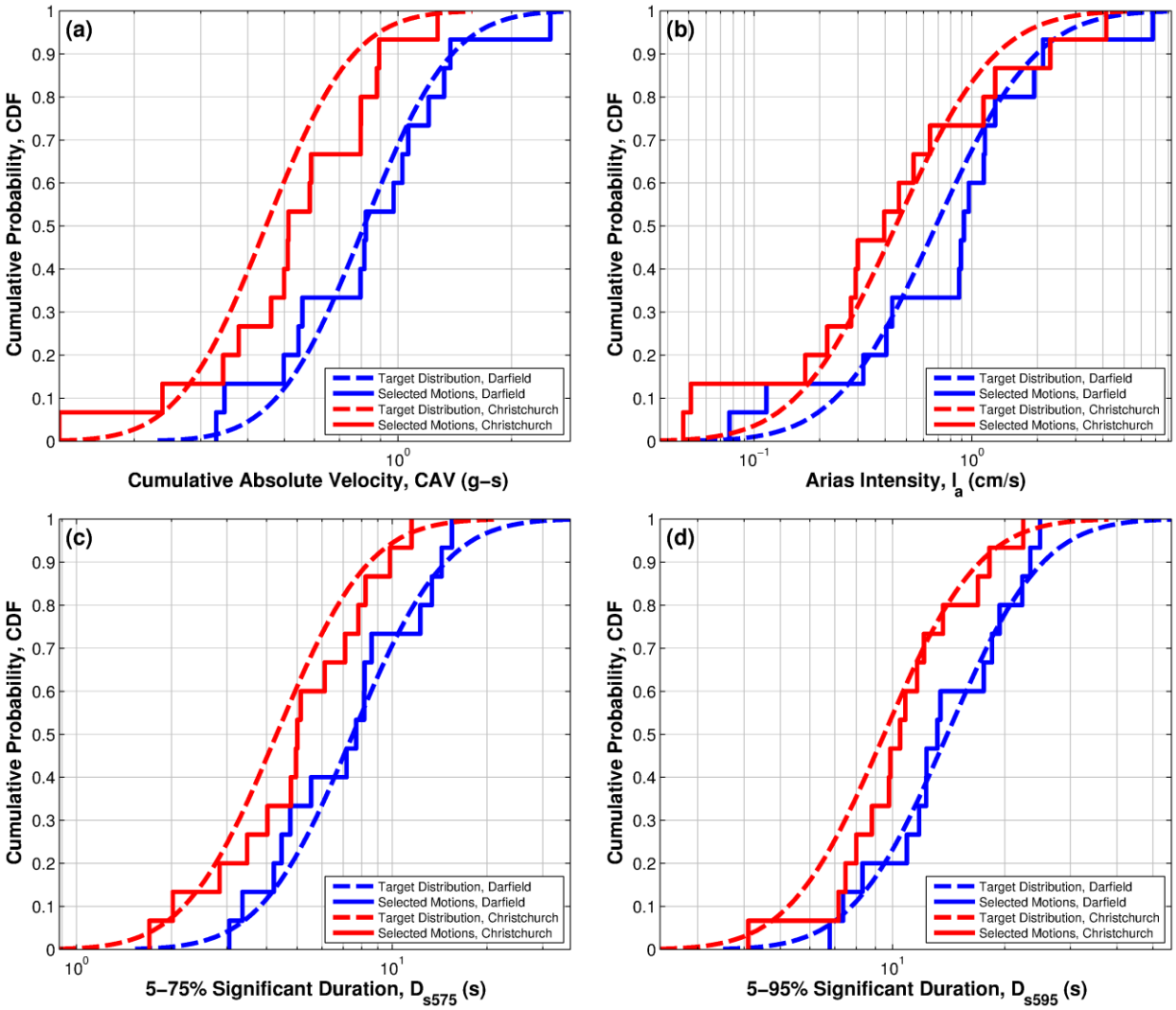

Figure B.3 Cumulative distributions of the target and selected motions for the CACS SMS site for both the Darfield and Christchurch earthquakes: (a) CAV; (b) I_a; (c) D_{s575} ; and (d) D_{s595}.

Table B.4 Selected ground motion sets for the CACS SMS site for the Darfield earthquake

NGA No.	Event	M_w	R_{rup} (km)	V_{s30} (m/s)	Pulselike?	Scale Factor
1161	Kocaeli, Turkey	7.51	10.9	792.0	Yes	1.342
1347	Chi-Chi, Taiwan	7.62	61.1	996.5	No	1.586
1482	Chi-Chi, Taiwan	7.62	19.9	540.7	Yes	1.248
1485	Chi-Chi, Taiwan	7.62	26.0	704.6	Yes	1.639
1524	Chi-Chi, Taiwan	7.62	45.2	446.6	Yes	0.537
1528	Chi-Chi, Taiwan	7.62	2.1	389.4	Yes	0.813
178	Imperial Valley-06	6.53	12.9	162.9	Yes	0.692
179	Imperial Valley-06	6.53	7.1	208.9	Yes	0.790
184	Imperial Valley-06	6.53	5.1	202.3	Yes	0.803
185	Imperial Valley-06	6.53	7.5	202.9	Yes	0.716
6975	Darfield, New Zealand	7	6.1	249.3	Yes	0.500
754	Loma Prieta	6.93	20.8	295.0	No	1.148
761	Loma Prieta	6.93	39.9	284.8	No	2.000
807	Loma Prieta	6.93	47.6	400.6	No	2.000
879	Landers	7.28	2.2	1369.0	Yes	0.700

Table B.5 Selected ground motion sets for the CACS SMS site for the Christchurch earthquake

NGA No.	Event	M_w	R_{rup} (km)	V_{s30} (m/s)	Pulselike?	Scale Factor
1020	Northridge-01	6.69	21.4	602.1	No	1.595
2655	Chi-Chi, Taiwan-03	6.2	19.3	475.5	No	1.078
288	Irpinia, Italy-01	6.9	22.6	561.0	No	1.968
2897	Chi-Chi, Taiwan-04	6.2	33.6	652.9	No	1.416
3264	Chi-Chi, Taiwan-06	6.3	31.1	427.7	No	1.156
407	Coalinga-05	5.77	8.5	398.5	No	0.574
495	Nahanni, Canada	6.76	9.6	605.0	No	0.746
514	N. Palm Springs	6.06	7.9	376.9	No	0.816
65	San Fernando	6.61	46.8	308.4	No	2.000
68	San Fernando	6.61	22.8	316.5	No	0.895
802	Loma Prieta	6.93	8.5	380.9	Yes	0.534
8102	Christchurch, New Zealand	6.2	18.5	263.2	No	1.091
8124	Christchurch, New Zealand	6.2	9.4	293.0	No	1.010
964	Northridge-01	6.69	47.0	266.9	No	2.000
985	Northridge-01	6.69	29.9	297.1	No	0.722

Christchurch Botanical Gardens

(CBGS)

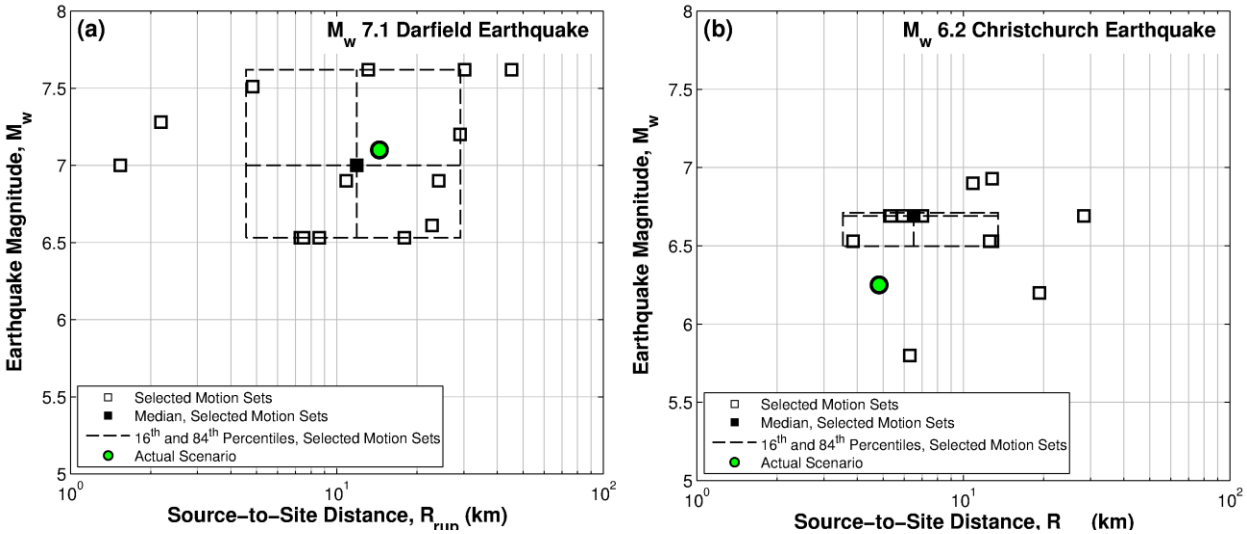

Figure B.4 Distributions of causal parameters, M_w and R_{rup}, for the selected motion sets for both the: (a) Darfield earthquake, and (b) Christchurch earthquake scenarios at the CBGS SMS site.

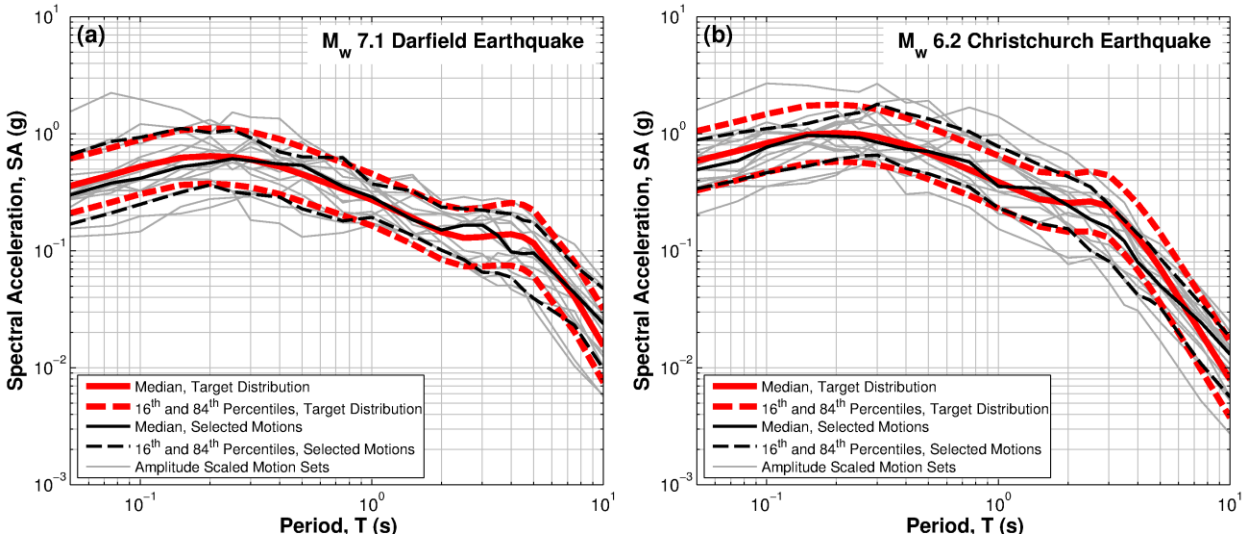

Figure B.5 5% damped response spectra of the target motions and selected motion for the CBGS SMS site for the: (a) Darfield earthquake, and (b) Christchurch earthquake.

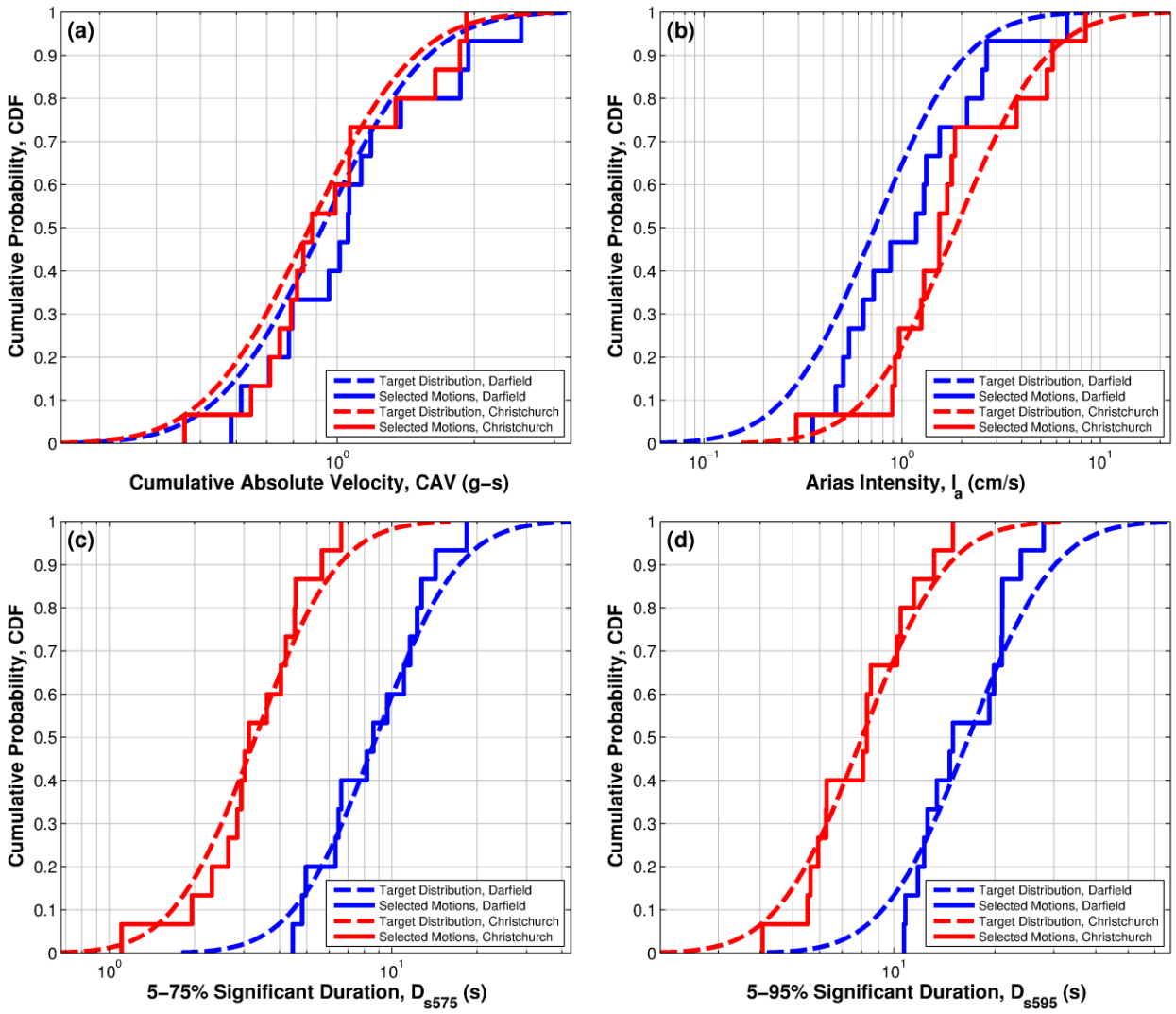

Figure B.6 Cumulative distributions of the target and selected motions for the CBGS SMS site for both the Darfield and Christchurch earthquakes: (a) CAV; (b) I_a; (c) D_{s575} ; and (d) D_{s595}.

Table B.6 Selected ground motion sets for the CBGS SMS site for the Darfield earthquake

NGA No.	Event	M_w	R_{rup} (km)	V_{s30} (m/s)	Pulselike?	Scale Factor
1176	Kocaeli, Turkey	7.51	4.8	297.0	Yes	0.810
1477	Chi-Chi, Taiwan	7.62	30.2	489.2	Yes	0.735
1524	Chi-Chi, Taiwan	7.62	45.2	446.6	Yes	0.873
1548	Chi-Chi, Taiwan	7.62	13.1	599.6	Yes	0.715
165	Imperial Valley-06	6.53	7.3	242.1	No	1.063
173	Imperial Valley-06	6.53	8.6	202.9	Yes	1.719
175	Imperial Valley-06	6.53	17.9	196.9	No	2.000
185	Imperial Valley-06	6.53	7.5	202.9	Yes	1.118
292	Irpinia, Italy-01	6.9	10.8	382.0	Yes	1.320
5810	Iwate	6.9	24.1	655.5	Yes	1.895
5836	El Mayor-Cucapah	7.2	29.0	264.6	No	0.735
6893	Darfield, New Zealand	7	11.9	344.0	No	0.827
68	San Fernando	6.61	22.8	316.5	No	1.553
6962	Darfield, New Zealand	7	1.5	295.7	Yes	0.788
879	Landers	7.28	2.2	1369.0	Yes	0.500

Table B.7 Selected ground motion sets for the CBGS SMS site for the Christchurch earthquake

NGA No.	Event	M_w	R_{rup} (km)	V_{s30} (m/s)	Pulselike?	Scale Factor
1013	Northridge-01	6.69	5.9	629.0	Yes	1.632
1051	Northridge-01	6.69	7.0	2016.1	Yes	0.968
1063	Northridge-01	6.69	6.5	282.3	Yes	1.072
1084	Northridge-01	6.69	5.4	251.2	Yes	0.589
1086	Northridge-01	6.69	5.3	440.5	Yes	0.695
171	Imperial Valley-06	6.53	0.1	264.6	Yes	1.150
174	Imperial Valley-06	6.53	12.6	196.3	No	0.867
178	Imperial Valley-06	6.53	12.9	162.9	Yes	1.594
182	Imperial Valley-06	6.53	0.6	210.5	Yes	1.747
183	Imperial Valley-06	6.53	3.9	206.1	No	0.861
2655	Chi-Chi, Taiwan-03	6.2	19.3	475.5	No	1.665
292	Irpinia, Italy-01	6.9	10.8	382.0	Yes	1.679
568	San Salvador	5.8	6.3	489.3	Yes	0.707
767	Loma Prieta	6.93	12.8	349.9	Yes	0.765
987	Northridge-01	6.69	28.3	321.9	No	1.214

Christchurch Cathedral College

(CCCC)

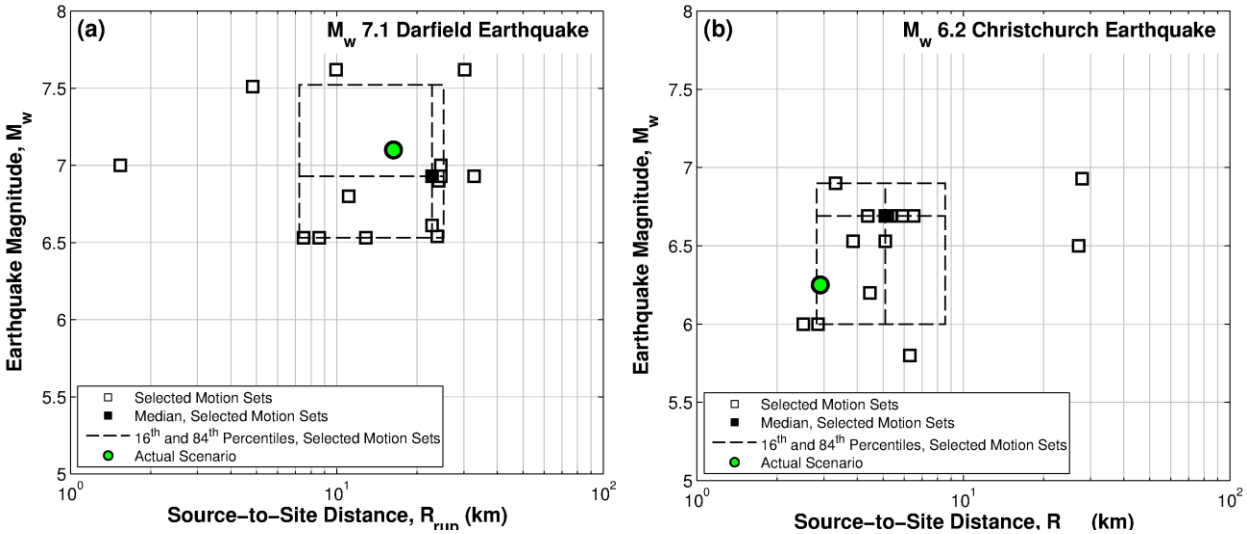

Figure B.7 Distributions of causal parameters, M_w and R_{rup}, for the selected motion sets for both the: (a) Darfield earthquake, and (b) Christchurch earthquake scenarios at the CCCC SMS site.

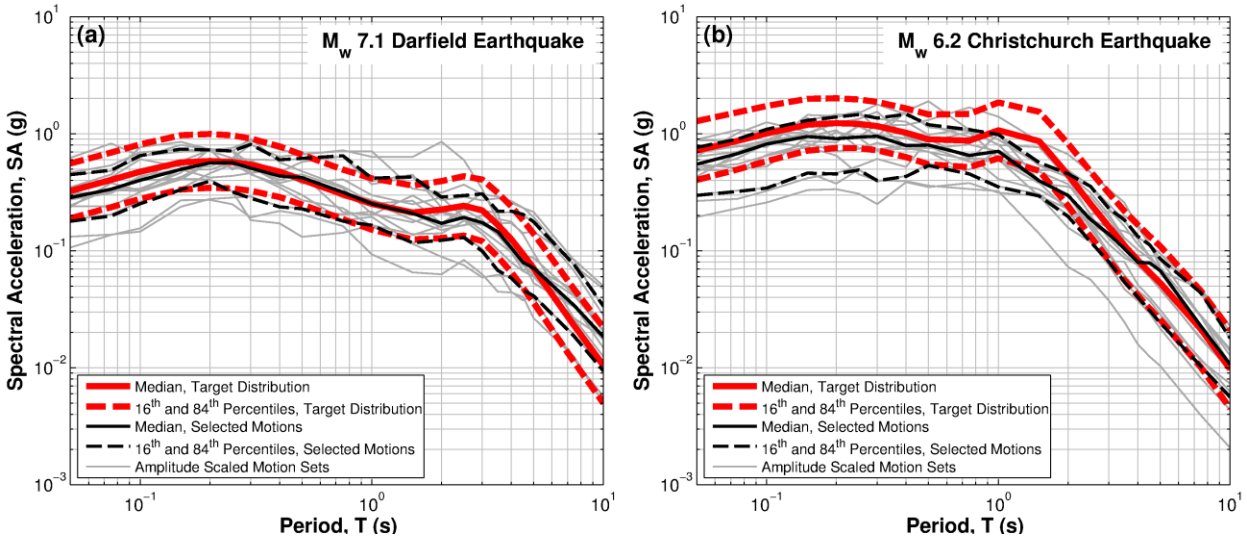

Figure B.8 5% damped response spectra of the target motions and selected motion for the CCCC SMS site for the: (a) Darfield earthquake, and (b) Christchurch earthquake.

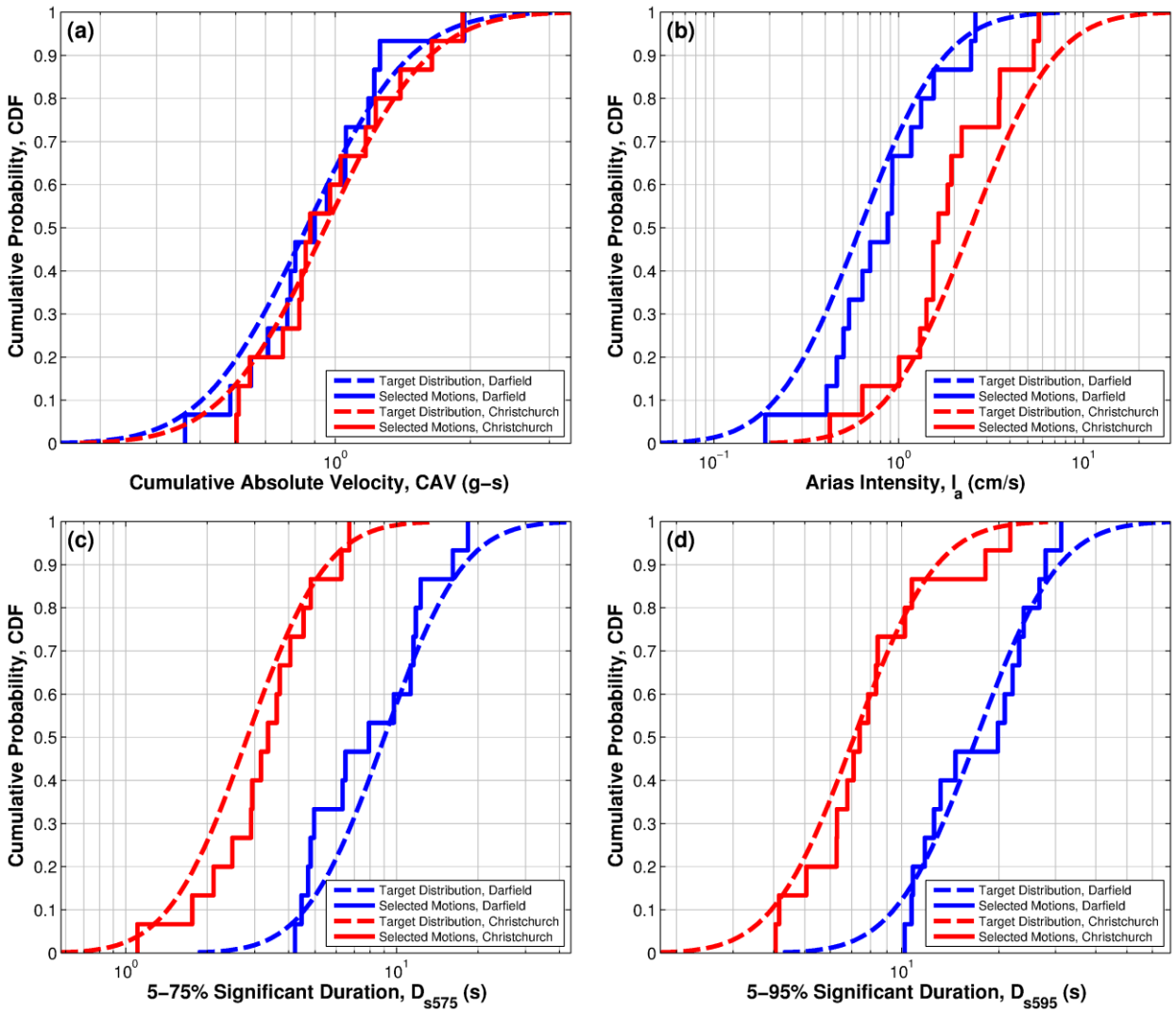

Figure B.9 Cumulative distributions of the target and selected motions for the CCCC SMS site for both the Darfield and Christchurch earthquakes: (a) CAV; (b) I_a; (c) D_{s575} ; and (d) D_{s595}.

Table B.8 Selected ground motion sets for the CCCC SMS site for the Darfield earthquake

NGA No.	Event	M_w	R_{rup} (km)	V_{s30} (m/s)	Pulselike?	Scale Factor
1176	Kocaeli, Turkey	7.51	4.8	297.0	Yes	1.208
1477	Chi-Chi, Taiwan	7.62	30.2	489.2	Yes	0.709
1595	Chi-Chi, Taiwan	7.62	9.9	258.9	Yes	0.669
173	Imperial Valley-06	6.53	8.6	202.9	Yes	1.242
178	Imperial Valley-06	6.53	12.9	162.9	Yes	0.818
185	Imperial Valley-06	6.53	7.5	202.9	Yes	0.874
4856	Chuetsu-oki	6.8	11.1	294.4	Yes	0.638
5810	Iwate	6.9	24.1	655.5	Yes	1.259
68	San Fernando	6.61	22.8	316.5	No	1.101
6953	Darfield, New Zealand	7	24.6	206.0	No	0.608
6962	Darfield, New Zealand	7	1.5	295.7	Yes	0.702
729	Superstition Hills-02	6.54	23.9	179.0	No	1.727
737	Loma Prieta	6.93	24.6	239.7	No	1.271
800	Loma Prieta	6.93	32.8	279.6	No	1.780
806	Loma Prieta	6.93	24.2	267.7	No	0.680

Table B.9 Selected ground motion sets for the CCCC SMS site for the Christchurch earthquake

NGA No.	Event	M_w	R_{rup} (km)	V_{s30} (m/s)	Pulselike?	Scale Factor
1013	Northridge-01	6.69	5.9	629.0	Yes	1.828
1063	Northridge-01	6.69	6.5	282.3	Yes	1.043
1084	Northridge-01	6.69	5.4	251.2	Yes	0.681
1085	Northridge-01	6.69	5.2	370.5	Yes	0.879
1114	Kobe, Japan	6.9	3.3	198.0	Yes	1.049
1119	Kobe, Japan	6.9	0.3	312.0	Yes	0.971
183	Imperial Valley-06	6.53	3.9	206.1	No	0.790
184	Imperial Valley-06	6.53	5.1	202.3	Yes	0.507
20	Northern Calif-03	6.5	27.0	219.3	Yes	1.531
4065	Parkfield-02, CA	6	2.9	383.9	Yes	1.882
4107	Parkfield-02, CA	6	2.5	178.3	Yes	1.512
568	San Salvador	5.8	6.3	489.3	Yes	1.098
776	Loma Prieta	6.93	27.9	282.1	No	1.987
8067	Christchurch, New Zealand	6.2	4.5	204.0	Yes	1.228
821	Erzican, Turkey	6.69	4.4	352.1	No	1.371

Christchurch Hospital

(CHHC)

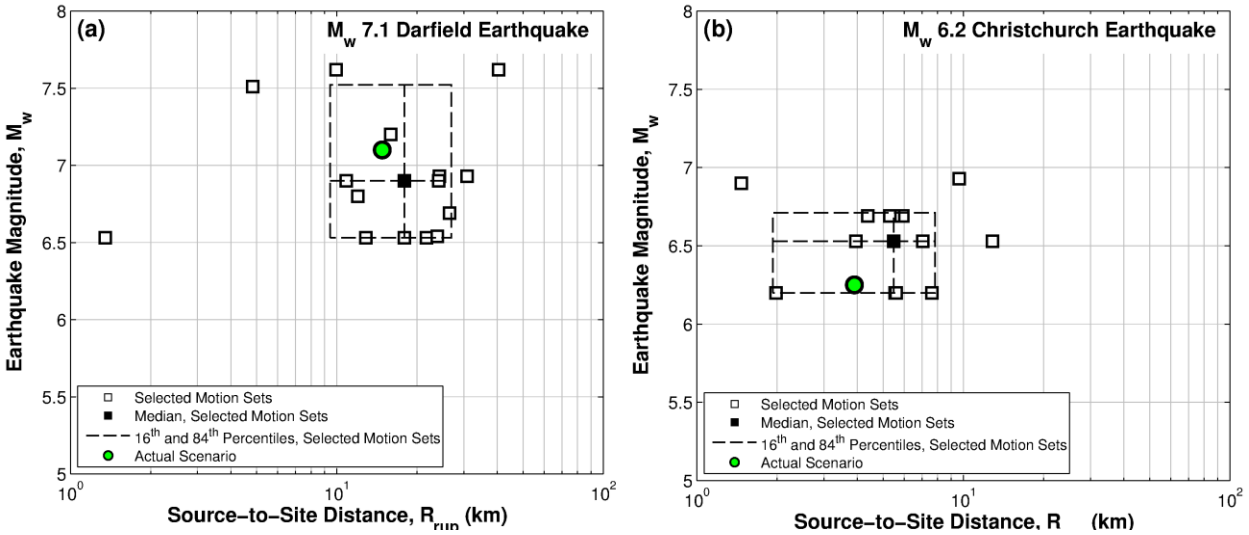

Figure B.10 Distributions of causal parameters, M_w and R_{rup}, for the selected motion sets for both the: (a) Darfield earthquake, and (b) Christchurch earthquake scenarios at the CHHC SMS site.

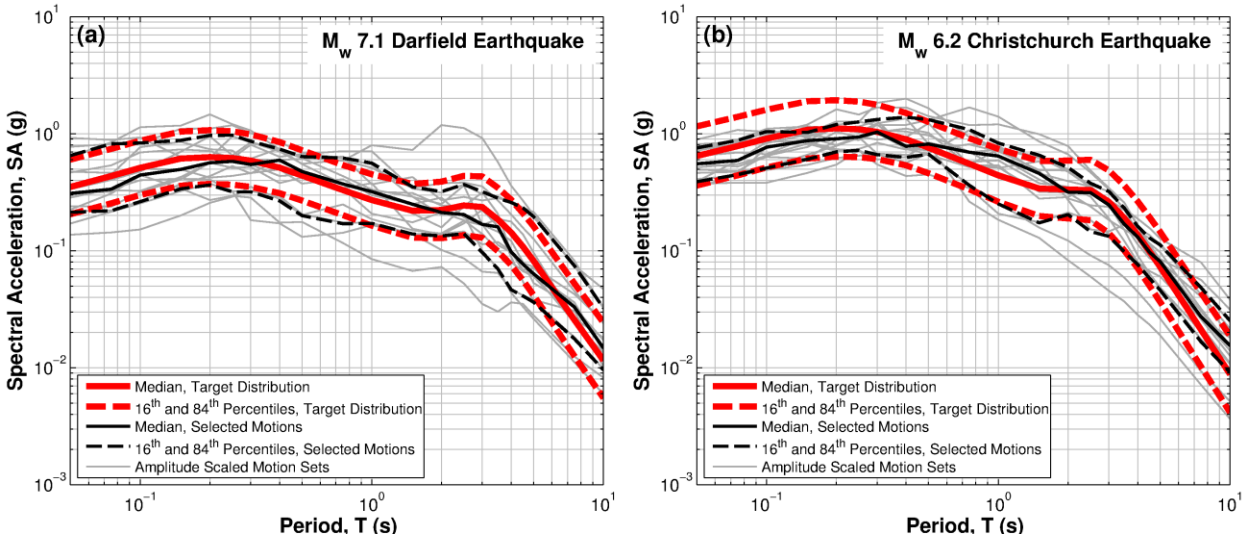

Figure B.11 5% damped response spectra of the target motions and selected motion for the CHHC SMS site for the: (a) Darfield earthquake, and (b) Christchurch earthquake.

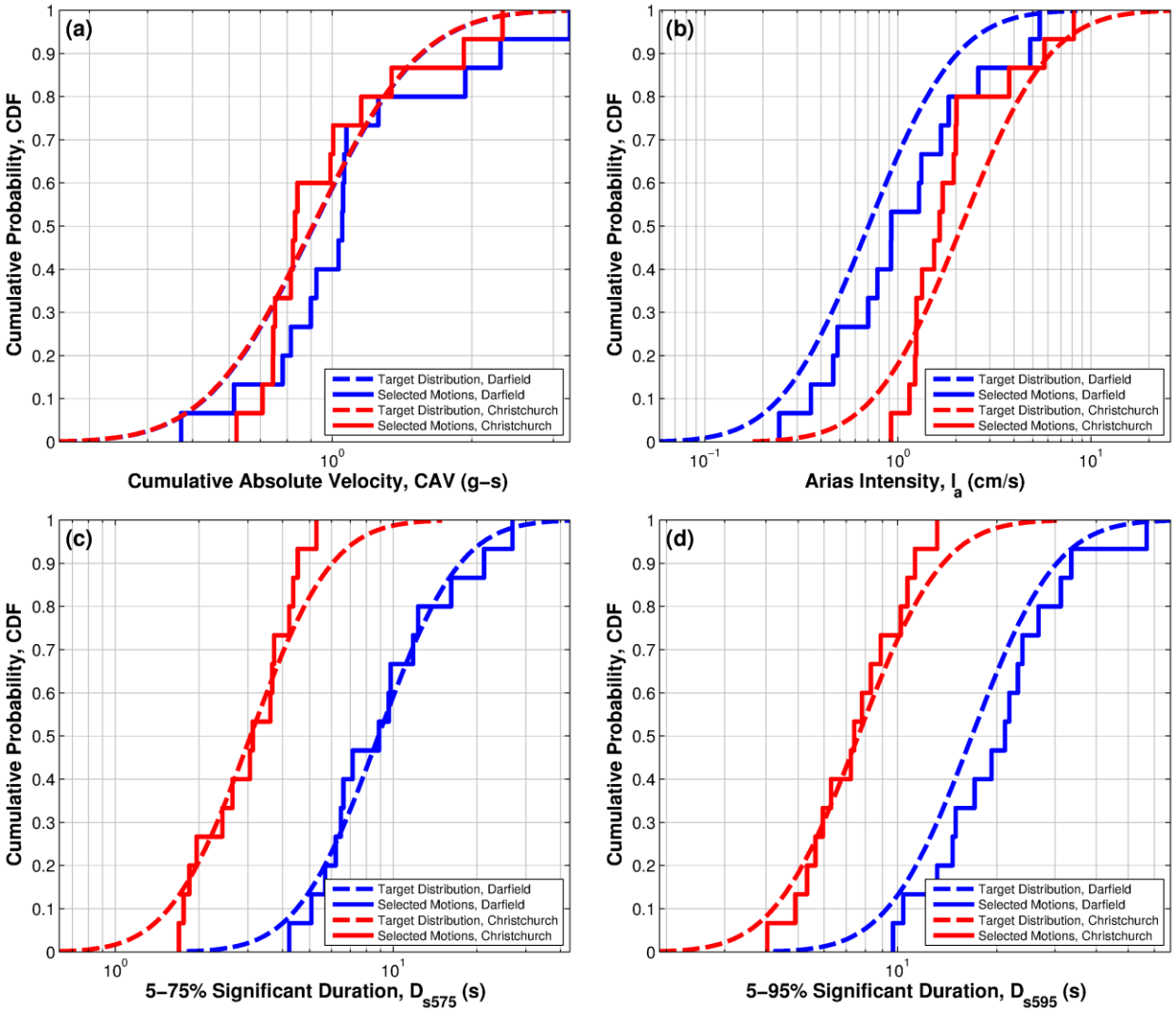

Figure B.12 Cumulative distributions of the target and selected motions for the CHHC SMS site for both the Darfield and Christchurch earthquakes: (a) CAV; (b) I_a; (c) D_{s575} ; and (d) D_{s595}.

Table B.10 Selected ground motion sets for the CHHC SMS site for the Darfield earthquake

NGA No.	Event	M_w	R_{rup} (km)	V_{s30} (m/s)	Pulselike?	Scale Factor
1077	Northridge-01	6.69	26.5	336.2	No	0.523
1176	Kocaeli, Turkey	7.51	4.8	297.0	Yes	0.514
1183	Chi-Chi, Taiwan	7.62	40.4	210.7	No	1.806
1595	Chi-Chi, Taiwan	7.62	9.9	258.9	Yes	0.856
172	Imperial Valley-06	6.53	21.7	237.3	No	0.903
175	Imperial Valley-06	6.53	17.9	196.9	No	1.814
178	Imperial Valley-06	6.53	12.9	162.9	Yes	1.734
181	Imperial Valley-06	6.53	1.4	203.2	Yes	1.679
292	Irpinia, Italy-01	6.9	10.8	382.0	Yes	1.205
4875	Chuetsu-oki	6.8	12.0	282.6	Yes	0.705
5810	Iwate	6.9	24.1	655.5	Yes	1.987
5827	El Mayor-Cucapah	7.2	15.9	242.1	No	0.827
729	Superstition Hills-02	6.54	23.9	179.0	No	0.669
786	Loma Prieta	6.93	30.8	209.9	No	2.000
806	Loma Prieta	6.93	24.2	267.7	No	1.000

Table B.11 Selected ground motion sets for the CHHC SMS site for the Christchurch earthquake

NGA No.	Event	M_w	R_{rup} (km)	V_{s30} (m/s)	Pulselike?	Scale Factor
1013	Northridge-01	6.69	5.9	629.0	Yes	1.071
1045	Northridge-01	6.69	5.5	285.9	Yes	1.247
1084	Northridge-01	6.69	5.4	251.2	Yes	0.826
1086	Northridge-01	6.69	5.3	440.5	Yes	0.668
1120	Kobe, Japan	6.9	1.5	256.0	Yes	0.585
178	Imperial Valley-06	6.53	12.9	162.9	Yes	0.642
179	Imperial Valley-06	6.53	7.1	208.9	Yes	0.722
180	Imperial Valley-06	6.53	4.0	205.6	Yes	1.605
182	Imperial Valley-06	6.53	0.6	210.5	Yes	0.873
2628	Chi-Chi, Taiwan-03	6.2	7.6	443.0	Yes	1.395
765	Loma Prieta	6.93	9.6	1428.1	No	2.000
8063	Christchurch, New Zealand	6.2	5.6	187.0	No	1.264
8119	Christchurch, New Zealand	6.2	2.0	206.0	Yes	1.009
8130	Christchurch, New Zealand	6.2	5.6	207.0	Yes	1.926
821	Erzican, Turkey	6.69	4.4	352.1	No	1.704

Cashmere High School

(CMHS)

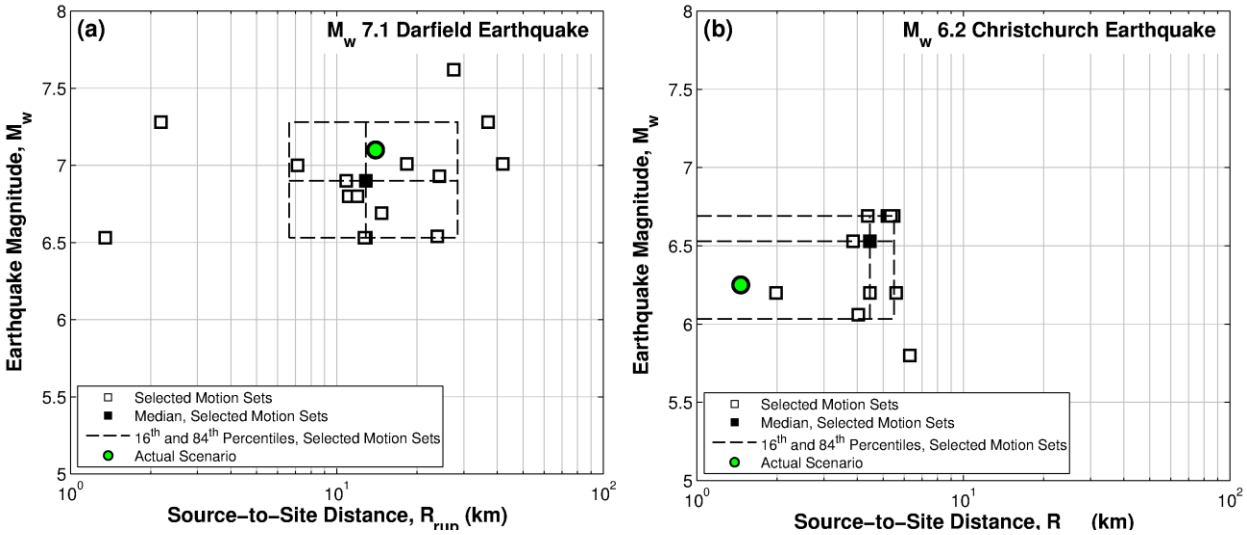

Figure B.13 Distributions of causal parameters, M_w and R_{rup}, for the selected motion sets for both the: (a) Darfield earthquake, and (b) Christchurch earthquake scenarios at the CMHS SMS site.

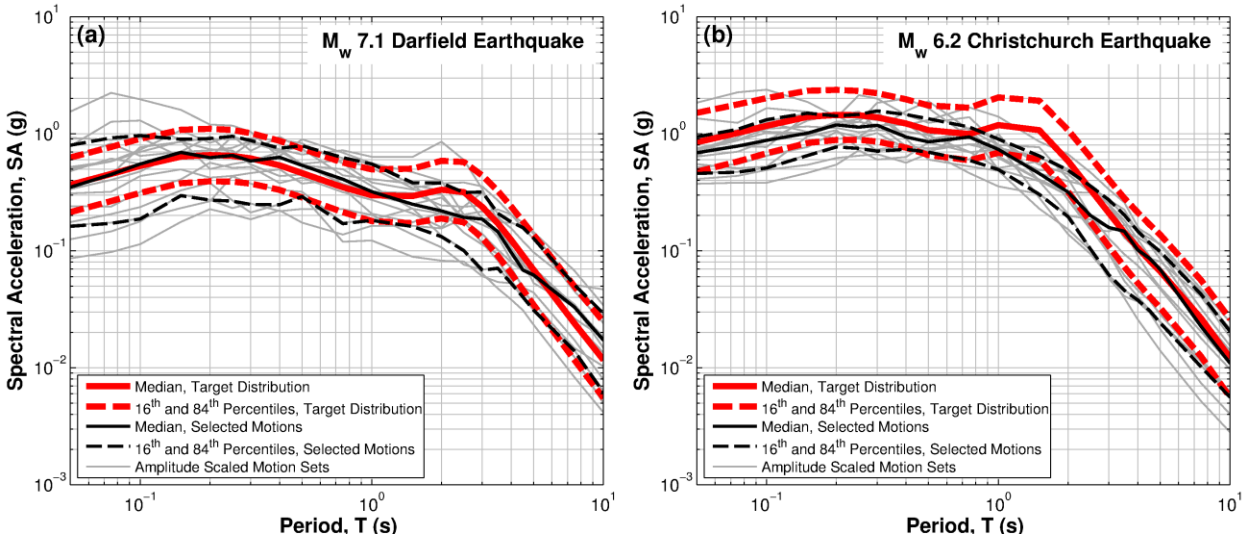

Figure B.14 5% damped response spectra of the target motions and selected motion for the CMHS SMS site for the: (a) Darfield earthquake, and (b) Christchurch earthquake.

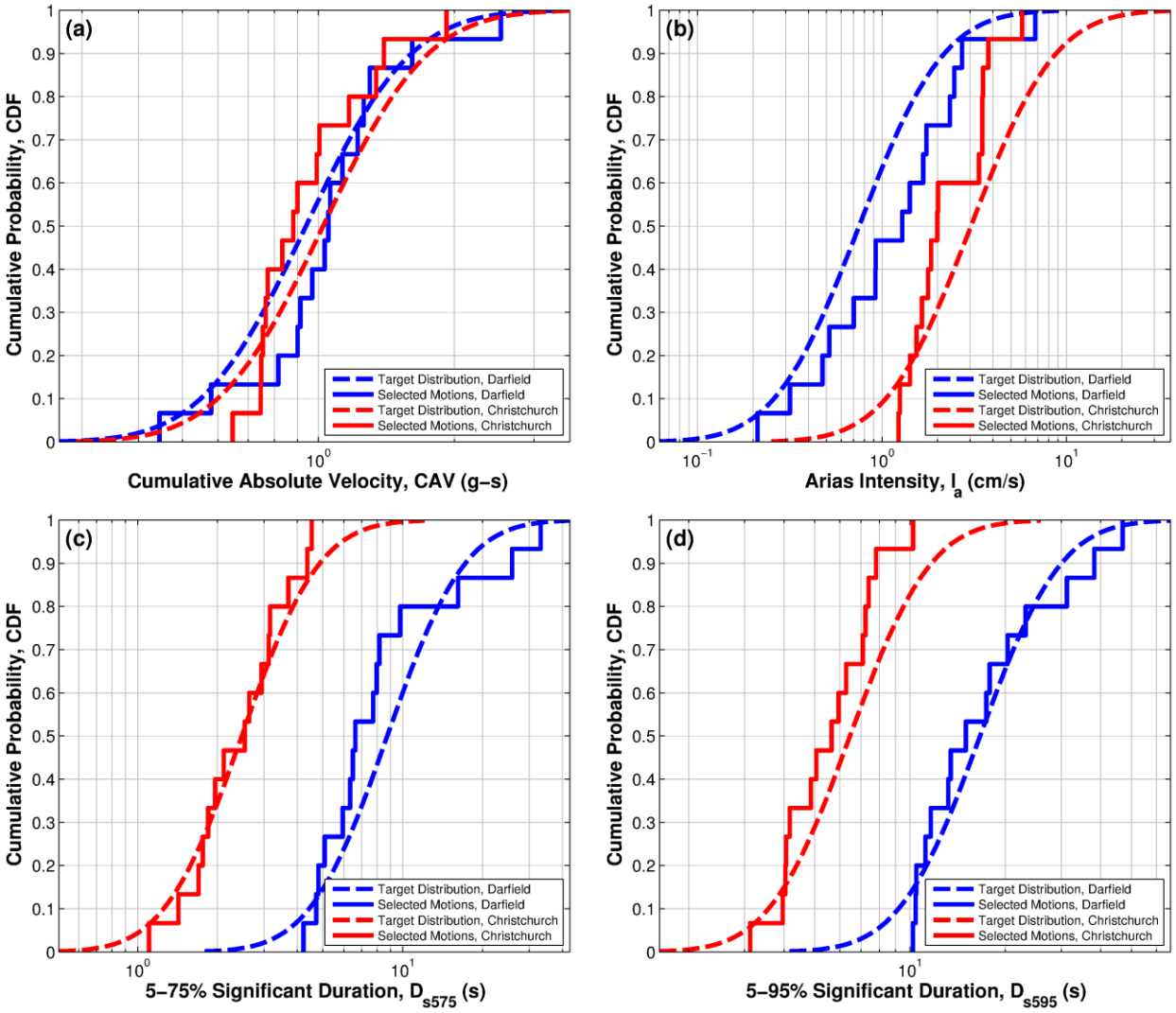

Figure B.15 Cumulative distributions of the target and selected motions for the CMHS SMS site for both the Darfield and Christchurch earthquakes: (a) CAV; (b) I_a; (c) D_{s575} ; and (d) D_{s595}.

Table B.12 Selected ground motion sets for the CMHS SMS site for the Darfield earthquake

NGA No.	Event	M_w	R_{rup} (km)	V_{s30} (m/s)	Pulselike?	Scale Factor
1538	Chi-Chi, Taiwan	7.62	27.5	190.5	No	1.522
178	Imperial Valley-06	6.53	12.9	162.9	Yes	1.035
181	Imperial Valley-06	6.53	1.4	203.2	Yes	0.578
187	Imperial Valley-06	6.53	12.7	348.7	No	1.355
292	Irpinia, Italy-01	6.9	10.8	382.0	Yes	0.961
3746	Cape Mendocino	7.01	18.3	459.0	Yes	0.835
3758	Landers	7.28	36.9	333.9	No	0.910
4847	Chuetsu-oki	6.8	11.9	383.4	Yes	1.712
4856	Chuetsu-oki	6.8	11.1	294.4	Yes	0.708
6927	Darfield, New Zealand	7	7.1	263.2	Yes	0.751
729	Superstition Hills-02	6.54	23.9	179.0	No	1.390
806	Loma Prieta	6.93	24.2	267.7	No	0.715
826	Cape Mendocino	7.01	42.0	337.5	No	2.000
879	Landers	7.28	2.2	1369.0	Yes	0.510
959	Northridge-01	6.69	14.7	267.5	No	0.500

Table B.13 Selected ground motion sets for the CMHS SMS site for the Christchurch earthquake

NGA No.	Event	M_w	R_{rup} (km)	V_{s30} (m/s)	Pulselike?	Scale Factor
1045	Northridge-01	6.69	5.5	285.9	Yes	2.000
1084	Northridge-01	6.69	5.4	251.2	Yes	0.654
1085	Northridge-01	6.69	5.2	370.5	Yes	2.000
1086	Northridge-01	6.69	5.3	440.5	Yes	1.352
1119	Kobe, Japan	6.9	0.3	312.0	Yes	2.000
182	Imperial Valley-06	6.53	0.6	210.5	Yes	2.000
183	Imperial Valley-06	6.53	3.9	206.1	No	1.236
451	Morgan Hill	6.19	0.5	561.4	Yes	1.424
529	N. Palm Springs	6.06	4.0	344.7	No	2.000
568	San Salvador	5.8	6.3	489.3	Yes	1.255
585	Baja California	5.5	4.5	471.5	No	1.341
8067	Christchurch, New Zealand	6.2	4.5	204.0	Yes	1.725
8119	Christchurch, New Zealand	6.2	2.0	206.0	Yes	1.300
8130	Christchurch, New Zealand	6.2	5.6	207.0	Yes	1.025
821	Erzican, Turkey	6.69	4.4	352.1	No	1.167

Hulverstone Drive Pumping Station

(HPSC)

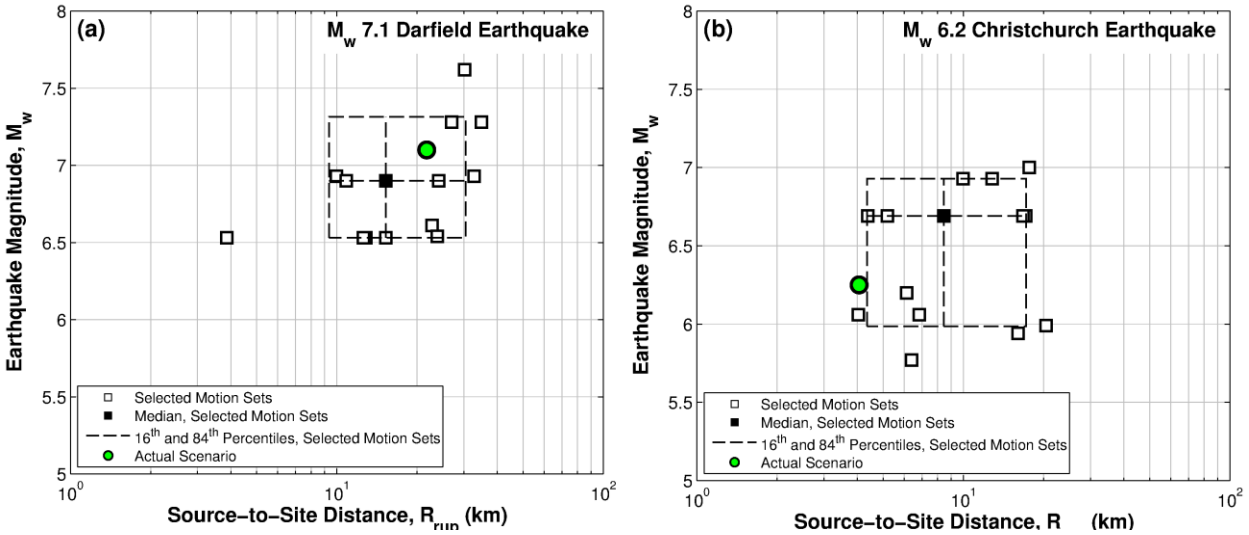

Figure B.16 Distributions of causal parameters, M_w and R_{rup}, for the selected motion sets for both the: (a) Darfield earthquake, and (b) Christchurch earthquake scenarios at the HPSC SMS site.

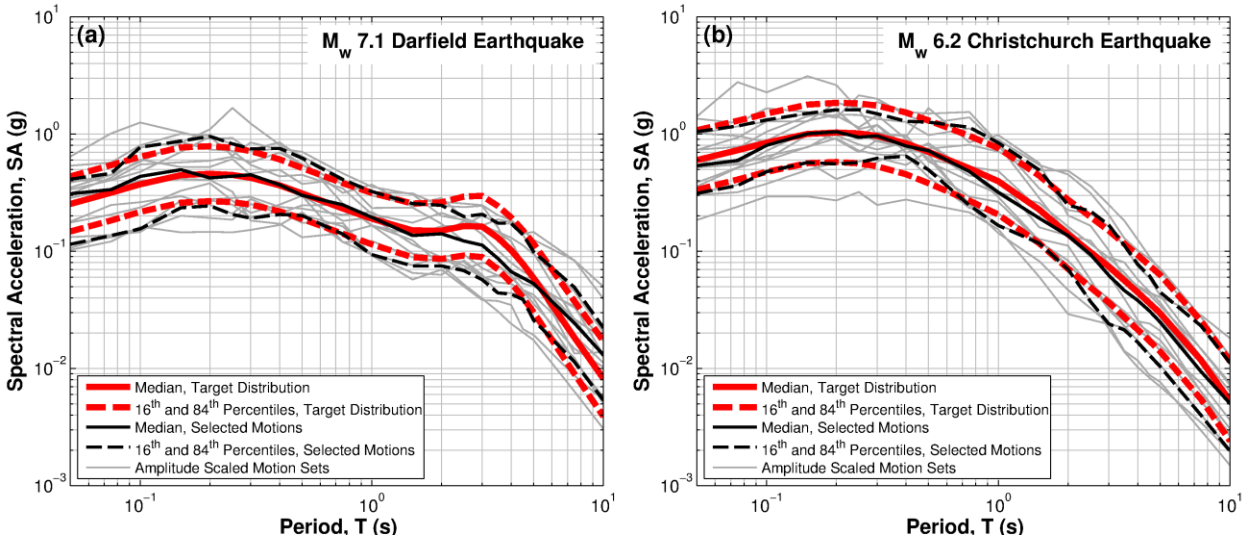

Figure B.17 5% damped response spectra of the target motions and selected motion for the HPSC SMS site for the: (a) Darfield earthquake, and (b) Christchurch earthquake.

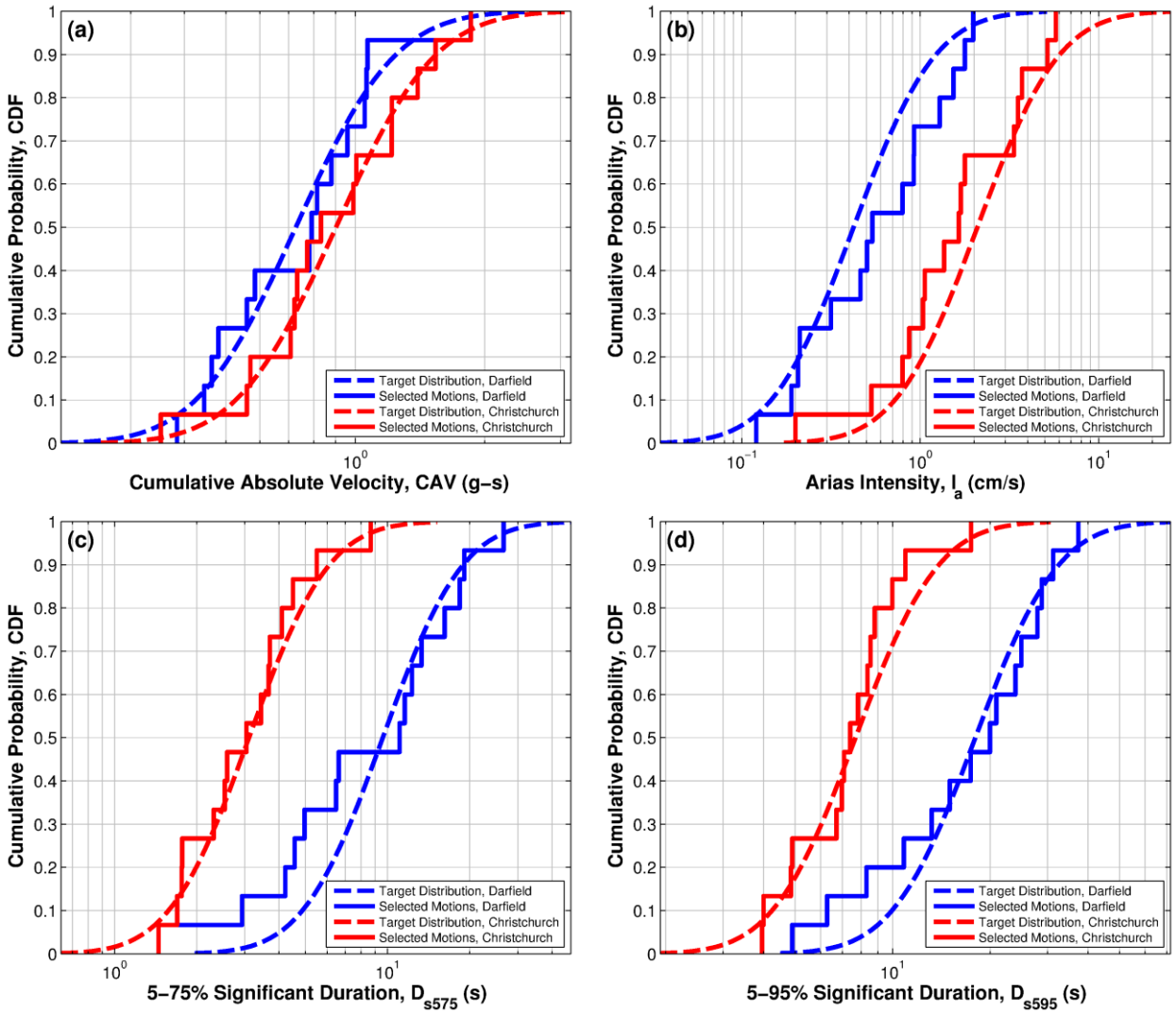

Figure B.18 Cumulative distributions of the target and selected motions for the HPSC SMS site for both the Darfield and Christchurch earthquakes: (a) CAV; (b) I_a; (c) D_{s575} ; and (d) D_{s595}.

Table B.14 Selected ground motion sets for the HPSC SMS site for the Darfield earthquake

NGA No.	Event	M_w	R_{rup} (km)	V_{s30} (m/s)	Pulselike?	Scale Factor
1477	Chi-Chi, Taiwan	7.62	30.2	489.2	Yes	0.896
1510	Chi-Chi, Taiwan	7.62	0.9	573.0	Yes	1.039
174	Imperial Valley-06	6.53	12.6	196.3	No	1.015
178	Imperial Valley-06	6.53	12.9	162.9	Yes	1.288
183	Imperial Valley-06	6.53	3.9	206.1	No	0.676
187	Imperial Valley-06	6.53	12.7	348.7	No	0.941
192	Imperial Valley-06	6.53	15.3	193.7	No	1.041
292	Irpinia, Italy-01	6.9	10.8	382.0	Yes	0.772
5810	Iwate	6.9	24.1	655.5	Yes	1.539
68	San Fernando	6.61	22.8	316.5	No	1.822
729	Superstition Hills-02	6.54	23.9	179.0	No	0.611
763	Loma Prieta	6.93	10.0	729.7	No	1.530
800	Loma Prieta	6.93	32.8	279.6	No	1.385
838	Landers	7.28	34.9	370.1	Yes	1.089
880	Landers	7.28	27.0	355.4	No	1.044

Table B.15 Selected ground motion sets for the HPSC SMS site for the Christchurch earthquake

NGA No.	Event	M_w	R_{rup} (km)	V_{s30} (m/s)	Pulselike?	Scale Factor
1004	Northridge-01	6.69	8.4	380.1	Yes	1.765
1078	Northridge-01	6.69	16.7	715.1	No	0.869
1085	Northridge-01	6.69	5.2	370.5	Yes	0.649
250	Mammoth Lakes-06	5.94	16.0	537.2	Yes	0.852
451	Morgan Hill	6.19	0.5	561.4	Yes	0.502
517	N. Palm Springs	6.06	6.8	359.0	No	0.652
529	N. Palm Springs	6.06	4.0	344.7	No	1.604
547	Chalfant Valley-01	5.77	6.4	316.2	No	1.117
668	Whittier Narrows-01	5.99	20.4	279.5	Yes	1.554
6890	Darfield, New Zealand	7	17.6	204.0	No	2.000
763	Loma Prieta	6.93	10.0	729.7	No	1.941
767	Loma Prieta	6.93	12.8	349.9	Yes	1.244
8158	Christchurch, New Zealand	6.2	6.1	649.7	Yes	0.778
821	Erzican, Turkey	6.69	4.4	352.1	No	1.860
953	Northridge-01	6.69	17.2	355.8	No	1.348

Heathcote Valley School

(HVSC)

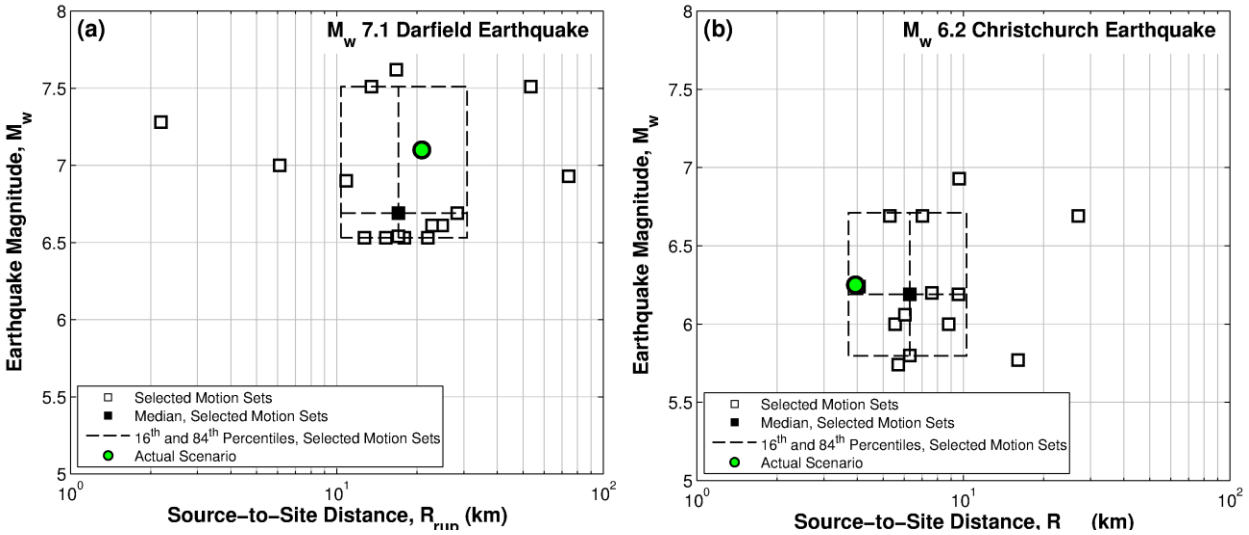

Figure B.19 Distributions of causal parameters, M_w and R_{rup}, for the selected motion sets for both the: (a) Darfield earthquake, and (b) Christchurch earthquake scenarios at the HVSC SMS site.

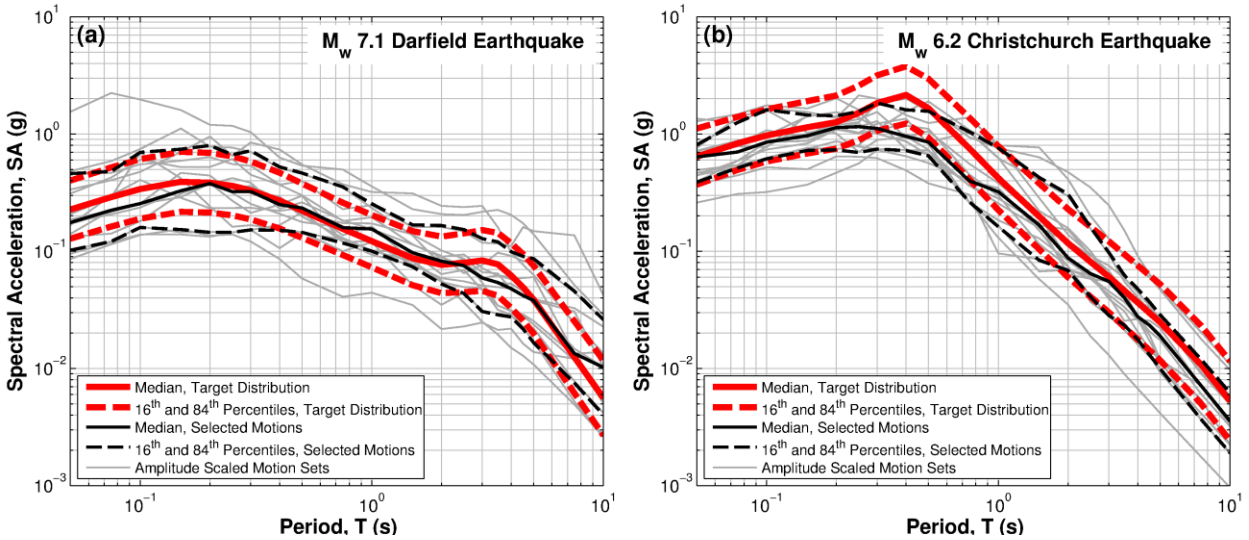

Figure B.20 5% damped response spectra of the target motions and selected motion for the HVSC SMS site for the: (a) Darfield earthquake, and (b) Christchurch earthquake.

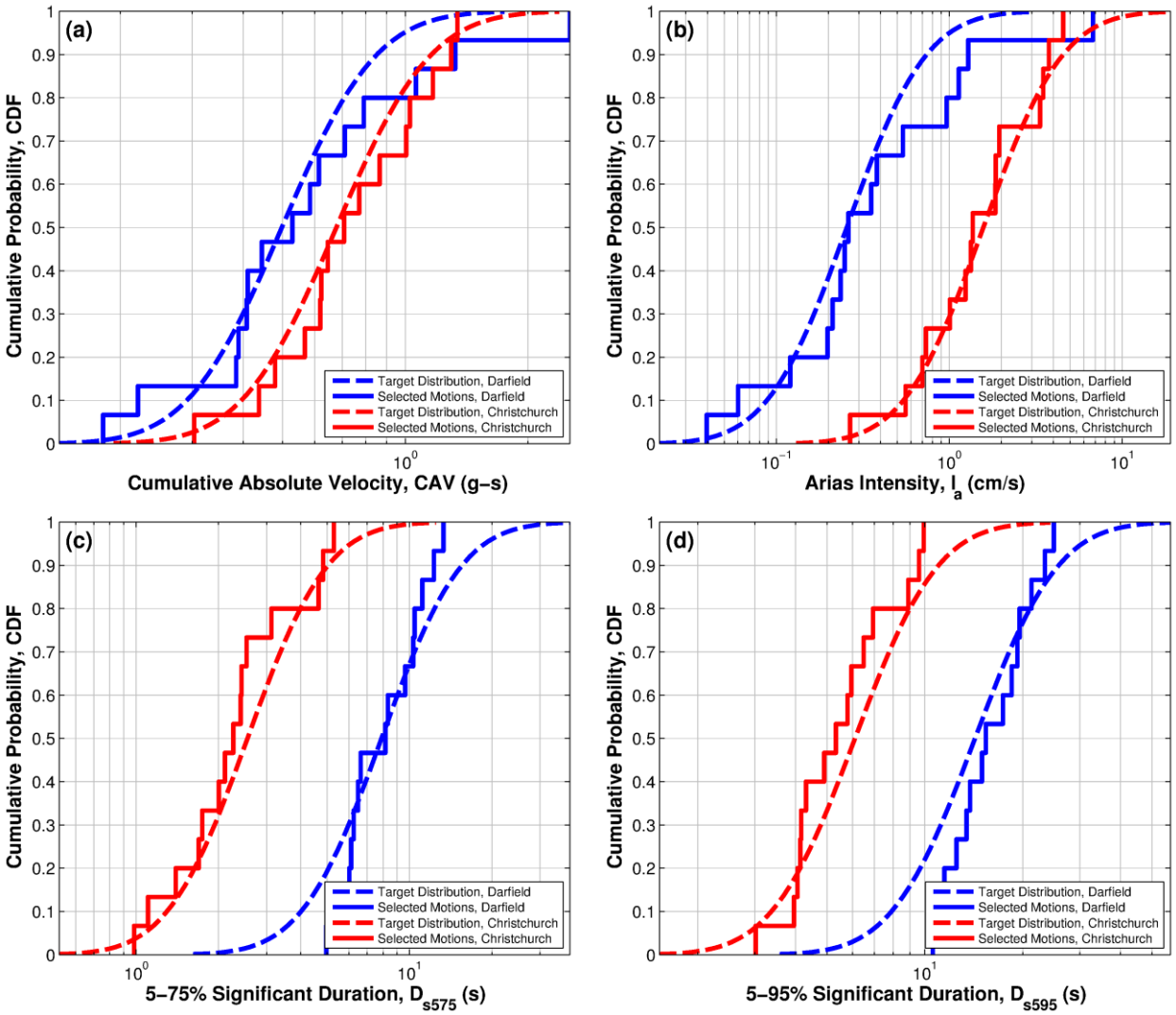

Figure B.21 Cumulative distributions of the target and selected motions for the HVSC SMS site for both the Darfield and Christchurch earthquakes: (a) CAV; (b) I_a; (c) D_{s575} ; and (d) D_{s595}.

Table B.16 Selected ground motion sets for the HVSC SMS site for the Darfield earthquake

NGA No.	Event	M_w	R_{rup} (km)	V_{s30} (m/s)	Pulselike?	Scale Factor
1148	Kocaeli, Turkey	7.51	13.5	523.0	Yes	1.250
1170	Kocaeli, Turkey	7.51	53.4	384.9	No	2.000
1486	Chi-Chi, Taiwan	7.62	16.7	465.6	Yes	0.551
175	Imperial Valley-06	6.53	17.9	196.9	No	0.695
176	Imperial Valley-06	6.53	22.0	249.9	No	1.197
187	Imperial Valley-06	6.53	12.7	348.7	No	0.962
192	Imperial Valley-06	6.53	15.3	193.7	No	0.881
292	Irpinia, Italy-01	6.9	10.8	382.0	Yes	0.584
68	San Fernando	6.61	22.8	316.5	No	1.626
6975	Darfield, New Zealand	7	6.1	249.3	Yes	0.619
719	Superstition Hills-02	6.54	17.0	208.7	No	1.337
797	Loma Prieta	6.93	74.1	873.1	No	1.861
879	Landers	7.28	2.2	1369.0	Yes	0.500
88	San Fernando	6.61	24.9	389.0	No	1.275
987	Northridge-01	6.69	28.3	321.9	No	0.918

Table B.17 Selected ground motion sets for the HVSC SMS site for the Christchurch earthquake

NGA No.	Event	M_w	R_{rup} (km)	V_{s30} (m/s)	Pulselike?	Scale Factor
1003	Northridge-01	6.69	27.0	308.7	Yes	0.705
1050	Northridge-01	6.69	7.0	2016.1	Yes	1.567
1086	Northridge-01	6.69	5.3	440.5	Yes	0.663
1119	Kobe, Japan	6.9	0.3	312.0	Yes	1.114
149	Coyote Lake	5.74	5.7	221.8	Yes	0.940
2628	Chi-Chi, Taiwan-03	6.2	7.6	443.0	Yes	1.030
30	Parkfield	6.19	9.6	289.6	No	0.862
4101	Parkfield-02, CA	6	5.6	397.4	Yes	1.739
4116	Parkfield-02, CA	6	8.8	246.1	Yes	1.611
411	Coalinga-05	5.77	16.1	257.4	No	1.353
451	Morgan Hill	6.19	0.5	561.4	Yes	1.306
540	N. Palm Springs	6.06	6.0	425.0	No	1.151
568	San Salvador	5.8	6.3	489.3	Yes	1.414
765	Loma Prieta	6.93	9.6	1428.1	No	0.630
95	Managua, Nicaragua-01	6.24	4.1	288.8	No	1.296

Kaipoi North School

(KPOC)

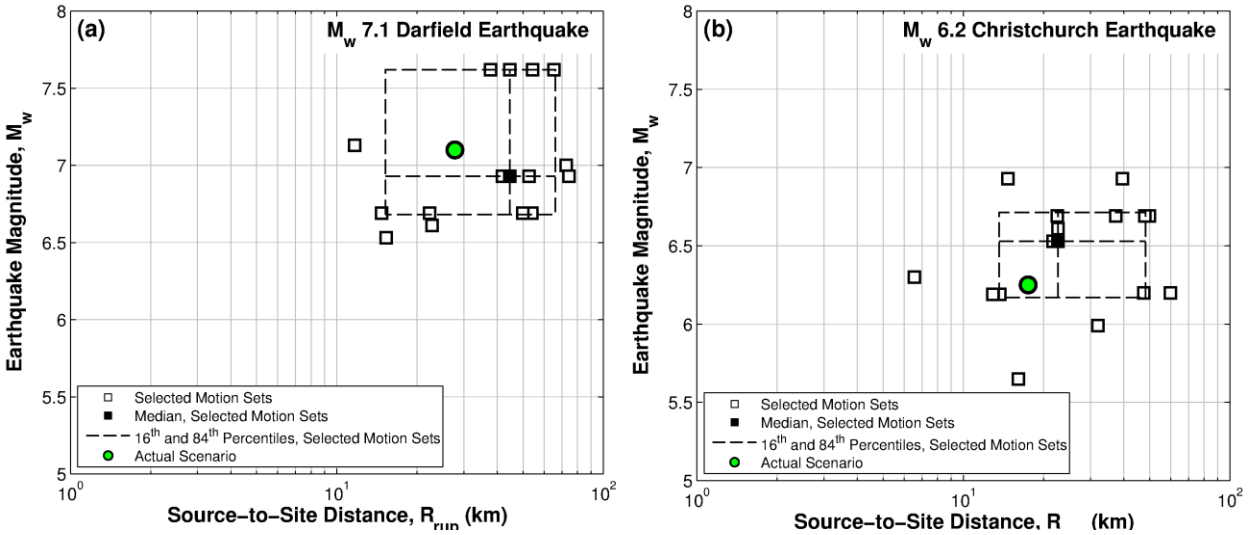

Figure B.22 Distributions of causal parameters, M_w and R_{rup}, for the selected motion sets for both the: (a) Darfield earthquake, and (b) Christchurch earthquake scenarios at the KPOC SMS site.

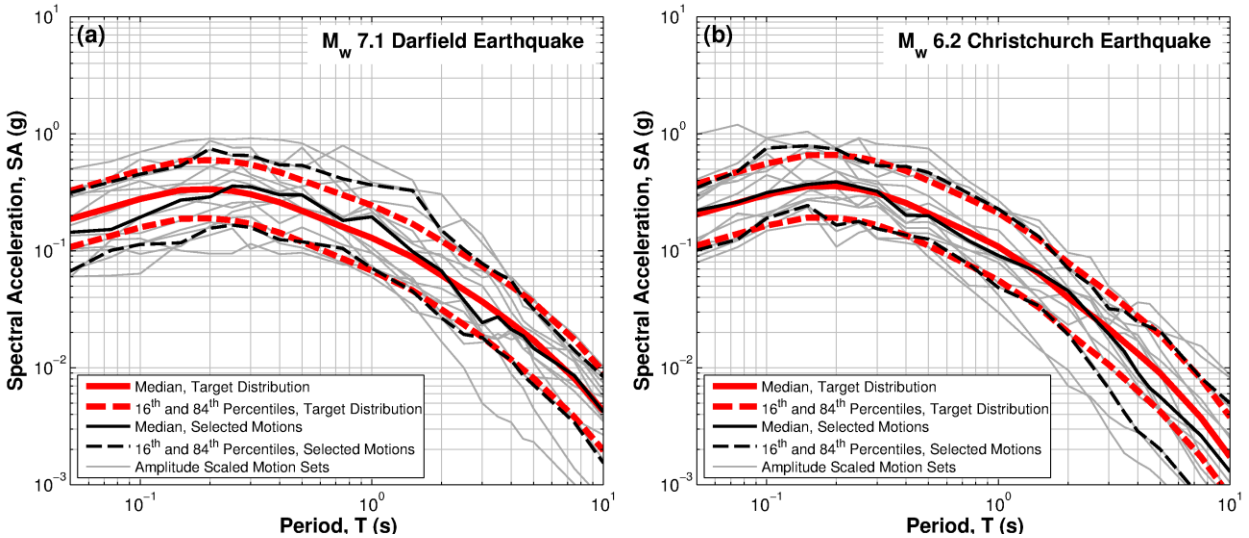

Figure B.23 5% damped response spectra of the target motions and selected motion for the KPOC SMS site for the: (a) Darfield earthquake, and (b) Christchurch earthquake.

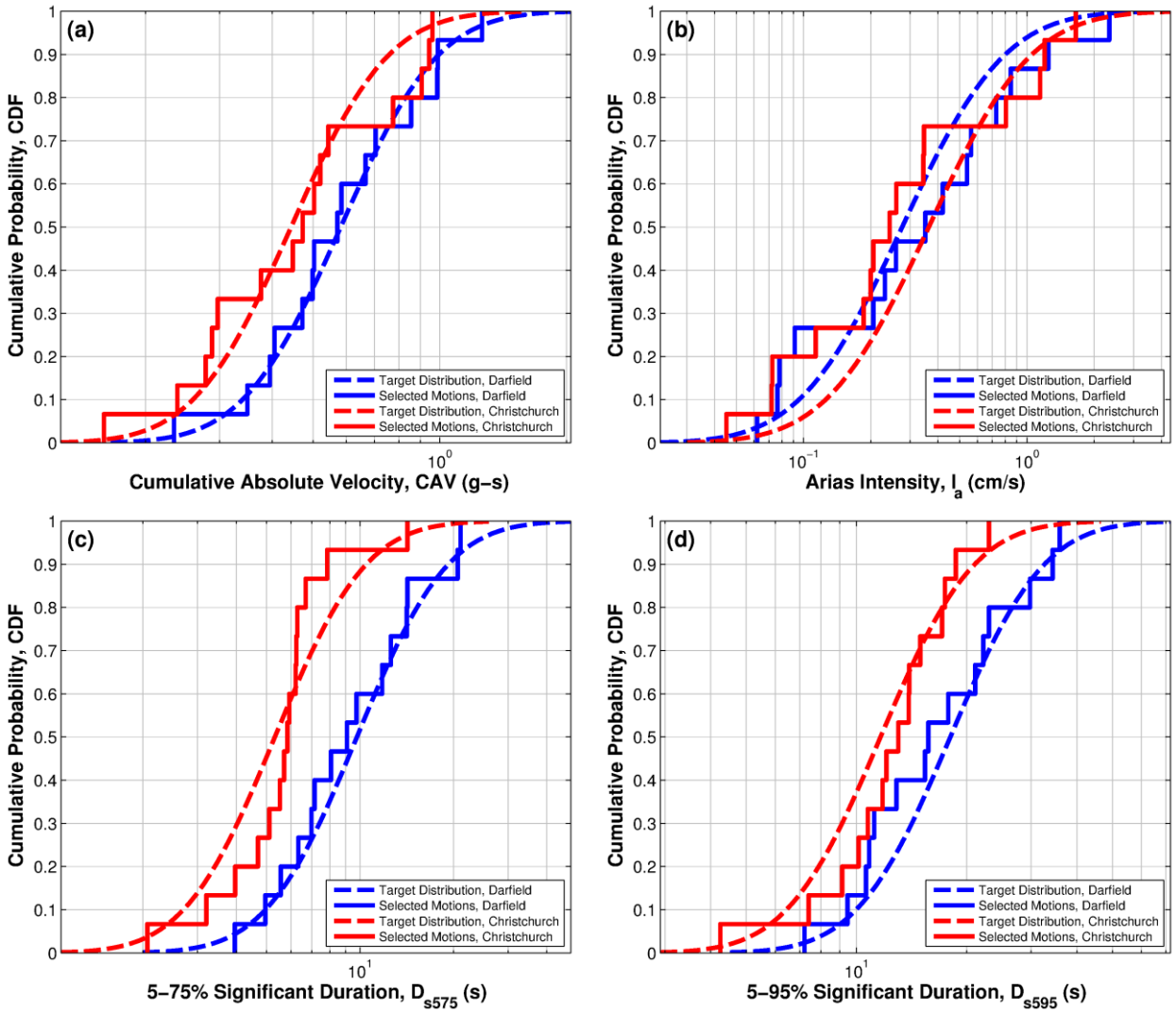

Figure B.24 Cumulative distributions of the target and selected motions for the KPOC SMS site for both the Darfield and Christchurch earthquakes: (a) CAV; (b) I_a; (c) D_{s575} ; and (d) D_{s595}.

Table B.18 Selected ground motion sets for the KPOC SMS site for the Darfield earthquake

NGA No.	Event	M_w	R_{rup} (km)	V_{s30} (m/s)	Pulselike?	Scale Factor
1089	Northridge-01	6.69	22.3	506.0	No	0.609
1245	Chi-Chi, Taiwan	7.62	37.7	804.4	No	2.000
1264	Chi-Chi, Taiwan	7.62	54.3	330.6	No	1.765
1270	Chi-Chi, Taiwan	7.62	44.5	626.4	No	1.185
1587	Chi-Chi, Taiwan	7.62	65.3	845.3	No	1.249
167	Imperial Valley-06	6.53	15.3	259.9	No	0.909
1787	Hector Mine	7.13	11.7	726.0	No	0.678
68	San Fernando	6.61	22.8	316.5	No	1.225
6980	Darfield, New Zealand	7	72.5	484.5	No	1.039
731	Loma Prieta	6.93	41.9	391.9	No	1.146
733	Loma Prieta	6.93	52.7	271.1	No	0.561
783	Loma Prieta	6.93	74.3	248.6	Yes	0.557
959	Northridge-01	6.69	14.7	267.5	No	0.766
962	Northridge-01	6.69	49.8	160.6	No	0.635
975	Northridge-01	6.69	53.9	362.3	No	2.000

Table B.19 Selected ground motion sets for the KPOC SMS site for the Christchurch earthquake

NGA No.	Event	M_w	R_{rup} (km)	V_{s30} (m/s)	Pulselike?	Scale Factor
1006	Northridge-01	6.69	22.5	398.4	No	0.805
1028	Northridge-01	6.69	37.2	435.6	No	0.989
172	Imperial Valley-06	6.53	21.7	237.3	No	0.602
1740	Little Skull Mtn,NV	5.65	16.1	302.6	No	1.894
2946	Chi-Chi, Taiwan-05	6.2	59.8	544.7	No	1.414
31	Parkfield	6.19	12.9	256.8	No	1.140
3220	Chi-Chi, Taiwan-05	6.2	47.5	652.9	No	0.566
4482	LAquila, Italy	6.3	6.6	552.0	Yes	0.705
456	Morgan Hill	6.19	13.7	270.8	No	1.105
57	San Fernando	6.61	22.6	450.3	No	0.726
696	Whittier Narrows-01	5.99	31.9	393.7	No	2.000
762	Loma Prieta	6.93	39.5	367.6	No	1.493
801	Loma Prieta	6.93	14.7	671.8	No	0.534
950	Northridge-01	6.69	48.0	544.7	No	0.686
962	Northridge-01	6.69	49.8	160.6	No	2.000

North New Brighton School

(NNBS)

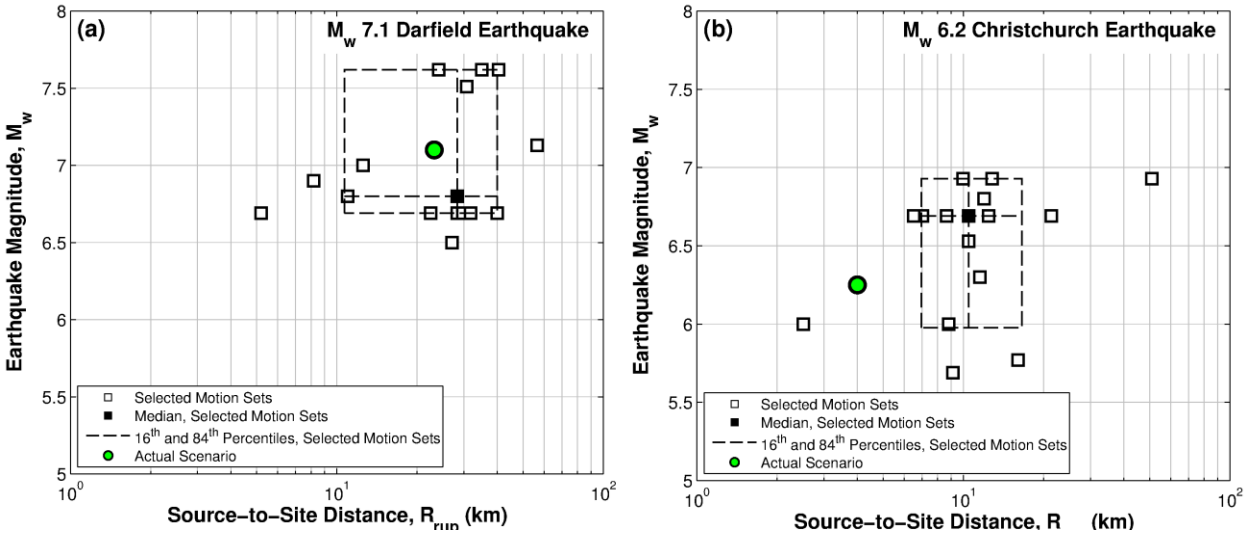

Figure B.25 Distributions of causal parameters, M_w and R_{rup}, for the selected motion sets for both the: (a) Darfield earthquake, and (b) Christchurch earthquake scenarios at the NNBS SMS site.

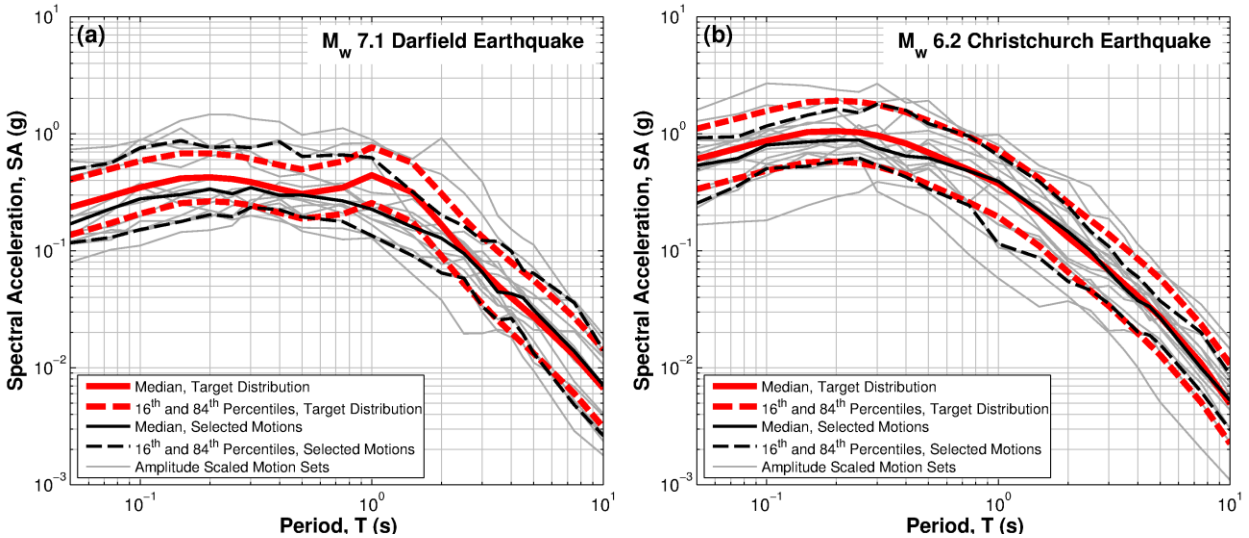

Figure B.26 5% damped response spectra of the target motions and selected motion for the NNBS SMS site for the: (a) Darfield earthquake, and (b) Christchurch earthquake.

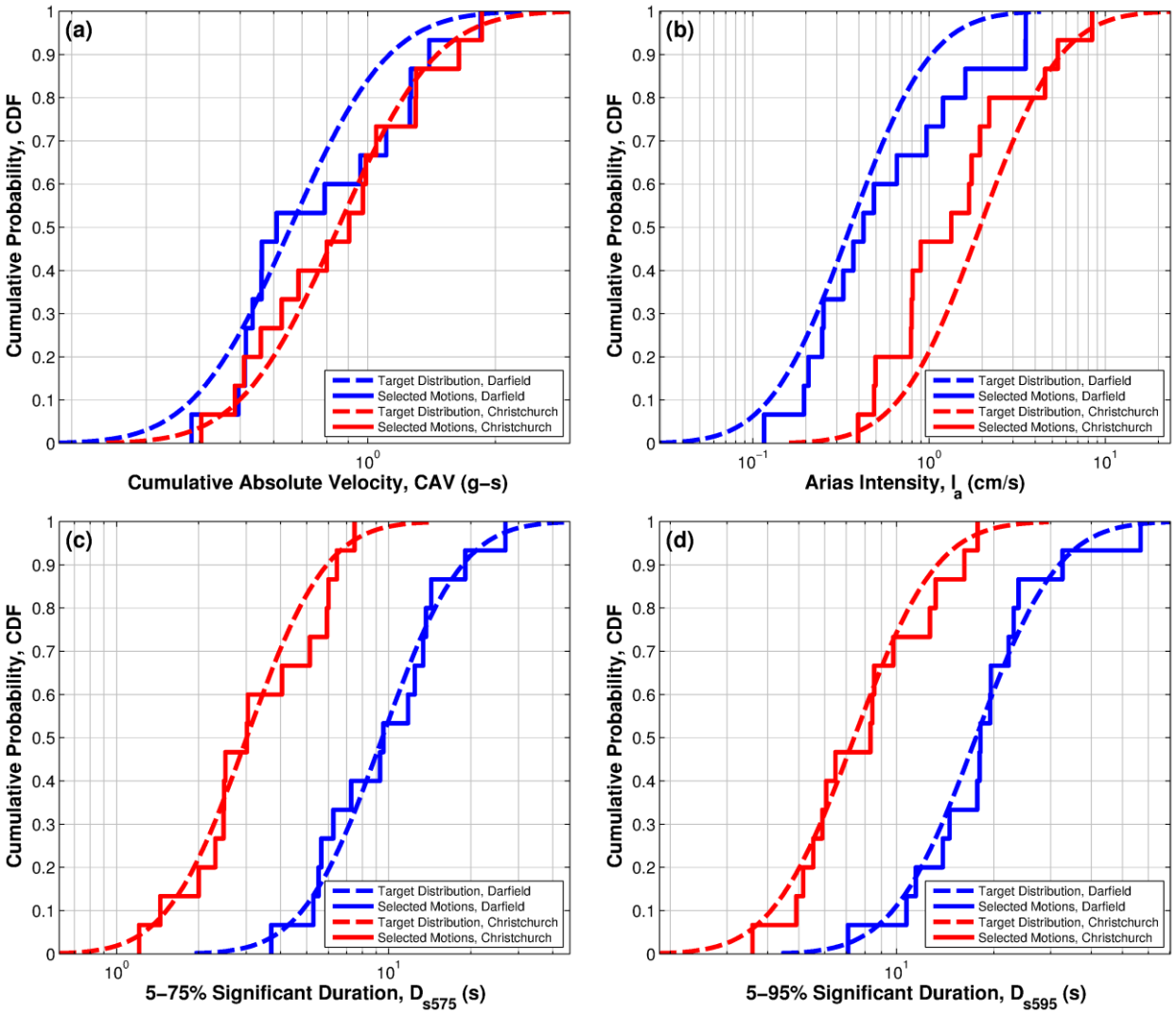

Figure B.27 Cumulative distributions of the target and selected motions for the NNBS SMS site for both the Darfield and Christchurch earthquakes: (a) CAV; (b) I_a; (c) D_{s575} ; and (d) D_{s595}.

Table B.20 Selected ground motion sets for the NNBS SMS site for the Darfield earthquake

NGA No.	Event	M_w	R_{rup} (km)	V_{s30} (m/s)	Pulselike?	Scale Factor
1006	Northridge-01	6.69	22.5	398.4	No	1.639
1008	Northridge-01	6.69	29.7	329.5	No	1.049
1026	Northridge-01	6.69	39.9	311.9	No	1.064
1057	Northridge-01	6.69	31.7	345.7	No	1.558
1085	Northridge-01	6.69	5.2	370.5	Yes	0.500
1166	Kocaeli, Turkey	7.51	30.7	476.6	No	0.955
1183	Chi-Chi, Taiwan	7.62	40.4	210.7	No	0.616
1208	Chi-Chi, Taiwan	7.62	24.1	442.2	No	1.322
1487	Chi-Chi, Taiwan	7.62	35.0	520.4	Yes	0.676
1776	Hector Mine	7.13	56.4	359.0	No	1.794
20	Northern Calif-03	6.5	27.0	219.3	Yes	1.305
285	Irpinia, Italy-01	6.9	8.2	649.7	Yes	2.000
4896	Chuetsu-oki	6.8	11.0	201.0	Yes	0.648
6930	Darfield, New Zealand	7	12.5	295.7	No	0.756
987	Northridge-01	6.69	28.3	321.9	No	0.519

Table B.21 Selected ground motion sets for the NNBS SMS site for the Christchurch earthquake

NGA No.	Event	M_w	R_{rup} (km)	V_{s30} (m/s)	Pulselike?	Scale Factor
1020	Northridge-01	6.69	21.4	602.1	No	1.702
1051	Northridge-01	6.69	7.0	2016.1	Yes	0.589
1063	Northridge-01	6.69	6.5	282.3	Yes	0.546
162	Imperial Valley-06	6.53	10.5	231.2	No	1.099
235	Mammoth Lakes-02	5.69	9.1	346.8	No	1.744
3473	Chi-Chi, Taiwan-06	6.3	11.5	443.0	Yes	1.219
4107	Parkfield-02, CA	6	2.5	178.3	Yes	1.415
4116	Parkfield-02, CA	6	8.8	246.1	Yes	0.904
412	Coalinga-05	5.77	16.1	257.4	No	2.000
4847	Chuetsu-oki	6.8	11.9	383.4	Yes	1.224
744	Loma Prieta	6.93	51.0	331.2	No	1.420
763	Loma Prieta	6.93	10.0	729.7	No	1.820
767	Loma Prieta	6.93	12.8	349.9	Yes	1.544
949	Northridge-01	6.69	8.7	297.7	No	1.175
960	Northridge-01	6.69	12.4	325.6	No	1.434

Papanui High School

(PPHS)

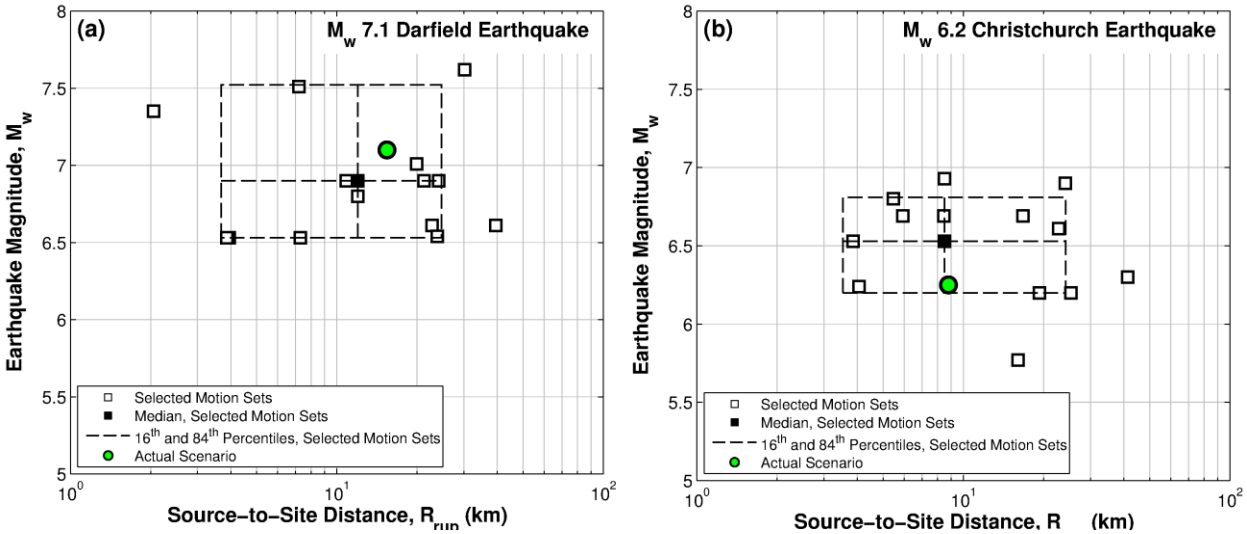

Figure B.28 Distributions of causal parameters, M_w and R_{rup}, for the selected motion sets for both the: (a) Darfield earthquake, and (b) Christchurch earthquake scenarios at the PPHS SMS site.

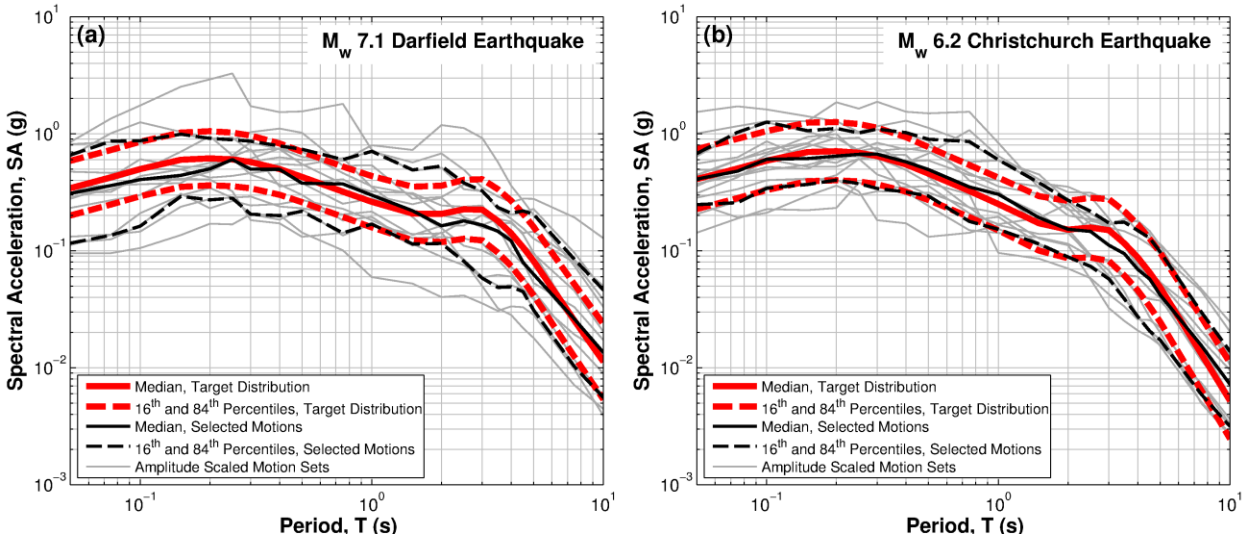

Figure B.29 5% damped response spectra of the target motions and selected motion for the PPHS SMS site for the: (a) Darfield earthquake, and (b) Christchurch earthquake.

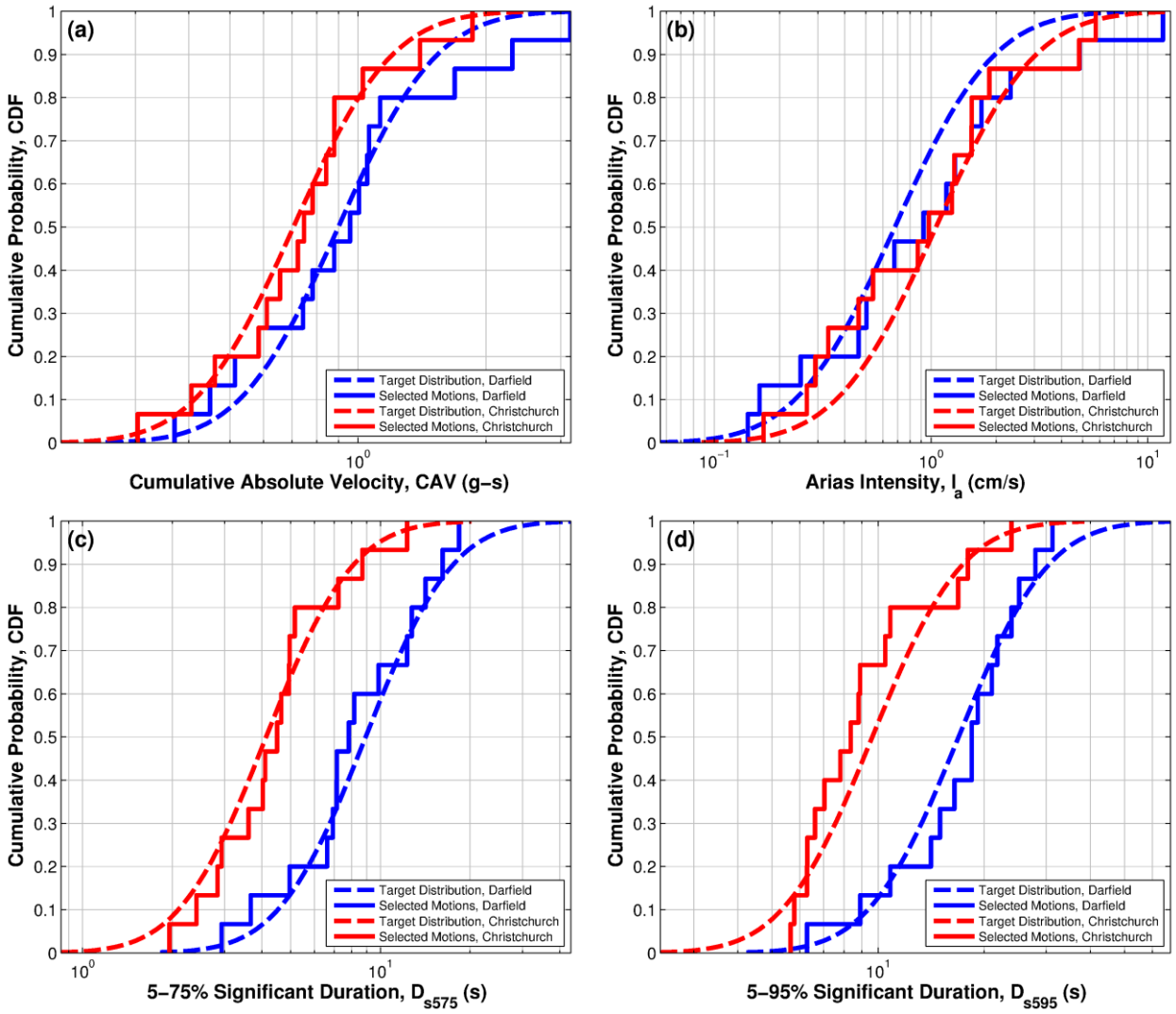

Figure B.30 Cumulative distributions of the target and selected motions for the PPHS SMS site for both the Darfield and Christchurch earthquakes: (a) CAV; (b) I_a; (c) D_{s575} ; and (d) D_{s595}.

Table B.22 Selected ground motion sets for the PPHS SMS site for the Darfield earthquake

NGA No.	Event	M_w	R_{rup} (km)	V_{s30} (m/s)	Pulselike?	Scale Factor
1165	Kocaeli, Turkey	7.51	7.2	811.0	Yes	2.000
143	Tabas, Iran	7.35	2.1	766.8	Yes	0.906
1477	Chi-Chi, Taiwan	7.62	30.2	489.2	Yes	1.153
1492	Chi-Chi, Taiwan	7.62	0.7	579.1	Yes	0.608
165	Imperial Valley-06	6.53	7.3	242.1	No	1.590
180	Imperial Valley-06	6.53	4.0	205.6	Yes	0.923
183	Imperial Valley-06	6.53	3.9	206.1	No	1.153
286	Irpinia, Italy-01	6.9	21.3	496.5	No	1.610
292	Irpinia, Italy-01	6.9	10.8	382.0	Yes	1.156
4875	Chuetsu-oki	6.8	12.0	282.6	Yes	0.636
5810	Iwate	6.9	24.1	655.5	Yes	1.495
68	San Fernando	6.61	22.8	316.5	No	1.082
729	Superstition Hills-02	6.54	23.9	179.0	No	0.747
827	Cape Mendocino	7.01	20.0	457.1	No	2.000
93	San Fernando	6.61	39.5	298.7	No	1.926

Table B.23 Selected ground motion sets for the PPHS SMS site for the Christchurch earthquake

NGA No.	Event	M_w	R_{rup} (km)	V_{s30} (m/s)	Pulselike?	Scale Factor
1004	Northridge-01	6.69	8.4	380.1	Yes	0.555
1013	Northridge-01	6.69	5.9	629.0	Yes	0.987
1078	Northridge-01	6.69	16.7	715.1	No	0.821
126	Gazli, USSR	6.8	5.5	259.6	No	0.500
158	Imperial Valley-06	6.53	0.3	259.9	No	0.929
182	Imperial Valley-06	6.53	0.6	210.5	Yes	0.593
183	Imperial Valley-06	6.53	3.9	206.1	No	1.428
2507	Chi-Chi, Taiwan-03	6.2	25.3	258.9	No	0.780
2655	Chi-Chi, Taiwan-03	6.2	19.3	475.5	No	1.648
3269	Chi-Chi, Taiwan-06	6.3	41.4	544.7	No	1.942
411	Coalinga-05	5.77	16.1	257.4	No	1.707
5810	Iwate	6.9	24.1	655.5	Yes	0.659
68	San Fernando	6.61	22.8	316.5	No	1.715
802	Loma Prieta	6.93	8.5	380.9	Yes	0.714
95	Managua, Nicaragua-01	6.24	4.1	288.8	No	1.951

Pages Road Pumping Station

(PRPC)

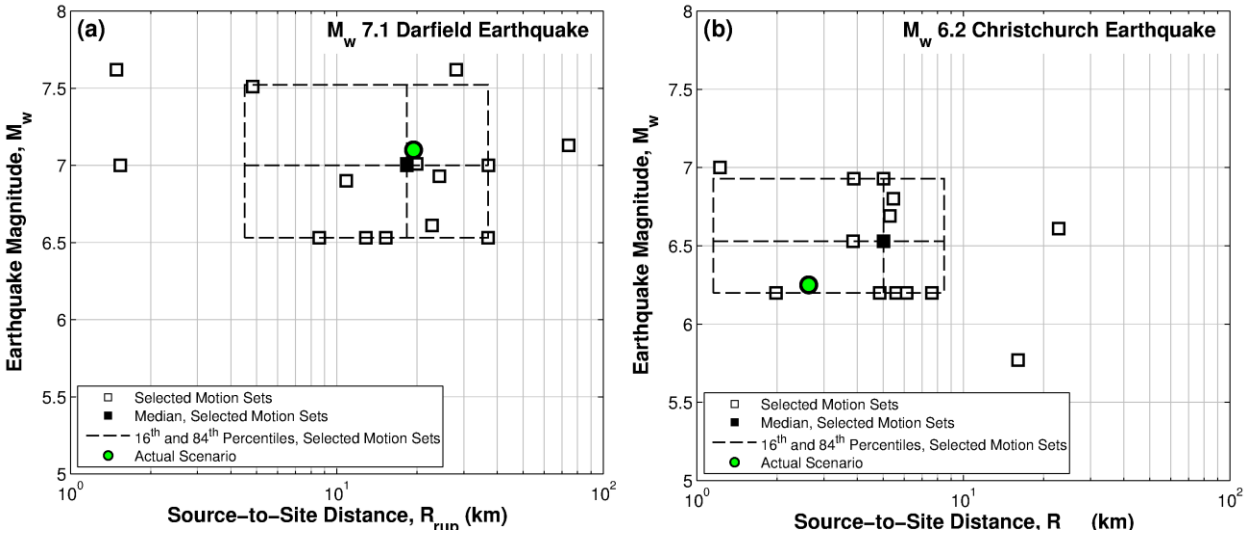

Figure B.31 Distributions of causal parameters, M_w and R_{rup}, for the selected motion sets for both the: (a) Darfield earthquake, and (b) Christchurch earthquake scenarios at the PRPC SMS site.

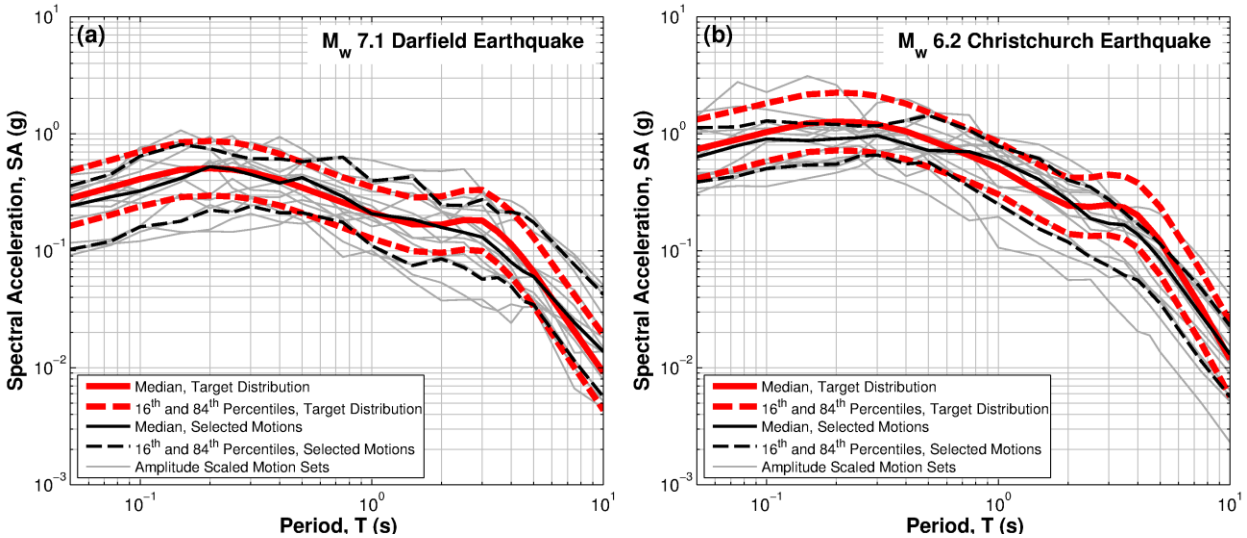

Figure B.32 5% damped response spectra of the target motions and selected motion for the PRPC SMS site for the: (a) Darfield earthquake, and (b) Christchurch earthquake.

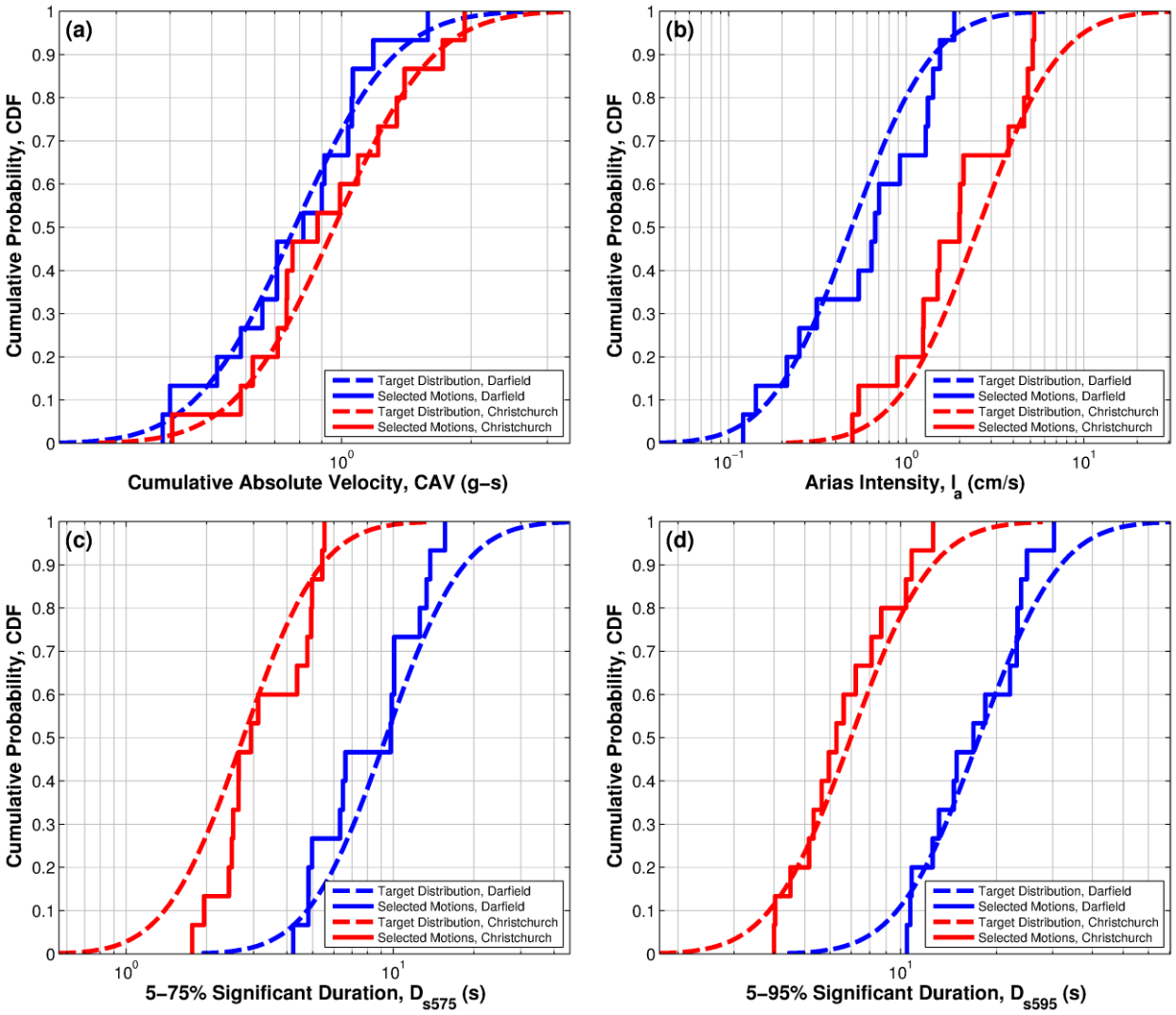

Figure B.33 Cumulative distributions of the target and selected motions for the PRPC SMS site for both the Darfield and Christchurch earthquakes: (a) CAV; (b) I_a; (c) D_{s575} ; and (d) D_{s595}.

Table B.24 Selected ground motion sets for the PRPC SMS site for the Darfield earthquake

NGA No.	Event	M_w	R_{rup} (km)	V_{s30} (m/s)	Pulselike?	Scale Factor
1176	Kocaeli, Turkey	7.51	4.8	297.0	Yes	0.661
1476	Chi-Chi, Taiwan	7.62	28.0	406.5	Yes	0.995
1529	Chi-Chi, Taiwan	7.62	1.5	714.3	Yes	0.892
173	Imperial Valley-06	6.53	8.6	202.9	Yes	1.350
178	Imperial Valley-06	6.53	12.9	162.9	Yes	0.866
1792	Hector Mine	7.13	74.0	282.1	No	0.892
186	Imperial Valley-06	6.53	36.9	212.0	No	1.544
192	Imperial Valley-06	6.53	15.3	193.7	No	2.000
292	Irpinia, Italy-01	6.9	10.8	382.0	Yes	0.564
3746	Cape Mendocino	7.01	18.3	459.0	Yes	0.821
6883	Darfield, New Zealand	7	37.0	295.7	No	1.022
68	San Fernando	6.61	22.8	316.5	No	0.707
6962	Darfield, New Zealand	7	1.5	295.7	Yes	1.230
806	Loma Prieta	6.93	24.2	267.7	No	0.930
827	Cape Mendocino	7.01	20.0	457.1	No	2.000

Table B.25 Selected ground motion sets for the PRPC SMS site for the Christchurch earthquake

NGA No.	Event	M_w	R_{rup} (km)	V_{s30} (m/s)	Pulselike?	Scale Factor
1086	Northridge-01	6.69	5.3	440.5	Yes	1.809
126	Gazli, USSR	6.8	5.5	259.6	No	1.672
171	Imperial Valley-06	6.53	0.1	264.6	Yes	1.401
182	Imperial Valley-06	6.53	0.6	210.5	Yes	1.839
183	Imperial Valley-06	6.53	3.9	206.1	No	1.651
2628	Chi-Chi, Taiwan-03	6.2	7.6	443.0	Yes	1.083
3548	Loma Prieta	6.93	5.0	1070.3	Yes	1.165
412	Coalinga-05	5.77	16.1	257.4	No	2.000
68	San Fernando	6.61	22.8	316.5	No	1.930
6906	Darfield, New Zealand	7	1.2	344.0	Yes	1.646
779	Loma Prieta	6.93	3.9	594.8	No	0.830
8066	Christchurch, New Zealand	6.2	4.9	194.0	Yes	0.675
8119	Christchurch, New Zealand	6.2	2.0	206.0	Yes	2.000
8130	Christchurch, New Zealand	6.2	5.6	207.0	Yes	1.424
8158	Christchurch, New Zealand	6.2	6.1	649.7	Yes	1.538

Christchurch Resthaven

(REHS)

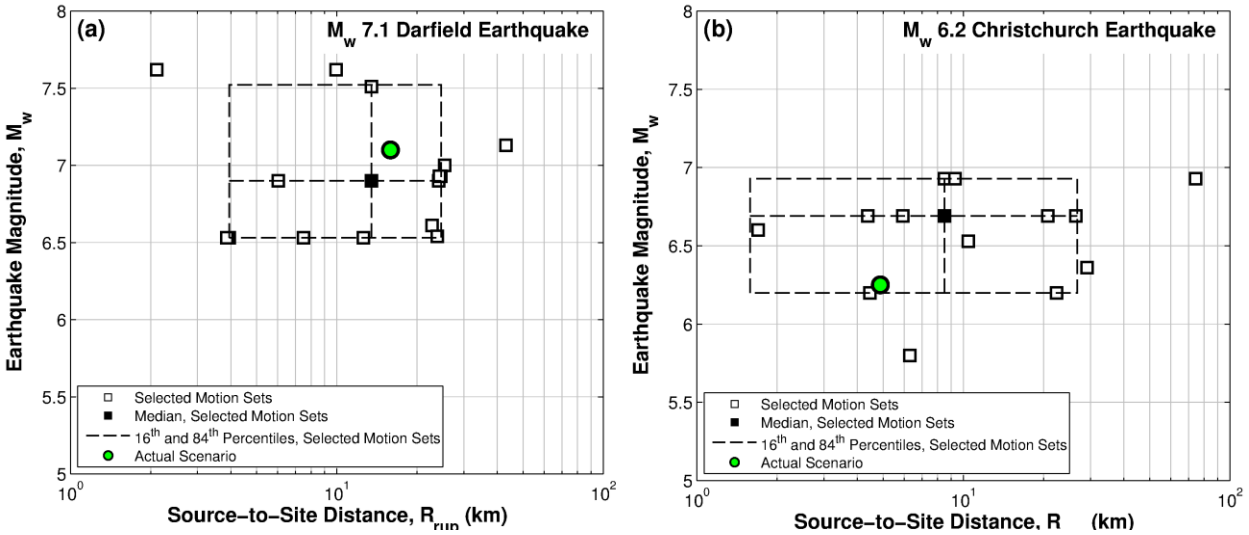

Figure B.34 Distributions of causal parameters, M_w and R_{rup}, for the selected motion sets for both the: (a) Darfield earthquake, and (b) Christchurch earthquake scenarios at the REHS SMS site.

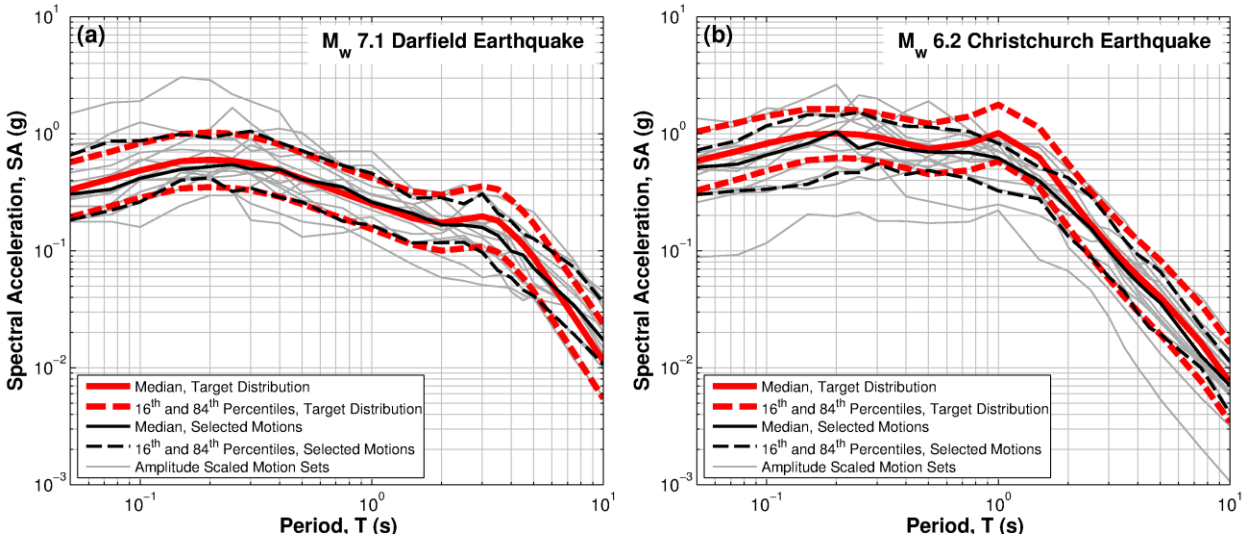

Figure B.35 5% damped response spectra of the target motions and selected motion for the REHS SMS site for the: (a) Darfield earthquake, and (b) Christchurch earthquake.

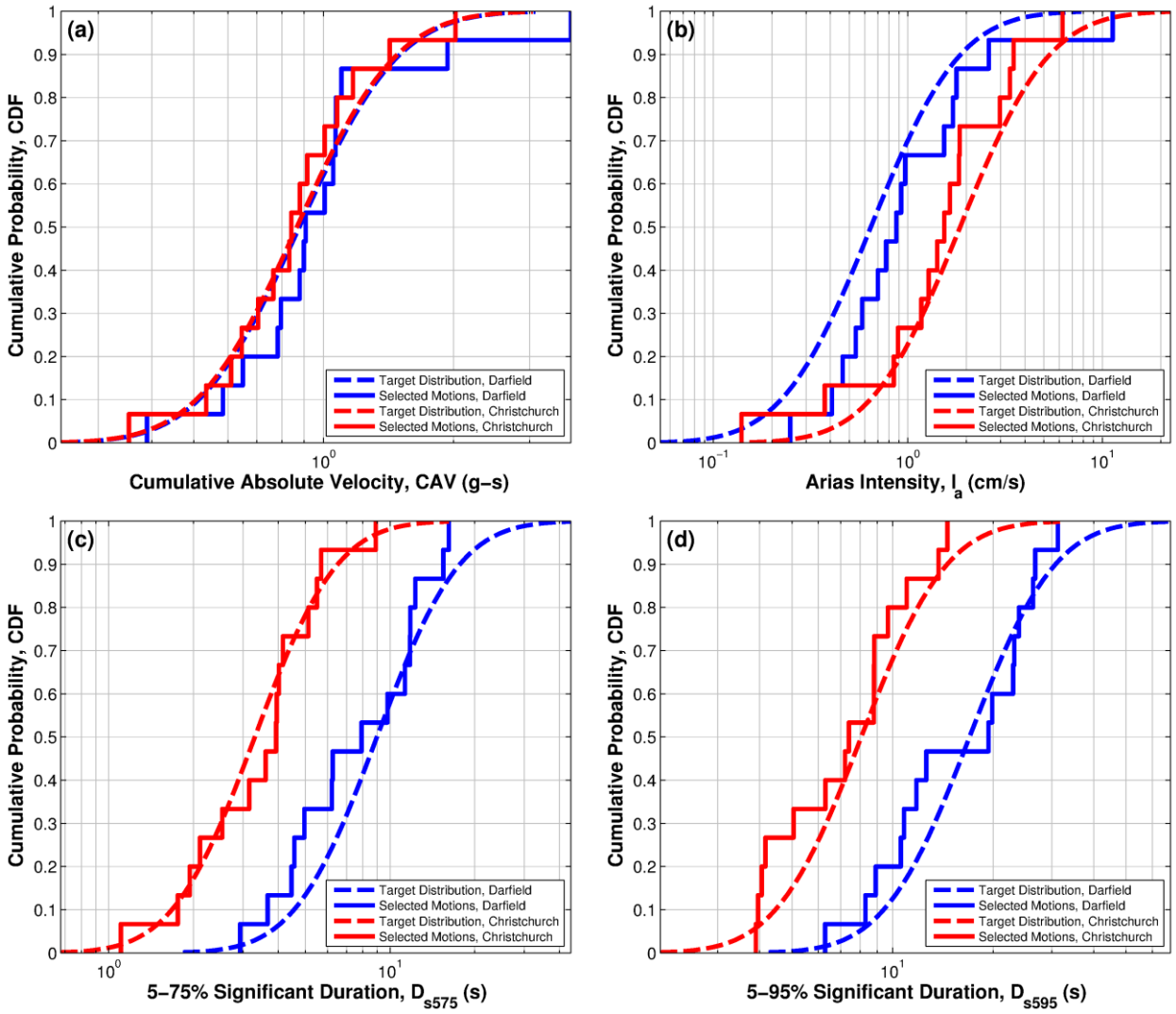

Figure B.36 Cumulative distributions of the target and selected motions for the REHS SMS site for both the Darfield and Christchurch earthquakes: (a) CAV; (b) I_a; (c) D_{s575} ; and (d) D_{s595}.

Table B.26 Selected ground motion sets for the REHS SMS site for the Darfield earthquake

NGA No.	Event	M_w	R_{rup} (km)	V_{s30} (m/s)	Pulselike?	Scale Factor
1148	Kocaeli, Turkey	7.51	13.5	523.0	Yes	1.139
1528	Chi-Chi, Taiwan	7.62	2.1	389.4	Yes	0.914
1595	Chi-Chi, Taiwan	7.62	9.9	258.9	Yes	0.655
174	Imperial Valley-06	6.53	12.6	196.3	No	0.745
1762	Hector Mine	7.13	43.1	382.9	No	1.136
180	Imperial Valley-06	6.53	4.0	205.6	Yes	0.654
183	Imperial Valley-06	6.53	3.9	206.1	No	0.645
185	Imperial Valley-06	6.53	7.5	202.9	Yes	1.763
5658	Iwate	6.9	6.0	371.1	Yes	1.762
5810	Iwate	6.9	24.1	655.5	Yes	0.870
68	San Fernando	6.61	22.8	316.5	No	1.140
6912	Darfield, New Zealand	7	25.4	206.0	No	0.622
729	Superstition Hills-02	6.54	23.9	179.0	No	1.045
737	Loma Prieta	6.93	24.6	239.7	No	1.525
806	Loma Prieta	6.93	24.2	267.7	No	0.888

Table B.27 Selected ground motion sets for the REHS SMS site for the Christchurch earthquake

NGA No.	Event	M_w	R_{rup} (km)	V_{s30} (m/s)	Pulselike?	Scale Factor
1013	Northridge-01	6.69	5.9	629.0	Yes	1.180
1077	Northridge-01	6.69	26.5	336.2	No	1.191
1119	Kobe, Japan	6.9	0.3	312.0	Yes	1.785
161	Imperial Valley-06	6.53	10.4	208.7	Yes	2.000
2495	Chi-Chi, Taiwan-03	6.2	22.4	496.2	Yes	2.000
360	Coalinga-01	6.36	29.1	284.2	No	1.967
4040	Bam, Iran	6.6	1.7	487.4	Yes	0.881
451	Morgan Hill	6.19	0.5	561.4	Yes	0.678
568	San Salvador	5.8	6.3	489.3	Yes	1.585
783	Loma Prieta	6.93	74.3	248.6	Yes	1.846
802	Loma Prieta	6.93	8.5	380.9	Yes	0.551
803	Loma Prieta	6.93	9.3	347.9	Yes	2.000
8067	Christchurch, New Zealand	6.2	4.5	204.0	Yes	0.954
821	Erzican, Turkey	6.69	4.4	352.1	No	0.748
963	Northridge-01	6.69	20.7	450.3	No	1.426

Riccarton High School

(RHSC)

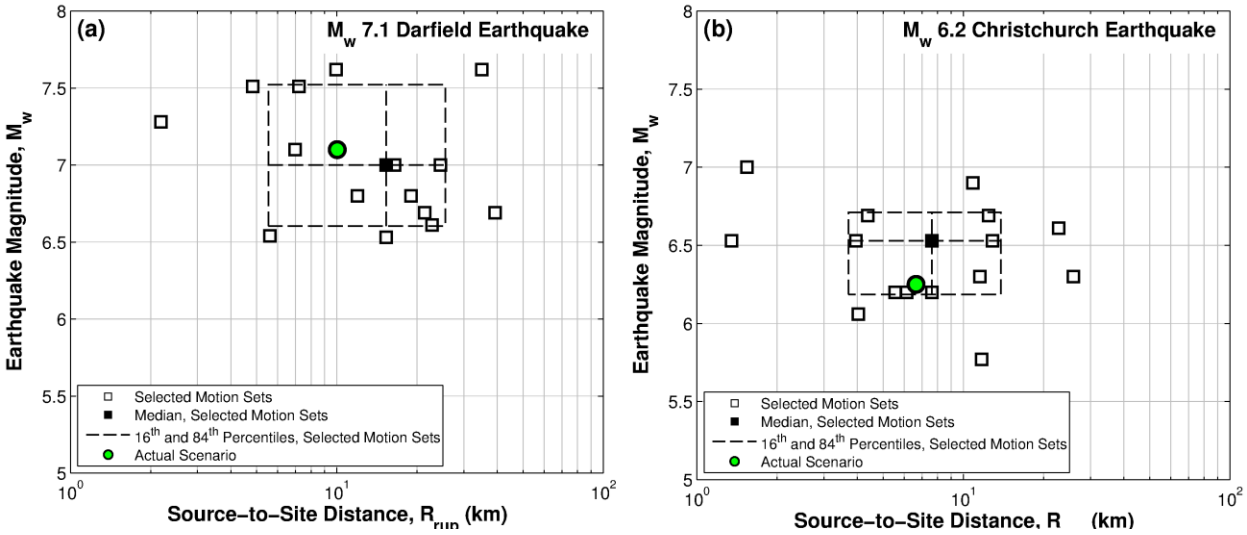

Figure B.37 Distributions of causal parameters, M_w and R_{rup}, for the selected motion sets for both the: (a) Darfield earthquake, and (b) Christchurch earthquake scenarios at the RHSC SMS site.

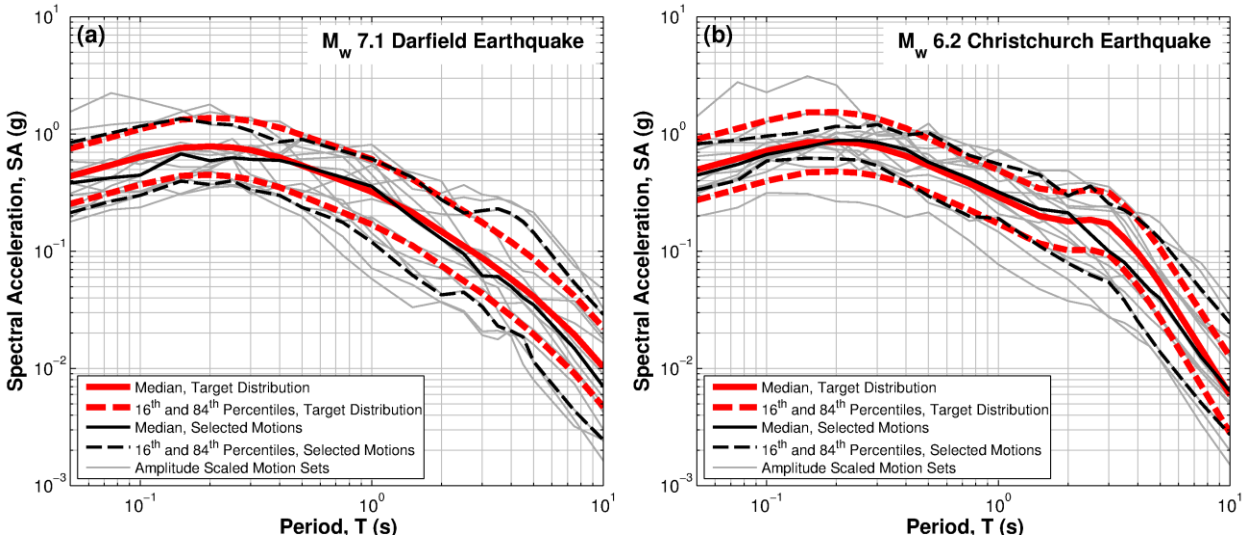

Figure B.38 5% damped response spectra of the target motions and selected motion for the RHSC SMS site for the: (a) Darfield earthquake, and (b) Christchurch earthquake.

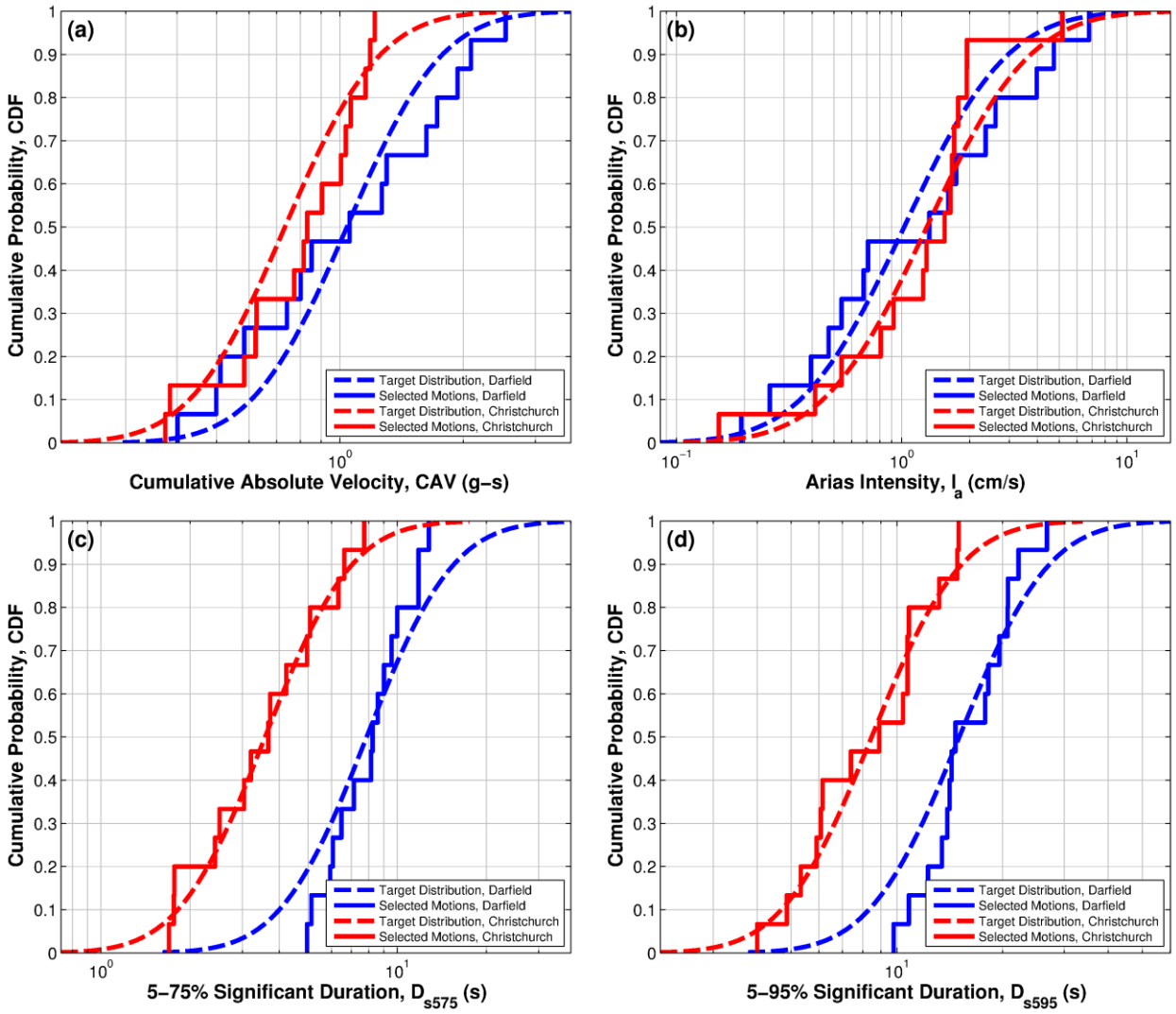

Figure B.39 Cumulative distributions of the target and selected motions for the RHSC SMS site for both the Darfield and Christchurch earthquakes: (a) CAV; (b) I_a; (c) D_{s575} ; and (d) D_{s595}.

Table B.28 Selected ground motion sets for the RHSC SMS site for the Darfield earthquake

NGA No.	Event	M_w	R_{rup} (km)	V_{s30} (m/s)	Pulselike?	Scale Factor
1020	Northridge-01	6.69	21.4	602.1	No	1.779
1035	Northridge-01	6.69	39.3	351.6	No	2.000
1165	Kocaeli, Turkey	7.51	7.2	811.0	Yes	1.099
1176	Kocaeli, Turkey	7.51	4.8	297.0	Yes	0.844
1487	Chi-Chi, Taiwan	7.62	35.0	520.4	Yes	1.699
1595	Chi-Chi, Taiwan	7.62	9.9	258.9	Yes	1.424
167	Imperial Valley-06	6.53	15.3	259.9	No	1.451
4451	Montenegro, Yugo.	7.1	7.0	462.2	Yes	0.802
4847	Chuetsu-oki	6.8	11.9	383.4	Yes	1.311
4879	Chuetsu-oki	6.8	19.0	265.8	Yes	2.000
68	San Fernando	6.61	22.8	316.5	No	1.947
6915	Darfield, New Zealand	7	24.5	422.0	No	1.165
6961	Darfield, New Zealand	7	16.5	295.7	No	2.000
727	Superstition Hills-02	6.54	5.6	362.4	No	1.056
879	Landers	7.28	2.2	1369.0	Yes	0.640

Table B.29 Selected ground motion sets for the RHSC SMS site for the Christchurch earthquake

NGA No.	Event	M_w	R_{rup} (km)	V_{s30} (m/s)	Pulselike?	Scale Factor
178	Imperial Valley-06	6.53	12.9	162.9	Yes	1.882
180	Imperial Valley-06	6.53	4.0	205.6	Yes	0.930
181	Imperial Valley-06	6.53	1.4	203.2	Yes	1.596
2628	Chi-Chi, Taiwan-03	6.2	7.6	443.0	Yes	1.456
292	Irpinia, Italy-01	6.9	10.8	382.0	Yes	1.675
3472	Chi-Chi, Taiwan-06	6.3	25.9	615.0	No	1.862
3473	Chi-Chi, Taiwan-06	6.3	11.5	443.0	Yes	0.574
413	Coalinga-05	5.77	11.7	480.3	No	0.592
529	N. Palm Springs	6.06	4.0	344.7	No	1.198
68	San Fernando	6.61	22.8	316.5	No	0.806
6962	Darfield, New Zealand	7	1.5	295.7	Yes	0.603
8063	Christchurch, New Zealand	6.2	5.6	187.0	No	0.869
8158	Christchurch, New Zealand	6.2	6.1	649.7	Yes	0.792
821	Erzican, Turkey	6.69	4.4	352.1	No	1.058
960	Northridge-01	6.69	12.4	325.6	No	1.166

Shirley Library

(SHLC)

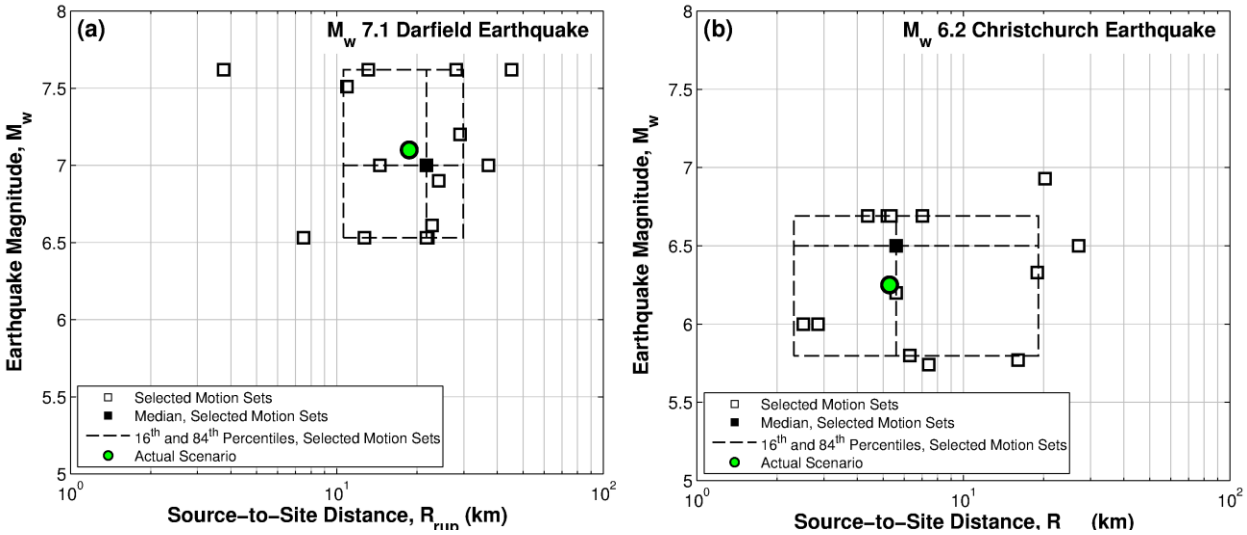

Figure B.40 Distributions of causal parameters, M_w and R_{rup}, for the selected motion sets for both the: (a) Darfield earthquake, and (b) Christchurch earthquake scenarios at the SHLC SMS site.

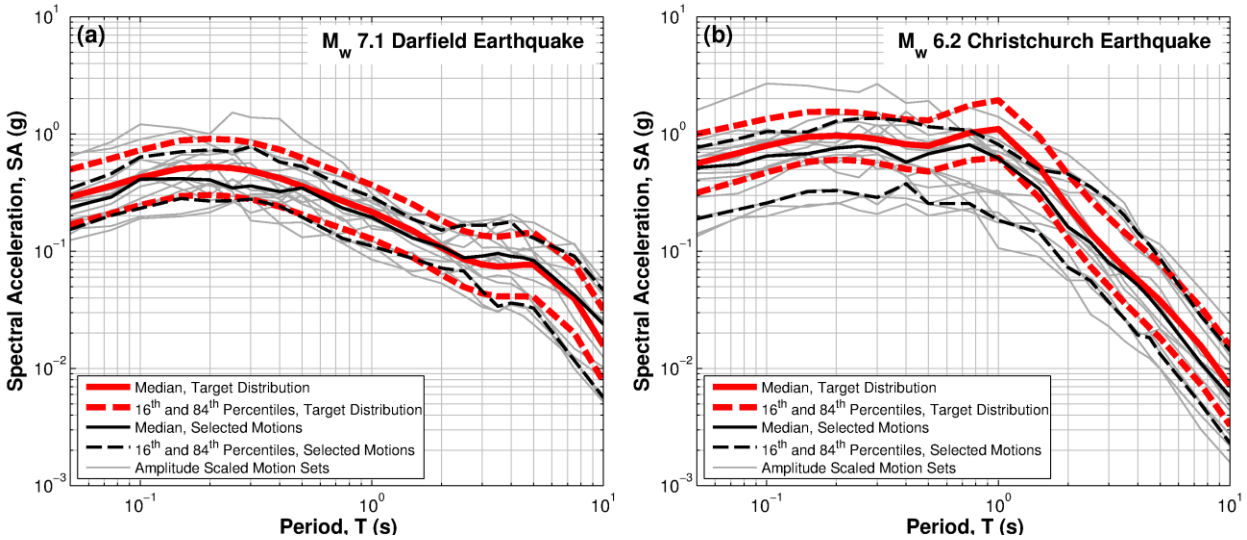

Figure B.41 5% damped response spectra of the target motions and selected motion for the SHLC SMS site for the: (a) Darfield earthquake, and (b) Christchurch earthquake.

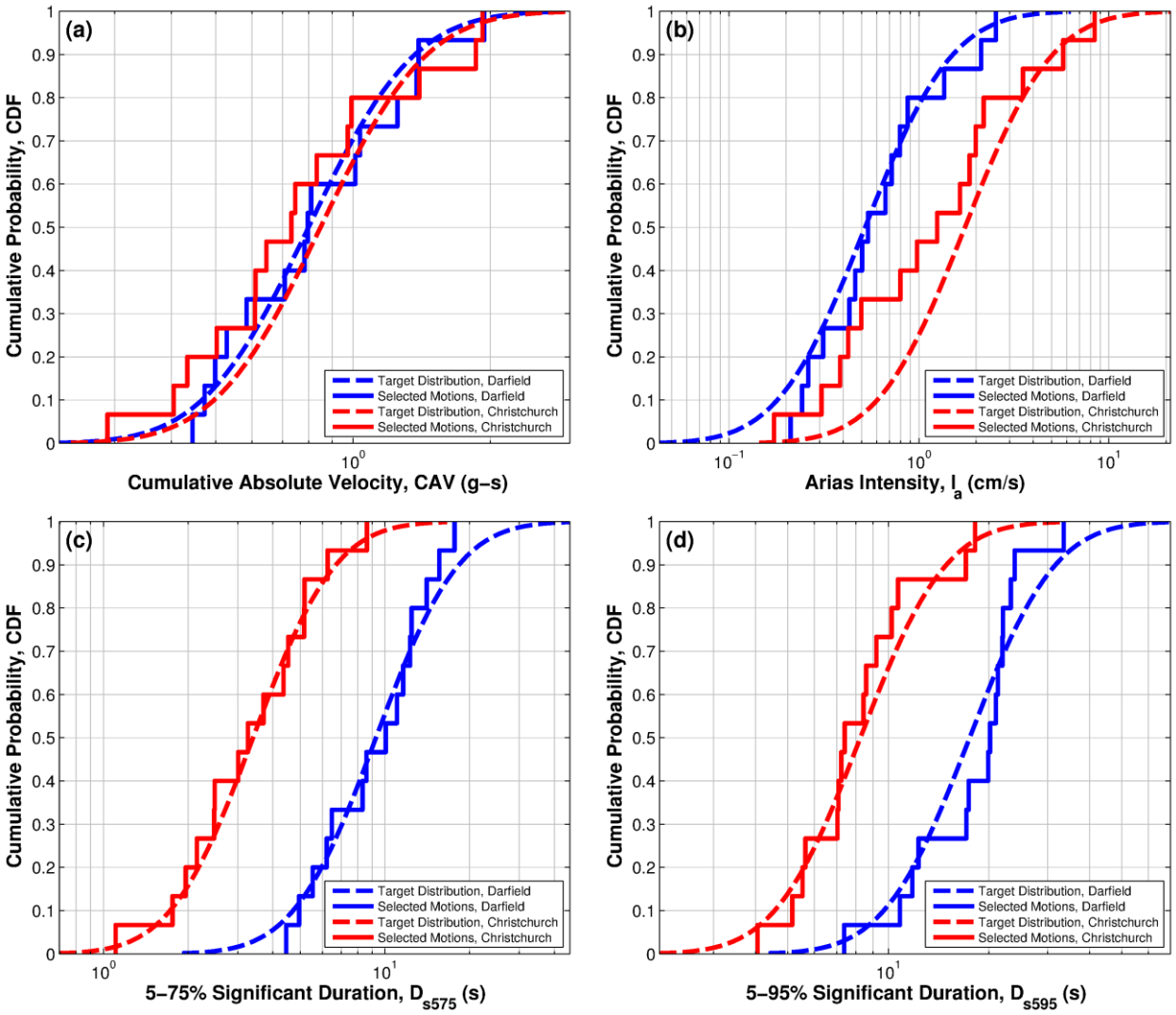

Figure B.42 Cumulative distributions of the target and selected motions for the SHLC SMS site for both the Darfield and Christchurch earthquakes: (a) CAV; (b) I_a; (c) D_{s575} ; and (d) D_{s595}.

Table B.30 Selected ground motion sets for the SHLC SMS site for the Darfield earthquake

NGA No.	Event	M_w	R_{rup} (km)	V_{s30} (m/s)	Pulselike?	Scale Factor
1161	Kocaeli, Turkey	7.51	10.9	792.0	Yes	1.092
1403	Chi-Chi, Taiwan	7.62	13.1	599.6	Yes	0.873
1476	Chi-Chi, Taiwan	7.62	28.0	406.5	Yes	0.857
1489	Chi-Chi, Taiwan	7.62	3.8	487.3	Yes	0.945
1524	Chi-Chi, Taiwan	7.62	45.2	446.6	Yes	0.902
1548	Chi-Chi, Taiwan	7.62	13.1	599.6	Yes	0.530
172	Imperial Valley-06	6.53	21.7	237.3	No	2.000
176	Imperial Valley-06	6.53	22.0	249.9	No	1.054
185	Imperial Valley-06	6.53	7.5	202.9	Yes	1.173
187	Imperial Valley-06	6.53	12.7	348.7	No	1.532
5810	Iwate	6.9	24.1	655.5	Yes	1.182
5836	El Mayor-Cucapah	7.2	29.0	264.6	No	0.500
6883	Darfield, New Zealand	7	37.0	295.7	No	1.745
6886	Darfield, New Zealand	7	14.5	280.3	No	0.699
68	San Fernando	6.61	22.8	316.5	No	1.371

Table B.31 Selected ground motion sets for the SHLC SMS site for the Christchurch earthquake

NGA No.	Event	M_w	R_{rup} (km)	V_{s30} (m/s)	Pulselike?	Scale Factor
1051	Northridge-01	6.69	7.0	2016.1	Yes	1.087
1084	Northridge-01	6.69	5.4	251.2	Yes	0.500
1085	Northridge-01	6.69	5.2	370.5	Yes	0.997
148	Coyote Lake	5.74	7.4	349.9	Yes	2.000
158	Imperial Valley-06	6.53	0.3	259.9	No	1.043
182	Imperial Valley-06	6.53	0.6	210.5	Yes	2.000
20	Northern Calif-03	6.5	27.0	219.3	Yes	2.000
266	Victoria, Mexico	6.33	19.0	242.1	No	0.823
4107	Parkfield-02, CA	6	2.5	178.3	Yes	1.324
4113	Parkfield-02, CA	6	2.9	372.3	Yes	1.668
412	Coalinga-05	5.77	16.1	257.4	No	1.783
568	San Salvador	5.8	6.3	489.3	Yes	1.923
739	Loma Prieta	6.93	20.3	488.8	No	1.039
8130	Christchurch, New Zealand	6.2	5.6	207.0	Yes	0.570
821	Erzican, Turkey	6.69	4.4	352.1	No	1.949

Styx Mill Transfer Station

(SMTC)

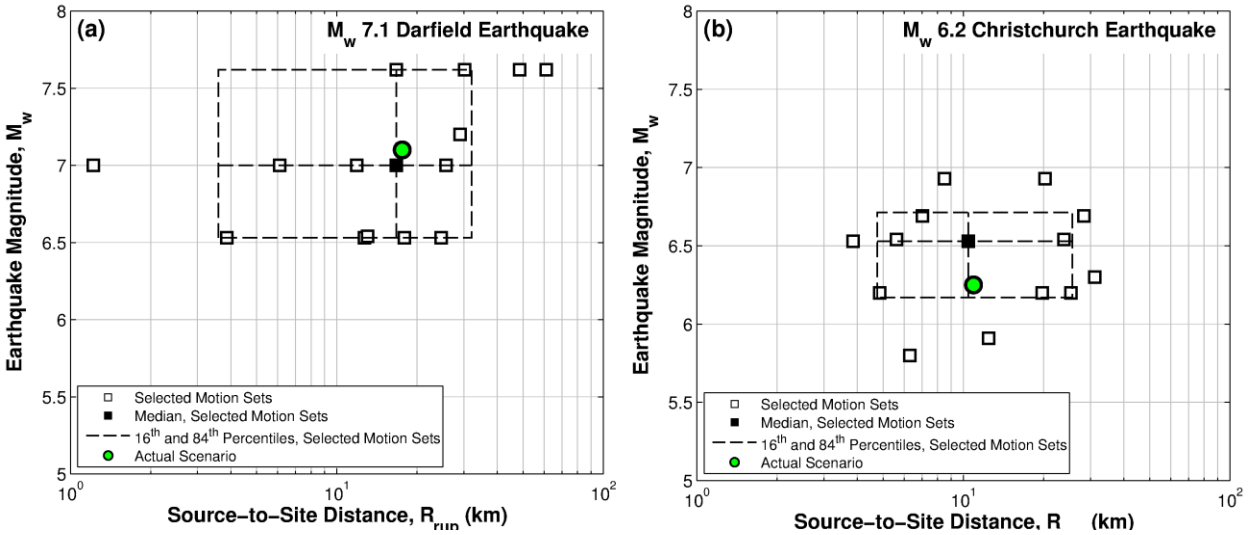

Figure B.43 Distributions of causal parameters, M_w and R_{rup}, for the selected motion sets for both the: (a) Darfield earthquake, and (b) Christchurch earthquake scenarios at the SMTC SMS site.

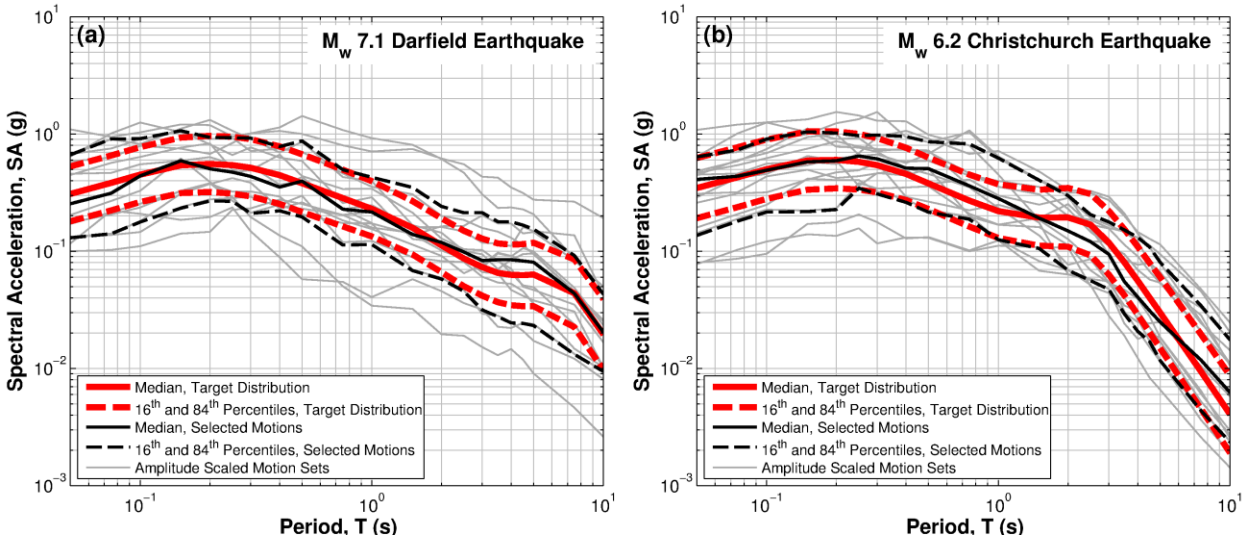

Figure B.44 5% damped response spectra of the target motions and selected motion for the SMTC SMS site for the: (a) Darfield earthquake, and (b) Christchurch earthquake.

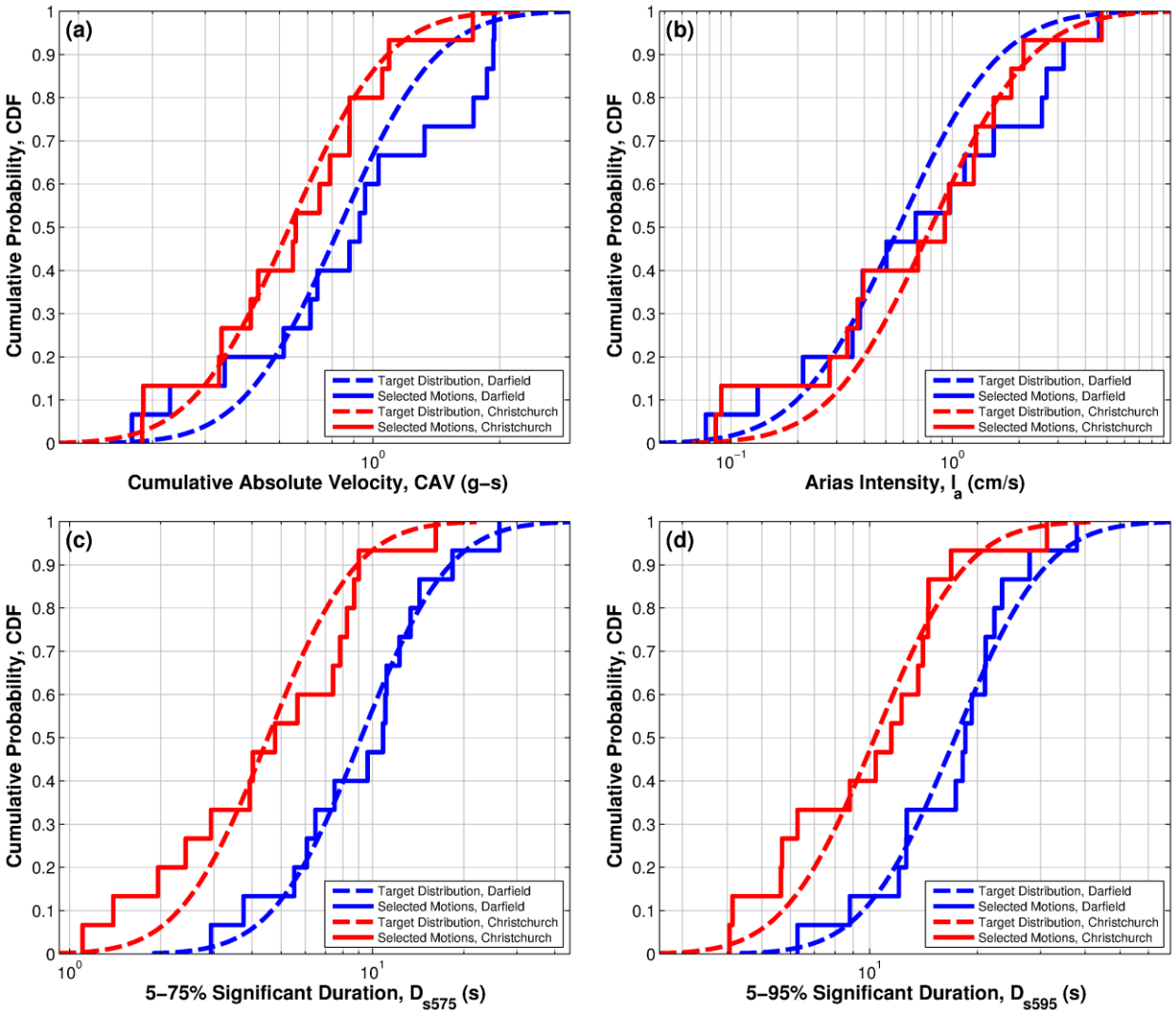

Figure B.45 Cumulative distributions of the target and selected motions for the SMTC SMS site for both the Darfield and Christchurch earthquakes: (a) CAV; (b) I_a; (c) D_{s575} ; and (d) D_{s595}.

Table B.32 Selected ground motion sets for the SMTC SMS site for the Darfield earthquake

NGA No.	Event	M_w	R_{rup} (km)	V_{s30} (m/s)	Pulselike?	Scale Factor
1212	Chi-Chi, Taiwan	7.62	48.5	172.1	No	1.433
1347	Chi-Chi, Taiwan	7.62	61.1	996.5	No	1.801
1477	Chi-Chi, Taiwan	7.62	30.2	489.2	Yes	1.079
1486	Chi-Chi, Taiwan	7.62	16.7	465.6	Yes	0.968
1505	Chi-Chi, Taiwan	7.62	0.3	487.3	Yes	0.575
175	Imperial Valley-06	6.53	17.9	196.9	No	1.639
183	Imperial Valley-06	6.53	3.9	206.1	No	0.616
187	Imperial Valley-06	6.53	12.7	348.7	No	0.964
190	Imperial Valley-06	6.53	24.6	362.4	No	2.000
5836	El Mayor-Cucapah	7.2	29.0	264.6	No	0.658
6893	Darfield, New Zealand	7	11.9	344.0	No	0.500
6906	Darfield, New Zealand	7	1.2	344.0	Yes	0.614
6928	Darfield, New Zealand	7	25.7	649.7	Yes	1.619
6975	Darfield, New Zealand	7	6.1	249.3	Yes	0.838
728	Superstition Hills-02	6.54	13.0	193.7	No	1.173

Table B.33 Selected ground motion sets for the SMTC SMS site for the Christchurch earthquake

NGA No.	Event	M_w	R_{rup} (km)	V_{s30} (m/s)	Pulselike?	Scale Factor
1050	Northridge-01	6.69	7.0	2016.1	Yes	0.964
161	Imperial Valley-06	6.53	10.4	208.7	Yes	0.619
182	Imperial Valley-06	6.53	0.6	210.5	Yes	0.663
183	Imperial Valley-06	6.53	3.9	206.1	No	0.516
236	Mammoth Lakes-03	5.91	12.4	382.1	No	1.823
2507	Chi-Chi, Taiwan-03	6.2	25.3	258.9	No	1.310
2699	Chi-Chi, Taiwan-04	6.2	19.7	427.7	No	2.000
3264	Chi-Chi, Taiwan-06	6.3	31.1	427.7	No	1.198
568	San Salvador	5.8	6.3	489.3	Yes	0.584
727	Superstition Hills-02	6.54	5.6	362.4	No	0.569
729	Superstition Hills-02	6.54	23.9	179.0	No	1.926
740	Loma Prieta	6.93	20.3	488.8	No	1.596
802	Loma Prieta	6.93	8.5	380.9	Yes	0.500
8066	Christchurch, New Zealand	6.2	4.9	194.0	Yes	0.500
987	Northridge-01	6.69	28.3	321.9	No	1.094

Appendix C: Profiles of MSF for the Christchurch SMS Sites

Profiles of MSF computed for both the M_w7.1 Darfield earthquake and the M_w6.2 Christchurch at each SMS using the Seed et al. (1975) and Green and Terri (2005) approaches for computing number of equivalent cycles are presented in Appendix C. The median, 16th and 84th percentile of the MSF values computed at the surface (per Seed et al. (1975)) and at the mid depth of the discretized soil layers (per Green and Terri (2005)) are represented in the plots. Also highlighted are the values computed at the critical layer corresponding to the lowest FS and at the reference depth where σ'_v = 1 atm. Further details on the critical depths at these sites can be found in Wotherspoon et al. (2015a,b).

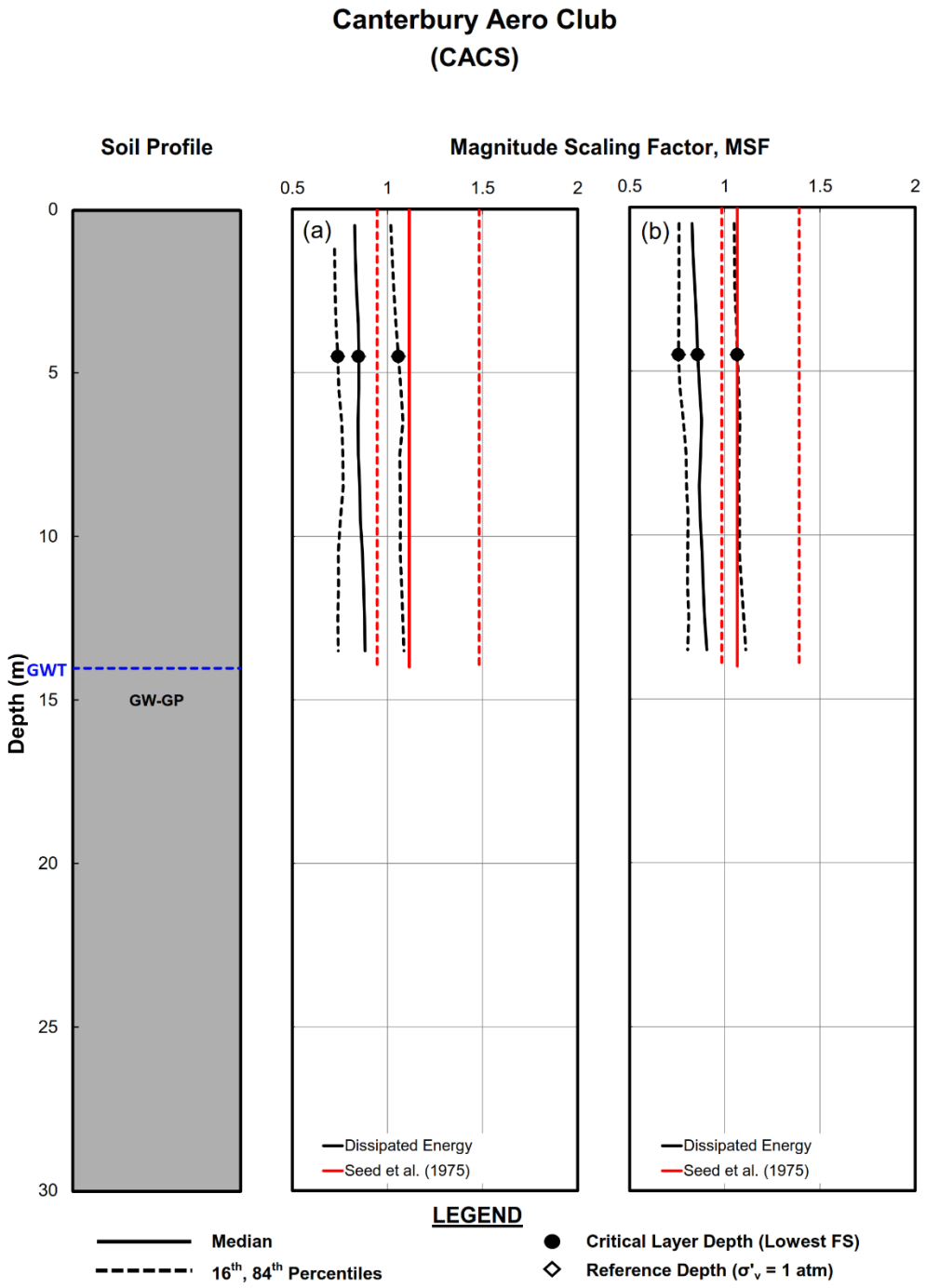

Figure C.1 MSF computed for the Canterbury Aero Club (CACS) SMS site using the Green and Terri (2005) and Seed et al. (1975) approaches for computing number of equivalent cycles for: (a) Darfield earthquake, and (b) Christchurch earthquake.

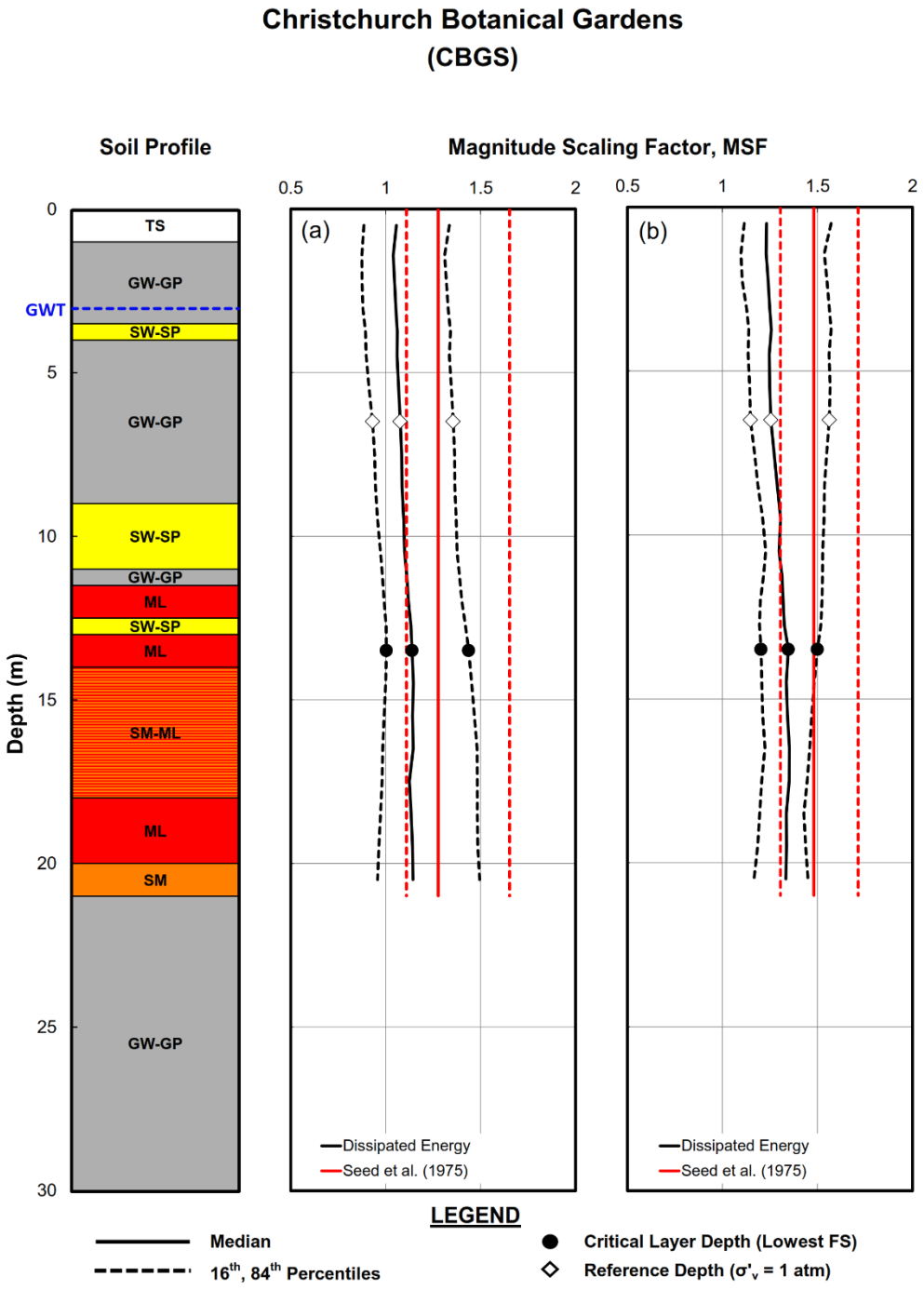

Figure C.2 MSF computed for the Christchurch Botanical Gardens (CBGS) SMS site using the Green and Terri (2005) and Seed et al. (1975) approaches for computing number of equivalent cycles for: (a) Darfield earthquake, and (b) Christchurch earthquake.

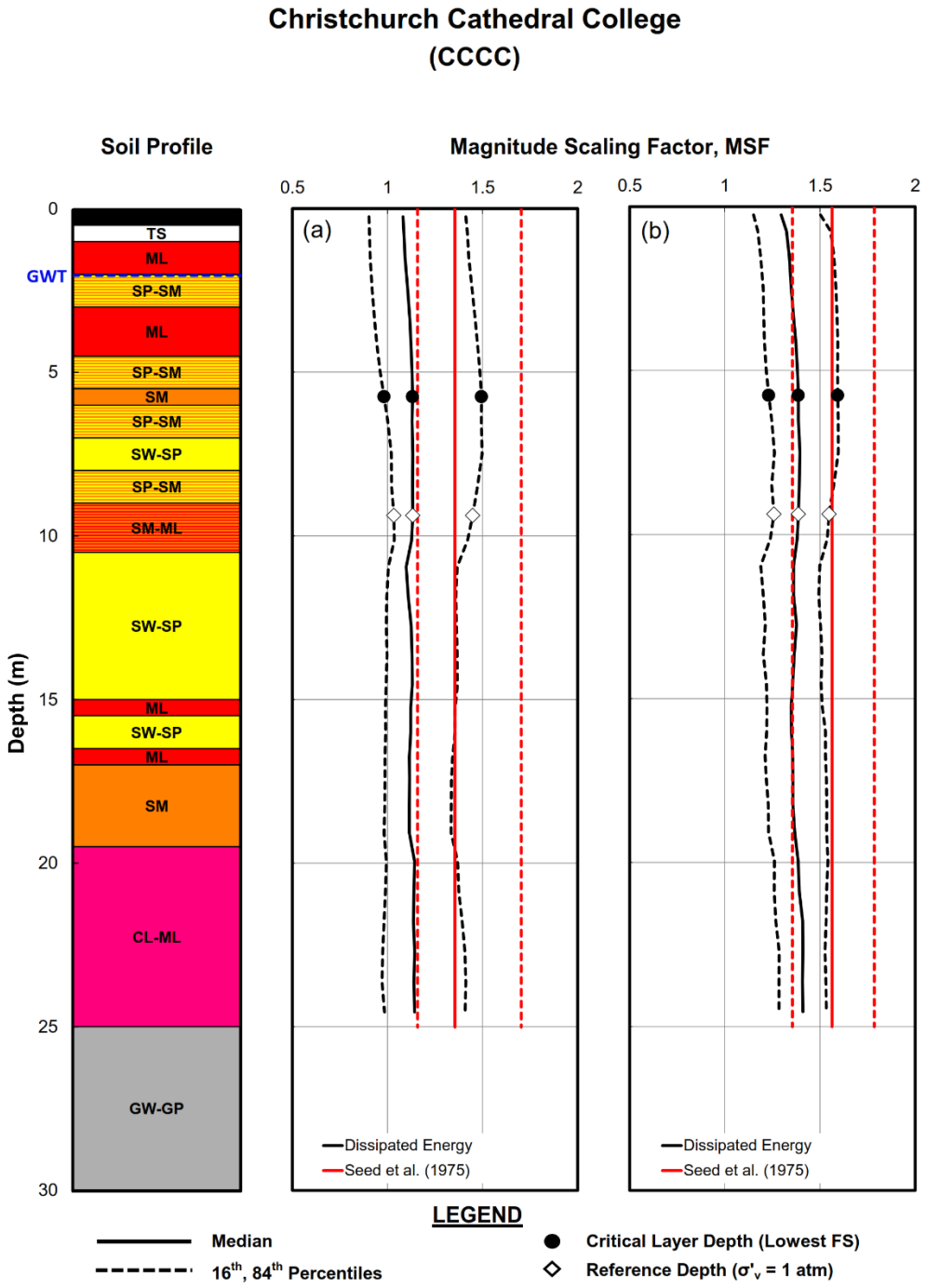

Figure C.3 MSF computed for the Christchurch Cathedral College (CCCC) SMS site using the Green and Terri (2005) and Seed et al. (1975) approaches for computing number of equivalent cycles for: (a) Darfield earthquake, and (b) Christchurch earthquake.

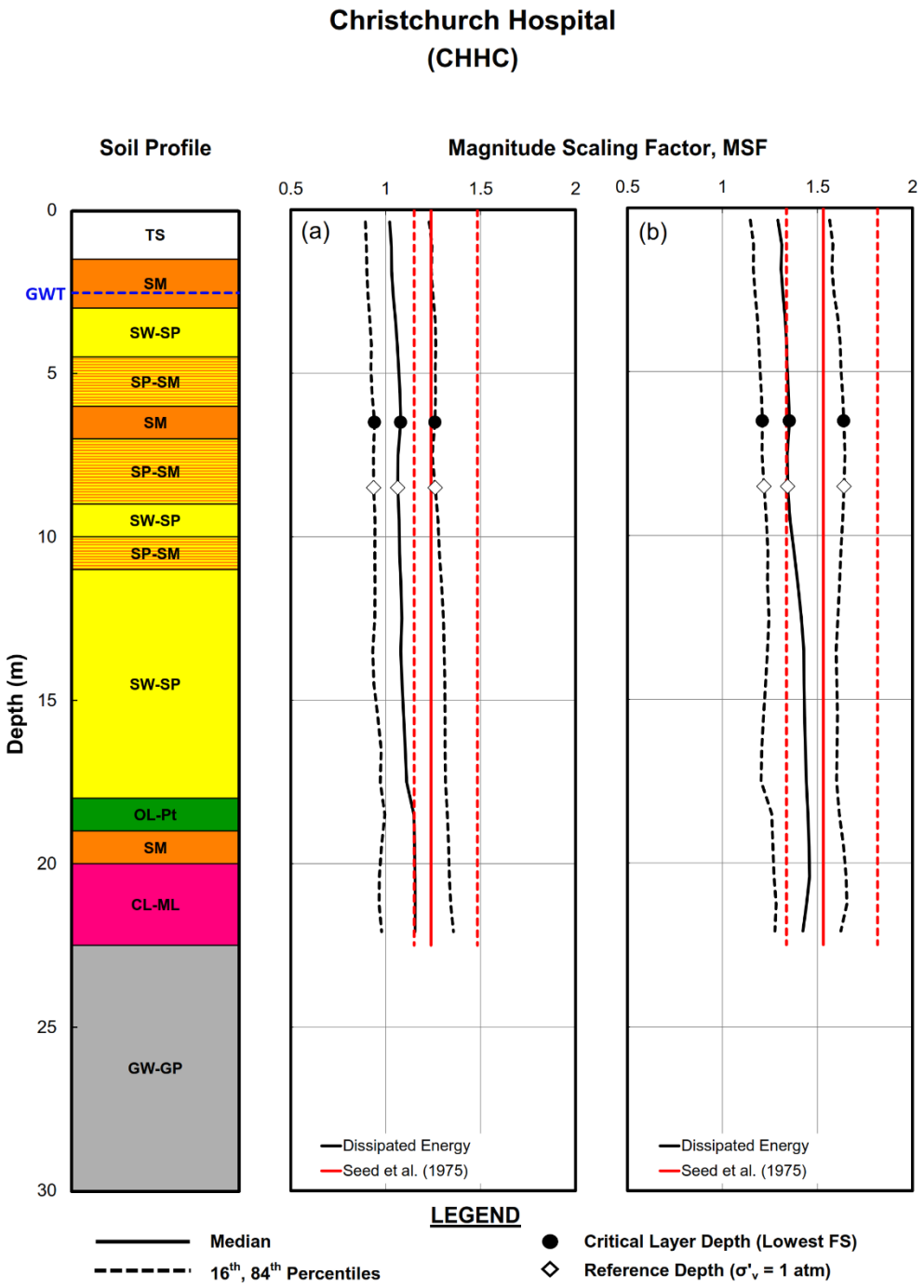

Figure C.4 MSF computed for the Christchurch Hospital (CHHC) SMS site using the Green and Terri (2005) and Seed et al. (1975) approaches for computing number of equivalent cycles for: (a) Darfield earthquake, and (b) Christchurch earthquake.

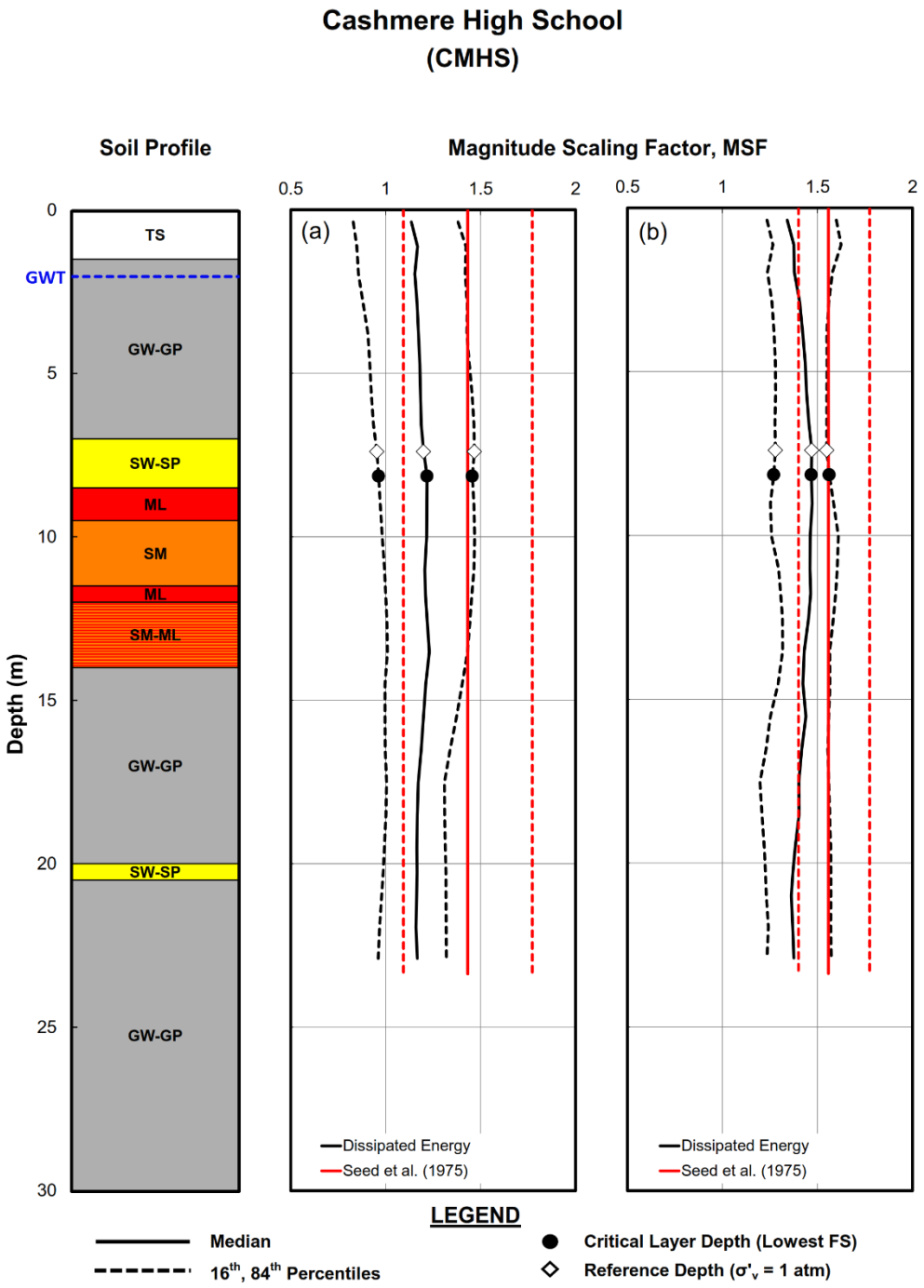

Figure C.5 MSF computed for the Cashmere High School (CMHS) SMS site using the Green and Terri (2005) and Seed et al. (1975) approaches for computing number of equivalent cycles for: (a) Darfield earthquake, and (b) Christchurch earthquake.

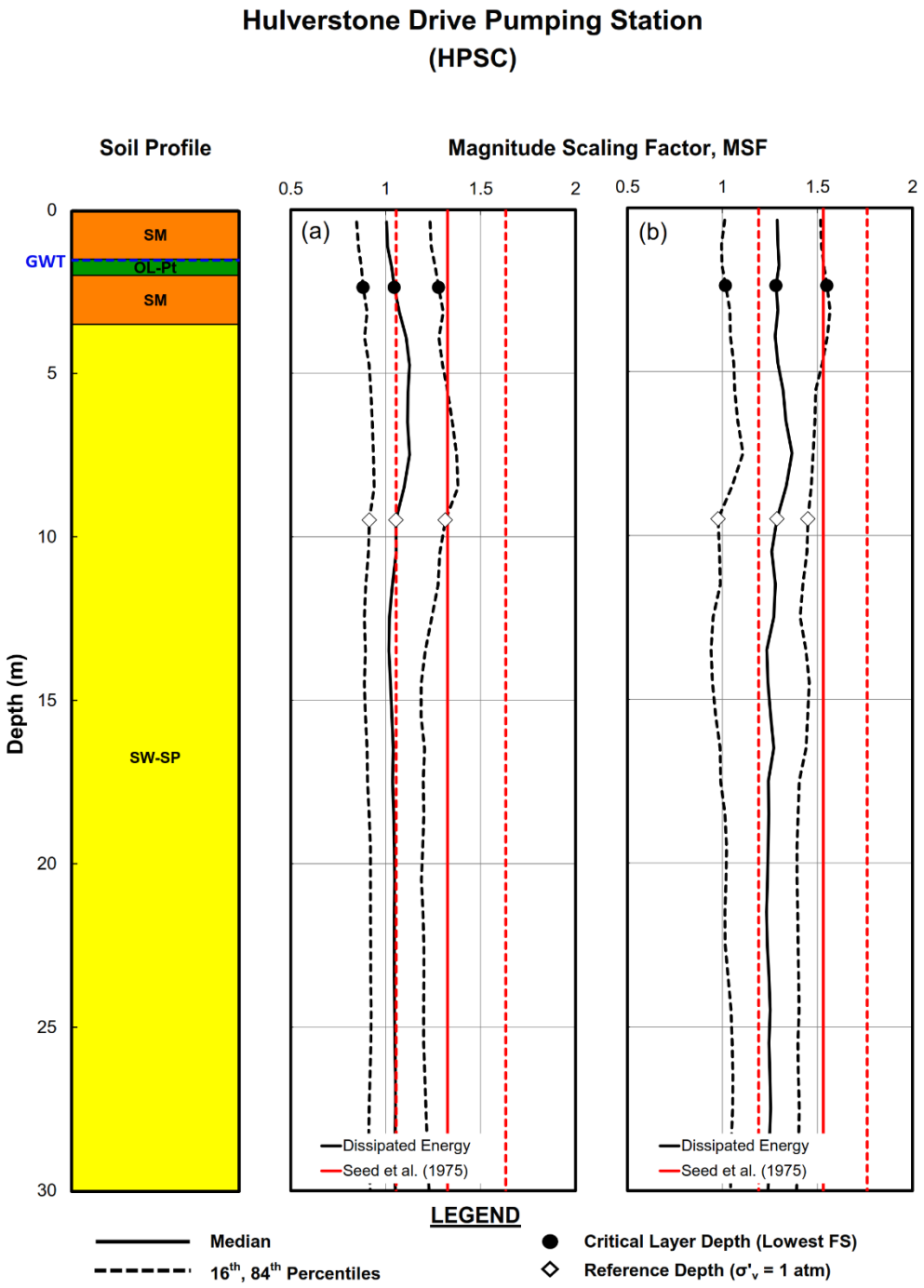

Figure C.6 MSF computed for the Hulverstone Drive Pumping Station (HPSC) SMS site using the Green and Terri (2005) and Seed et al. (1975) approaches for computing number of equivalent cycles for: (a) Darfield earthquake, and (b) Christchurch earthquake.

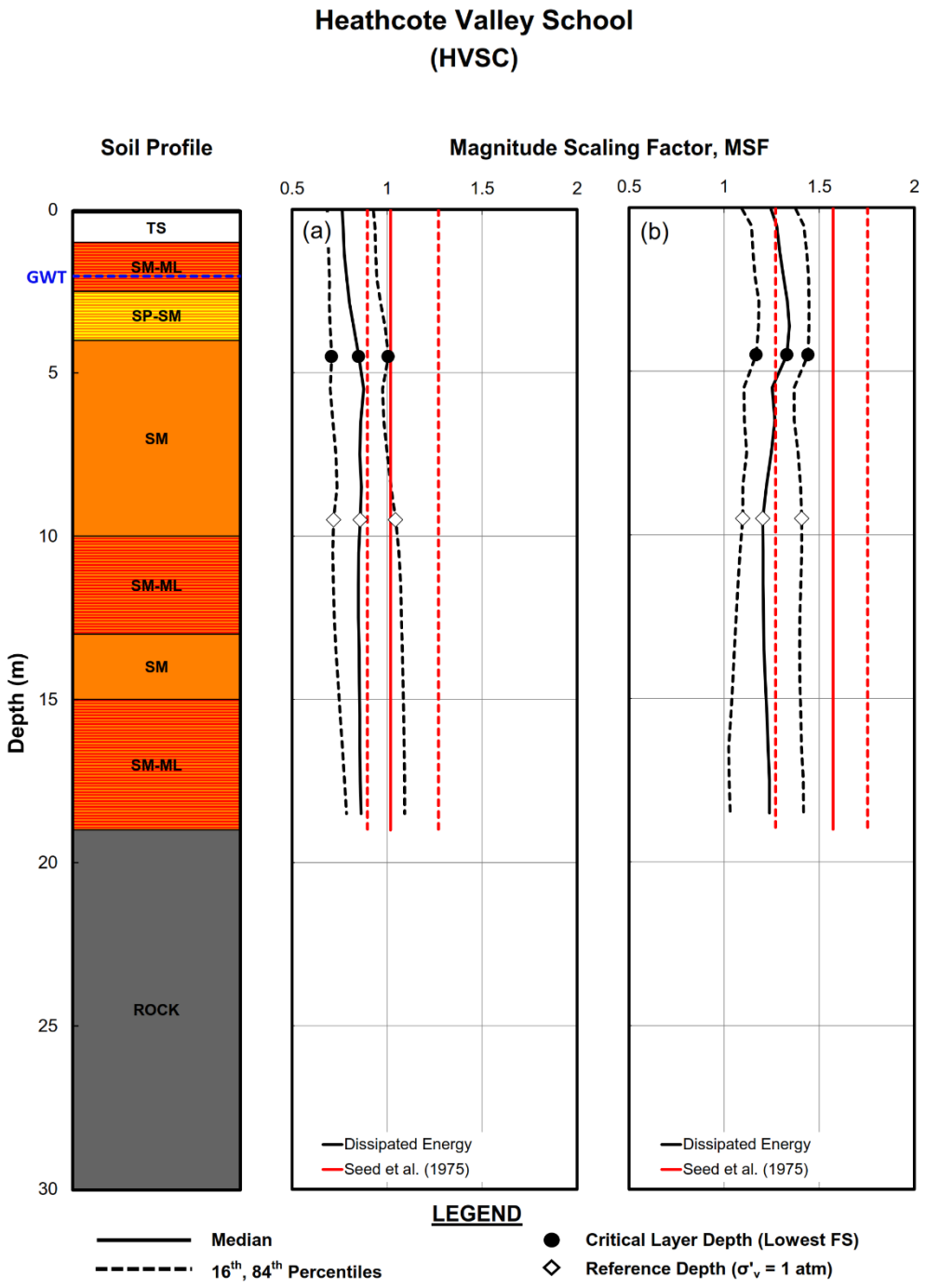

Figure C.7 MSF computed for the Heathcote Valley School (HVSC) SMS site using the Green and Terri (2005) and Seed et al. (1975) approaches for computing number of equivalent cycles for: (a) Darfield earthquake, and (b) Christchurch earthquake.

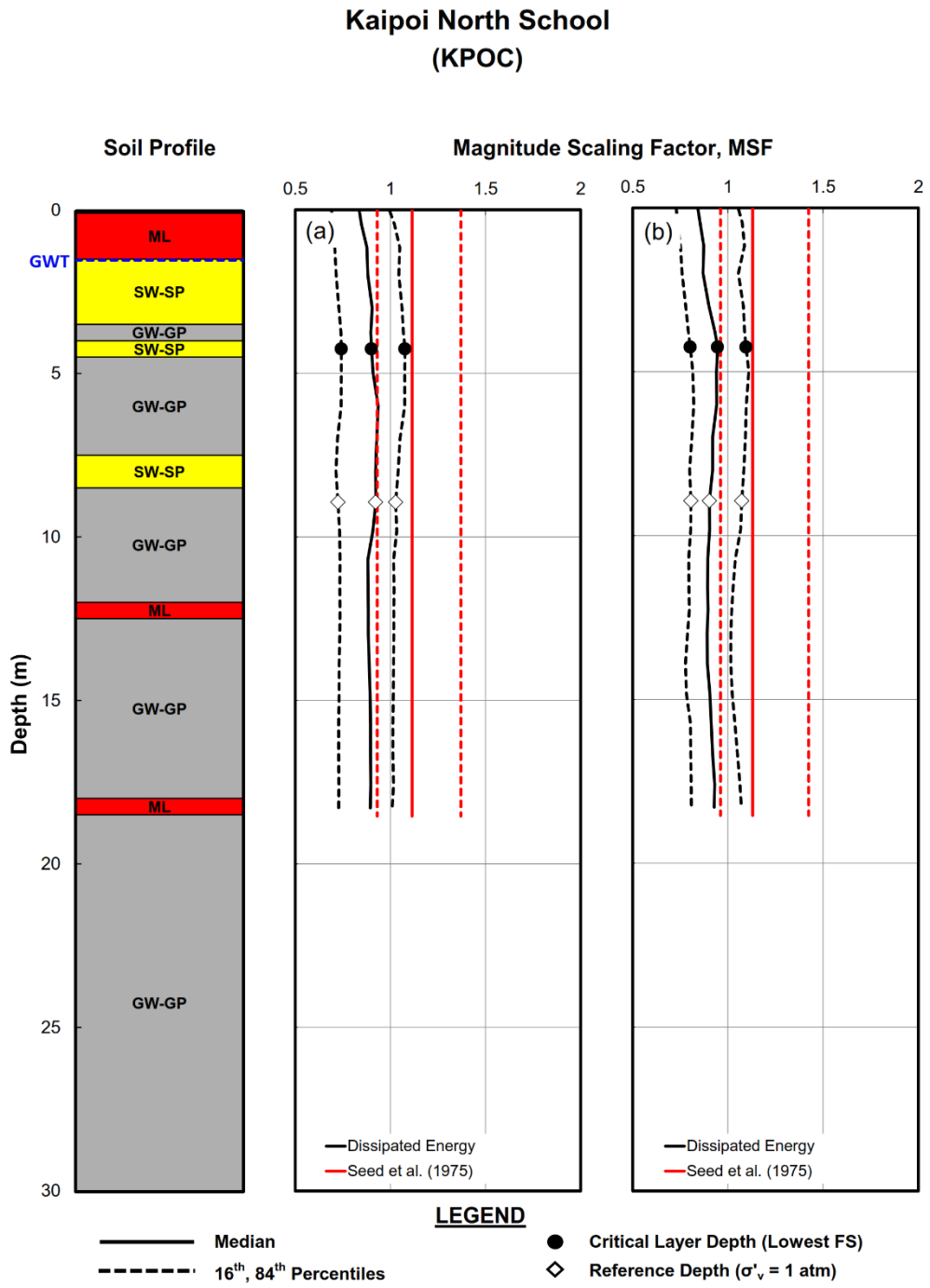

Figure C.8 MSF computed for the Kaipoi North School (KPOC) SMS site using the Green and Terri (2005) and Seed et al. (1975) approaches for computing number of equivalent cycles for: (a) Darfield earthquake, and (b) Christchurch earthquake.

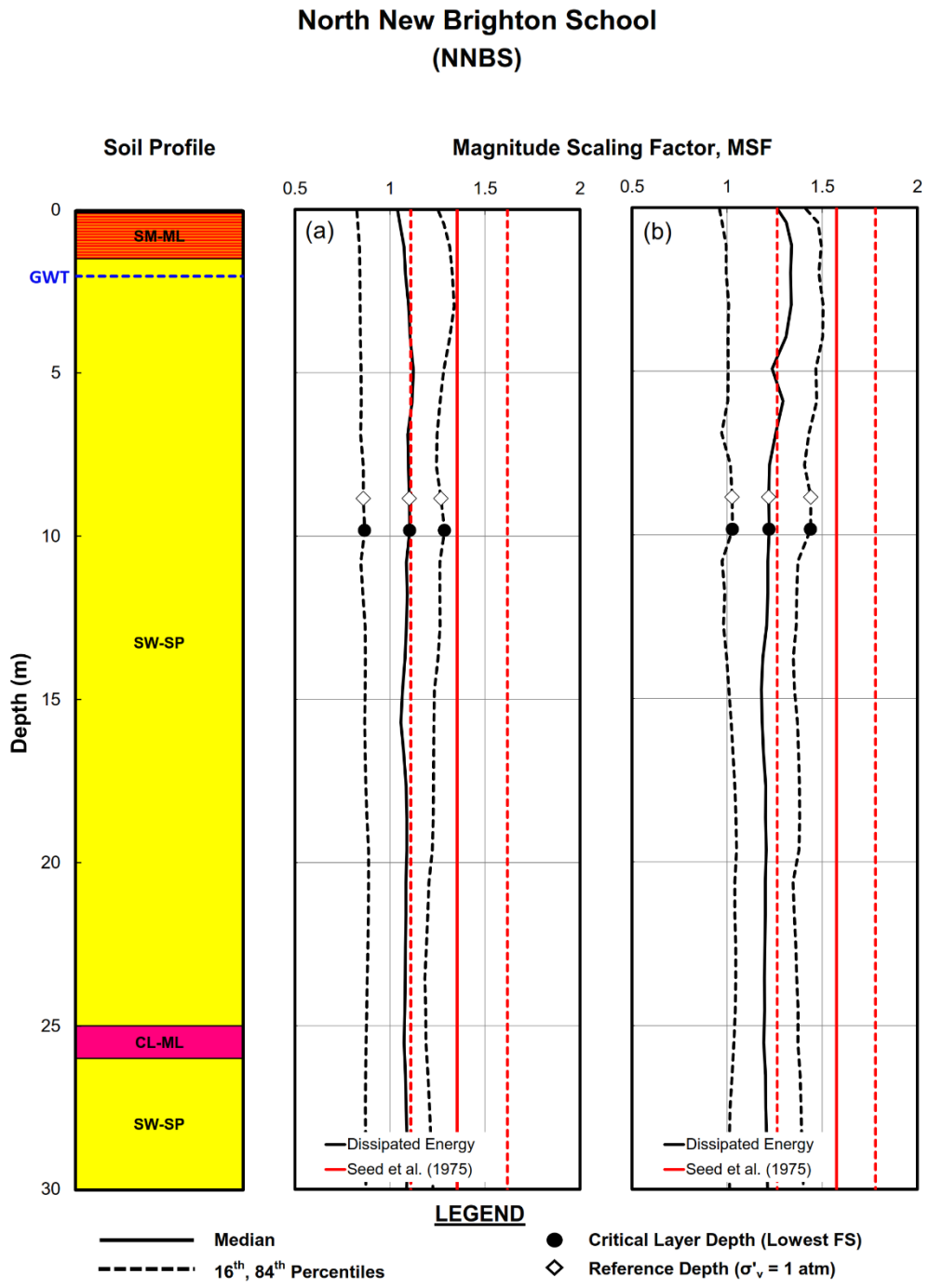

Figure C.9 MSF computed for the North New Brighton School (NNBS) SMS site using the Green and Terri (2005) and Seed et al. (1975) approaches for computing number of equivalent cycles for: (a) Darfield earthquake, and (b) Christchurch earthquake.

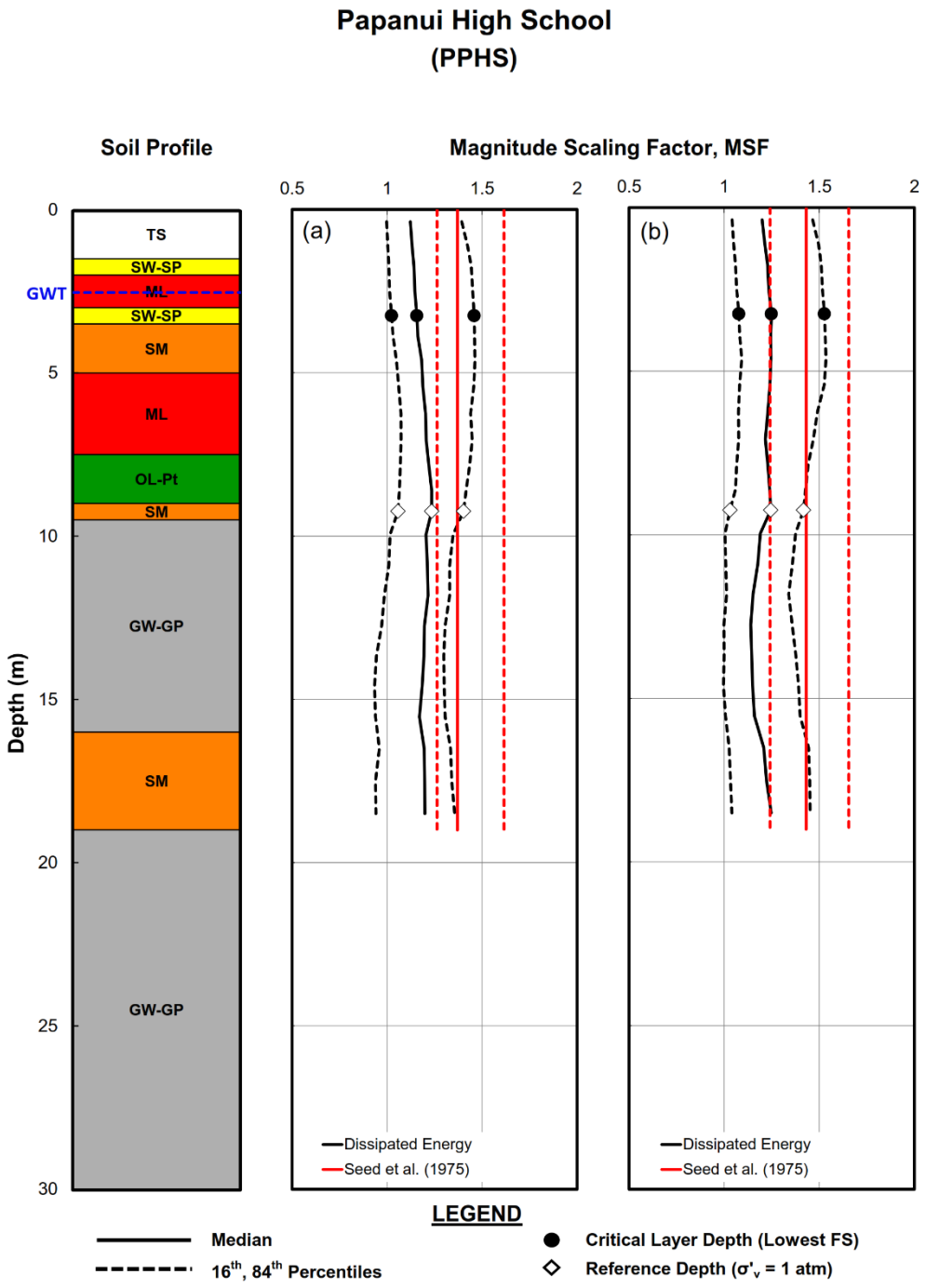

Figure C.10 MSF computed for the Papanui High School (PPHS) SMS site using the Green and Terri (2005) and Seed et al. (1975) approaches for computing number of equivalent cycles for: (a) Darfield earthquake, and (b) Christchurch earthquake.

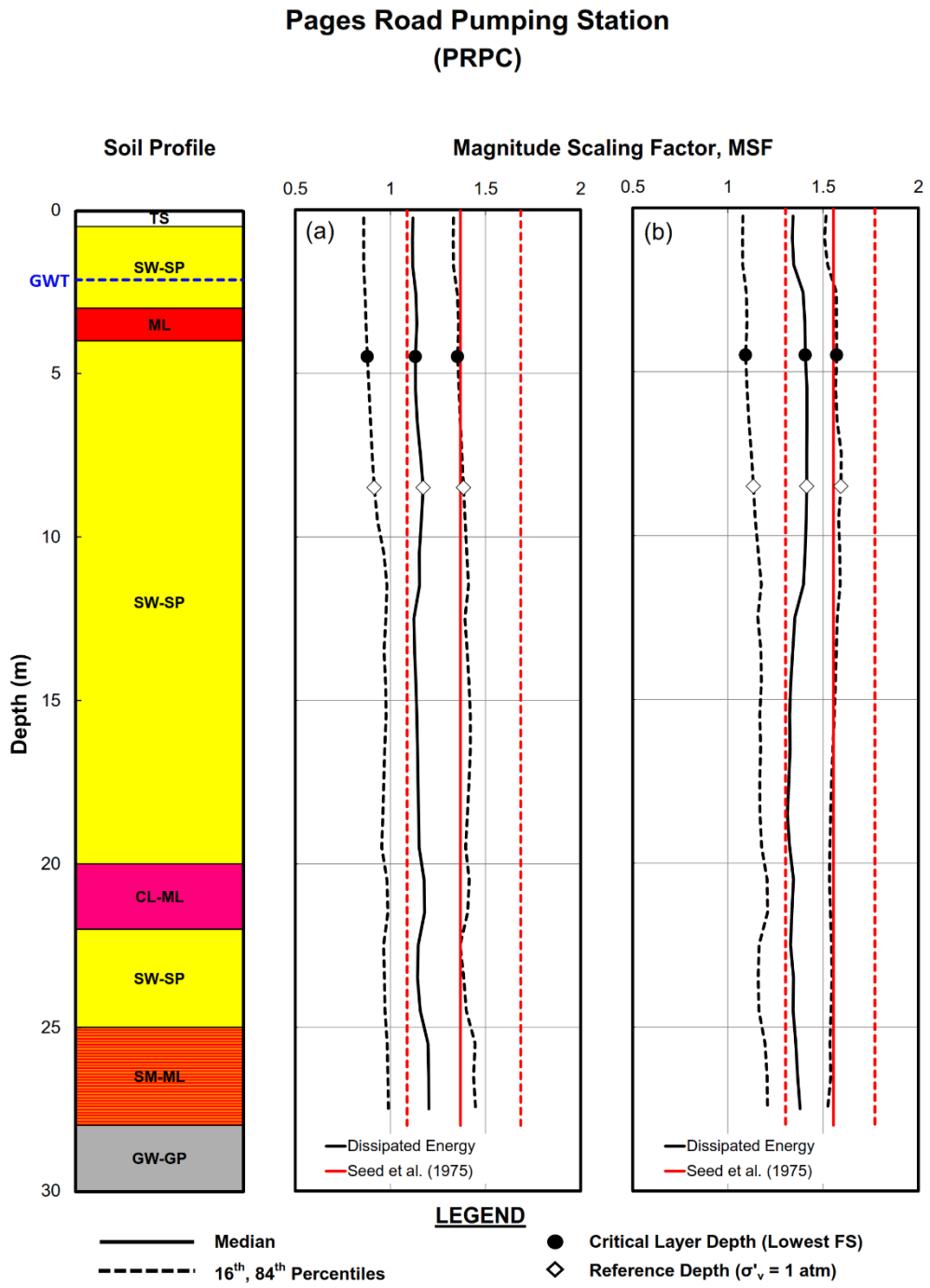

Figure C.11 MSF computed for the Pages Road Pumping Station (PRPC) SMS site using the Green and Terri (2005) and Seed et al. (1975) approaches for computing number of equivalent cycles for: (a) Darfield earthquake, and (b) Christchurch earthquake.

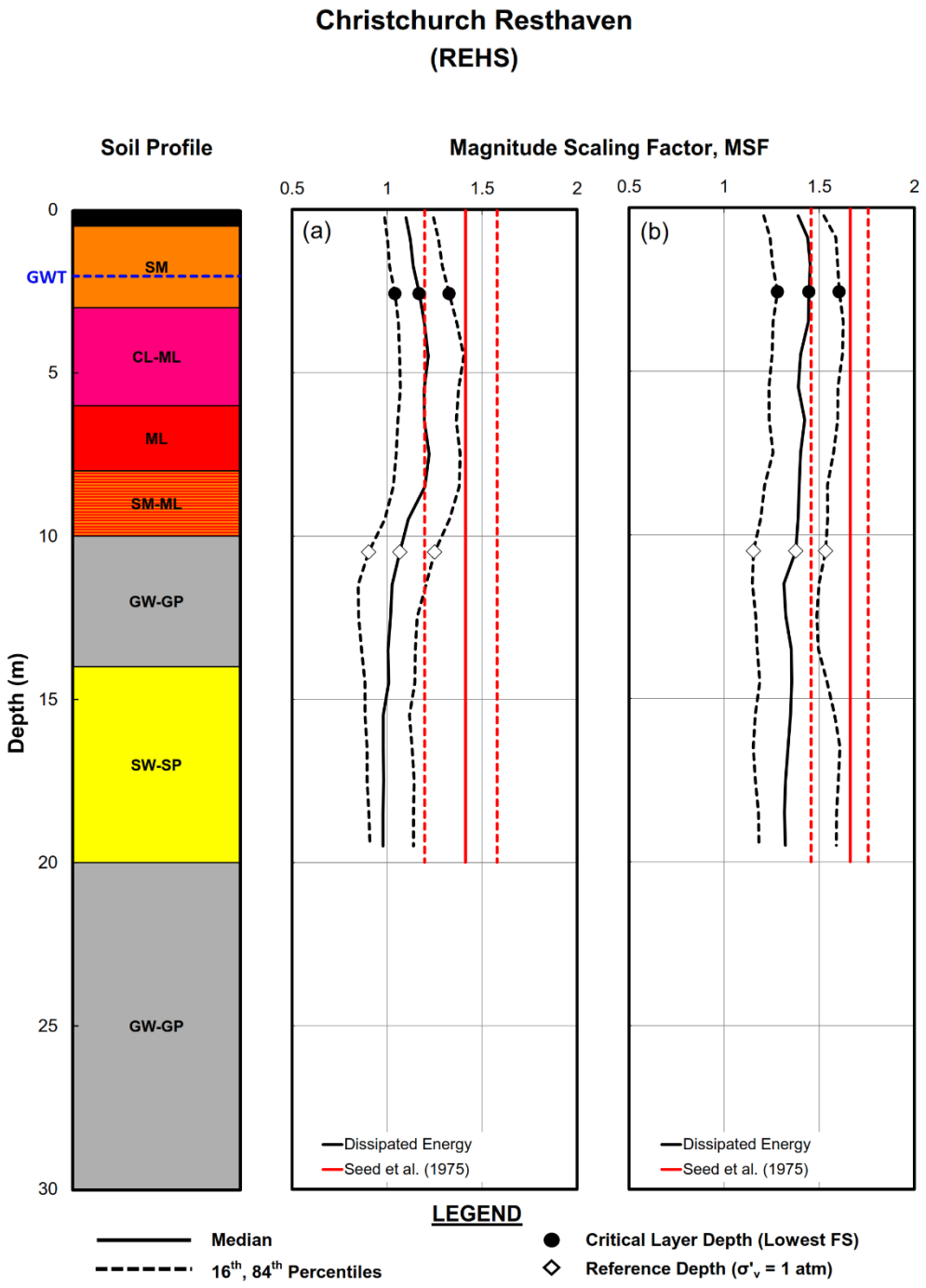

Figure C.12 MSF computed for the Christchurch Resthaven (REHS) SMS site using the Green and Terri (2005) and Seed et al. (1975) approaches for computing number of equivalent cycles for: (a) Darfield earthquake, and (b) Christchurch earthquake.

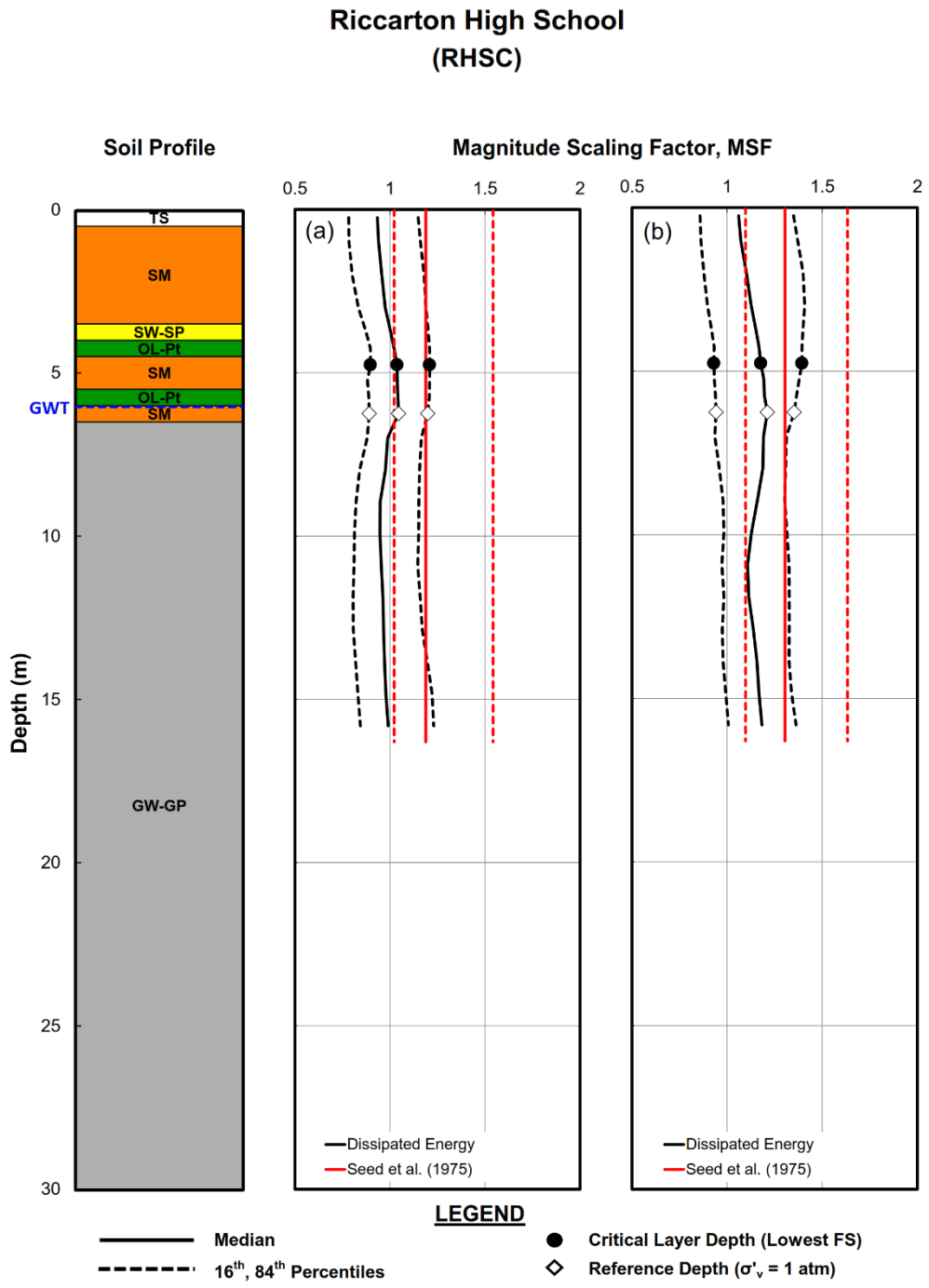

Figure C.13 MSF computed for the Riccarton High School (RHSC) SMS site using the Green and Terri (2005) and Seed et al. (1975) approaches for computing number of equivalent cycles for: (a) Darfield earthquake, and (b) Christchurch earthquake.

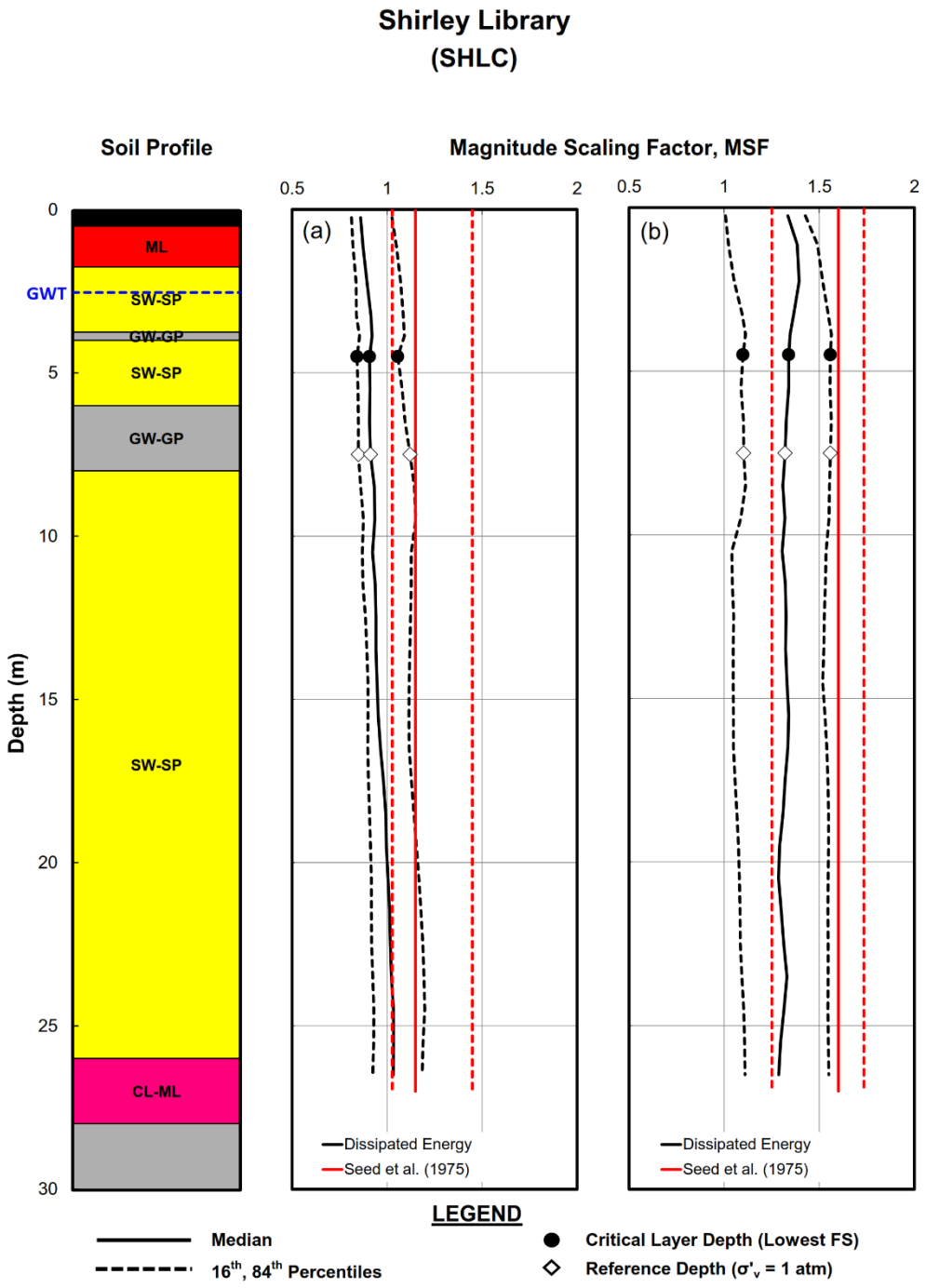

Figure C.14 MSF computed for the Shirley Library (SHLC) SMS site using the Green and Terri (2005) and Seed et al. (1975) approaches for computing number of equivalent cycles for: (a) Darfield earthquake, and (b) Christchurch earthquake.

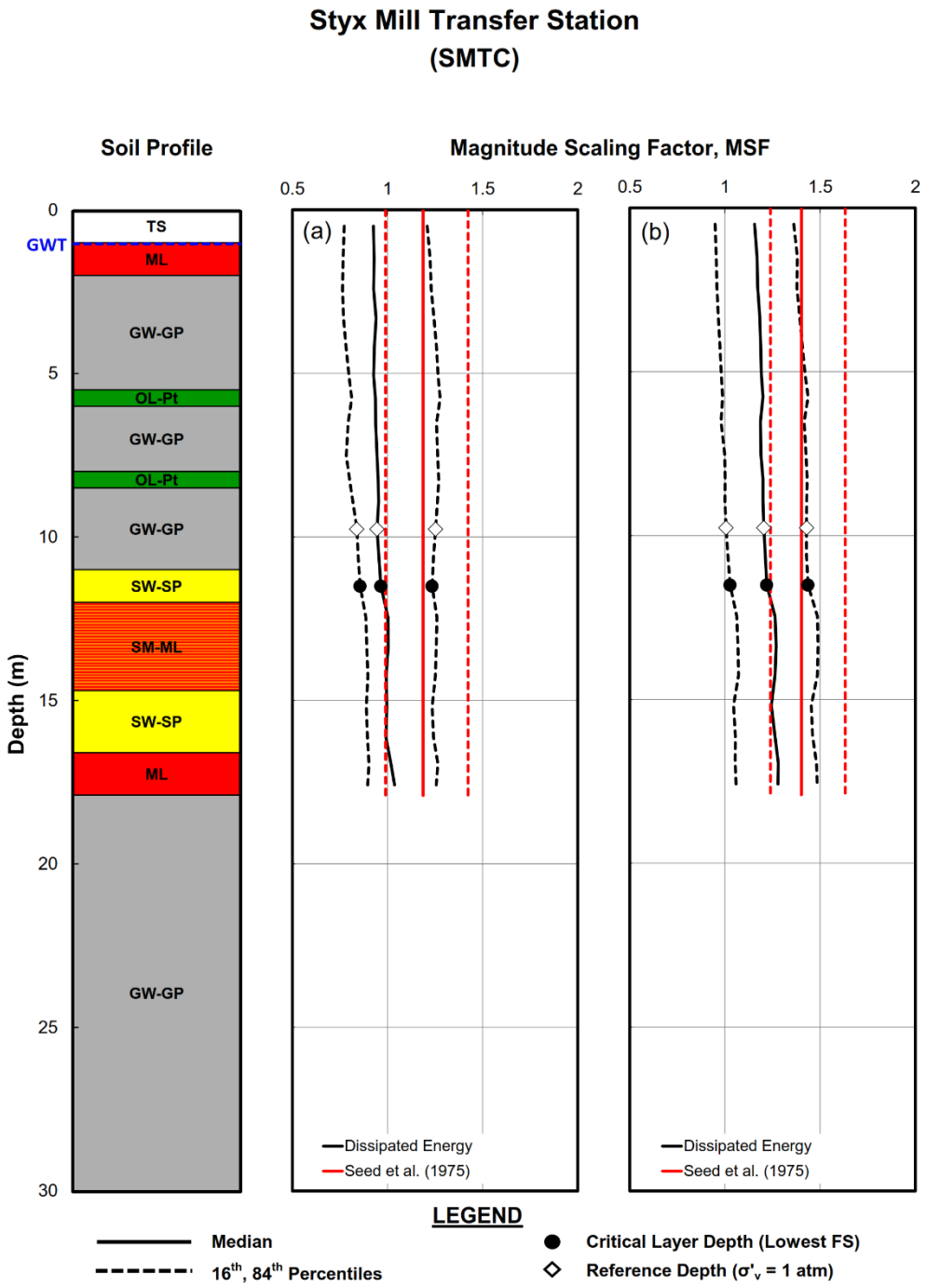

Figure C.15 MSF computed for the Styx Mill Transfer Station (SMTC) SMS site using the Green and Terri (2005) and Seed et al. (1975) approaches for computing number of equivalent cycles for: (a) Darfield earthquake, and (b) Christchurch earthquake.

Appendix D: Contour Plots Showing Spatial Variation of MSF across Christchurch

Contour plots of median MSF computed using the n_{eqM} from the Seed et al. (1975) and Green and Terri (2005) approaches for both the Darfield and Christchurch earthquakes are presented in Appendix D. The contours are superimposed on maps of the Christchurch region, with areas that experienced liquefaction colored in red. Because the MSF computed using the n_{eqM} from the Green and Terri (2005) approach vary to some extent with depth, the two sets of contour plots are developed from the MSF computed at the "critical" depth and the reference depth (σ'_v = 1 atm) for each of the SMSs. The critical depth is assumed to be that to the layer most susceptible to liquefaction (i.e., depth to the layer having the lowest computed factor of safety against liquefaction). Further details on the critical depths at these sites can be found in Wotherspoon et al. (2015a,b). For SMSs sites where no layers were deemed susceptible to liquefaction, the critical depth was taken as ~4.75 m which corresponds to the median critical depth of compiled liquefaction case histories (e.g., Cetin et al., 2004; Boulanger and Idriss, 2014).

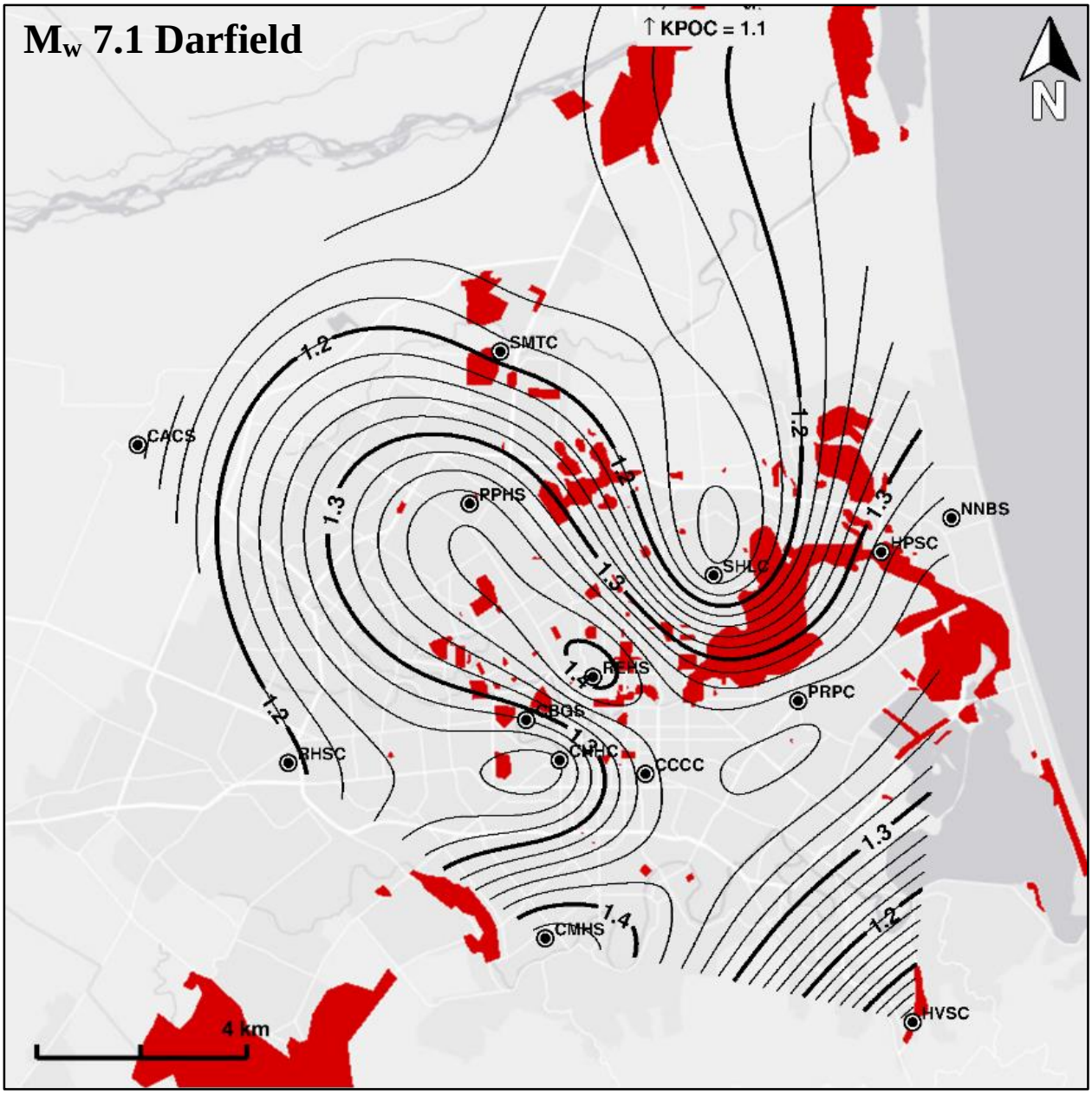

Figure D.1 Contour plot of MSF computed using n_{eqM} from the Seed et al. (1975) approach for the M_w 7.1 Darfield earthquake.

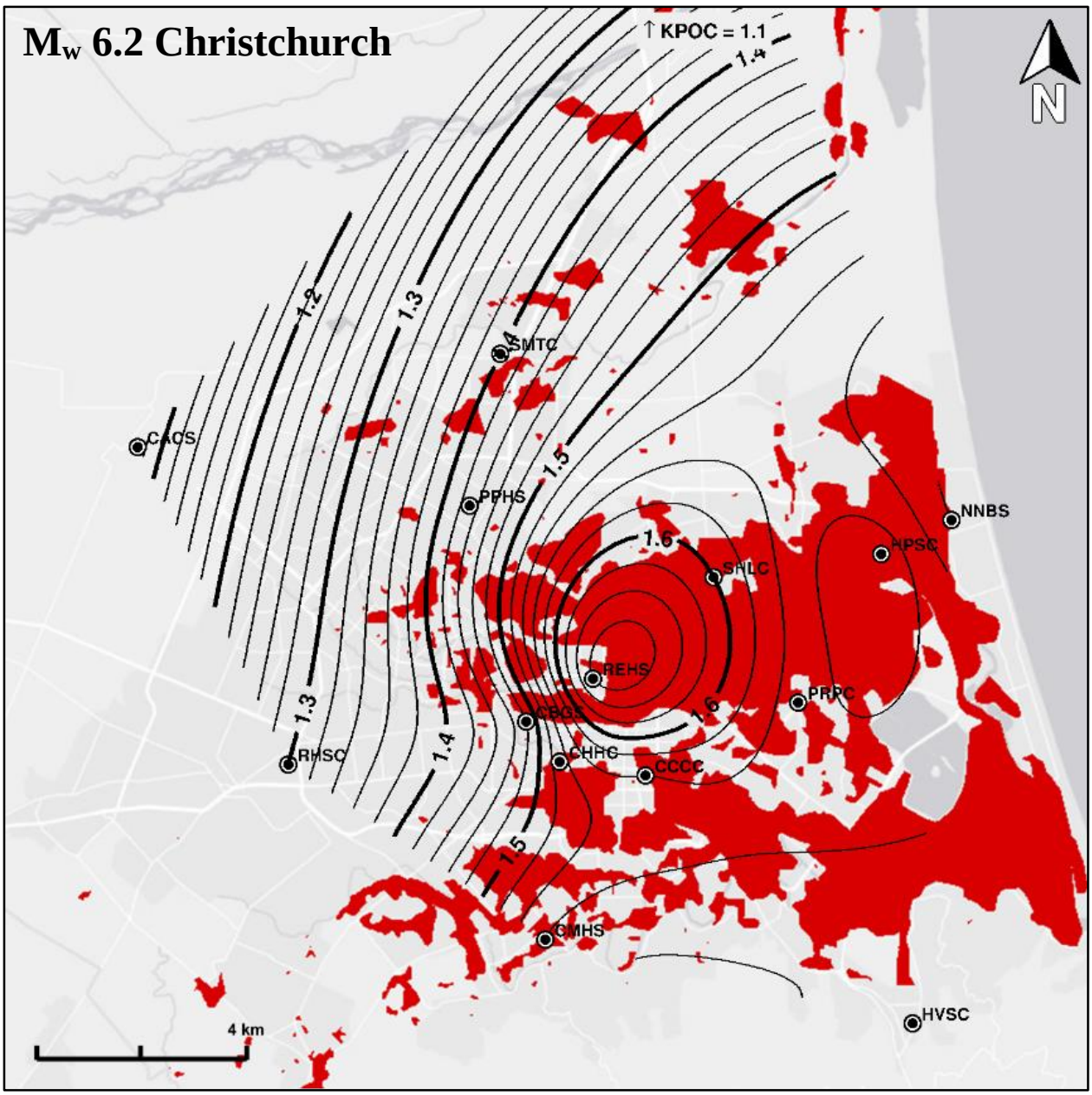

Figure D.2 Contour plots of MSF computed using n_{eqM} from the Seed et al. (1975) approach for the M_w 6.2 Christchurch earthquake.

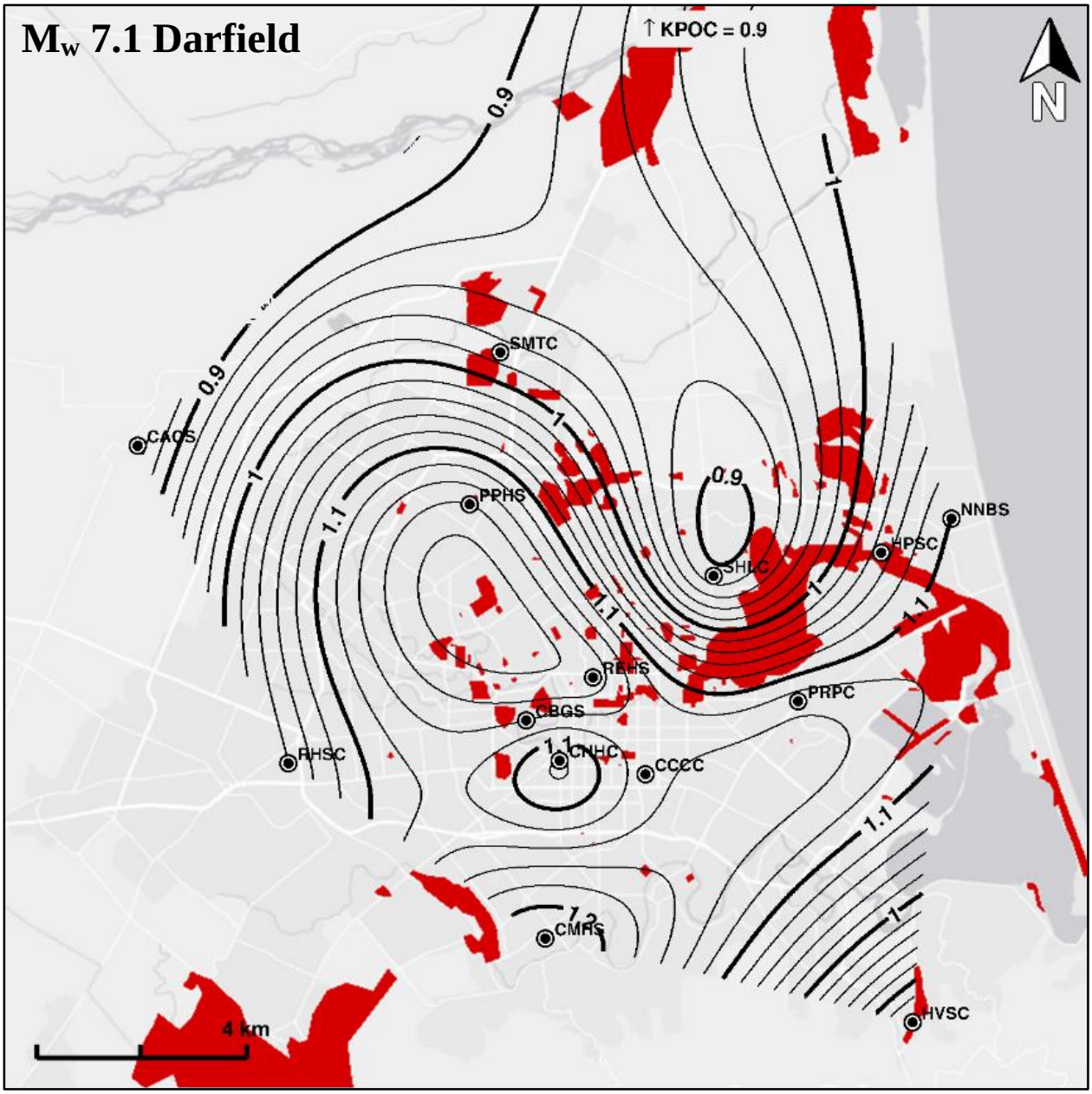

Figure D.3 Contour plots of MSF computed using n_{eqM} from the Green and Terri (2005) approach at the <u>critical depth</u> for the M_w 7.1 Darfield earthquake.

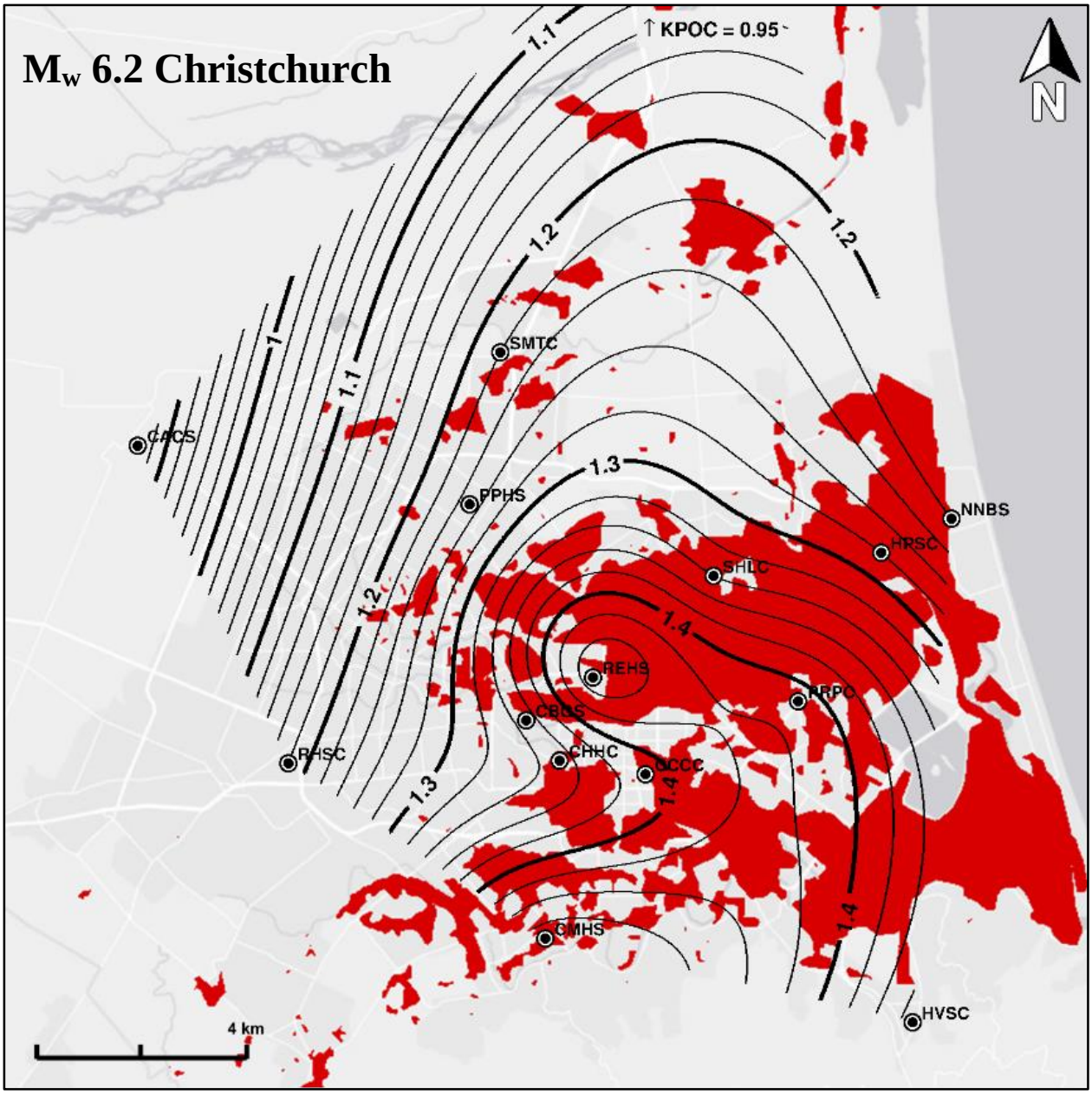

Figure D.4 Contour plots of MSF computed using n_{eqM} from the Green and Terri (2005) approach at the critical depth for the M_w 6.2 Christchurch earthquake.

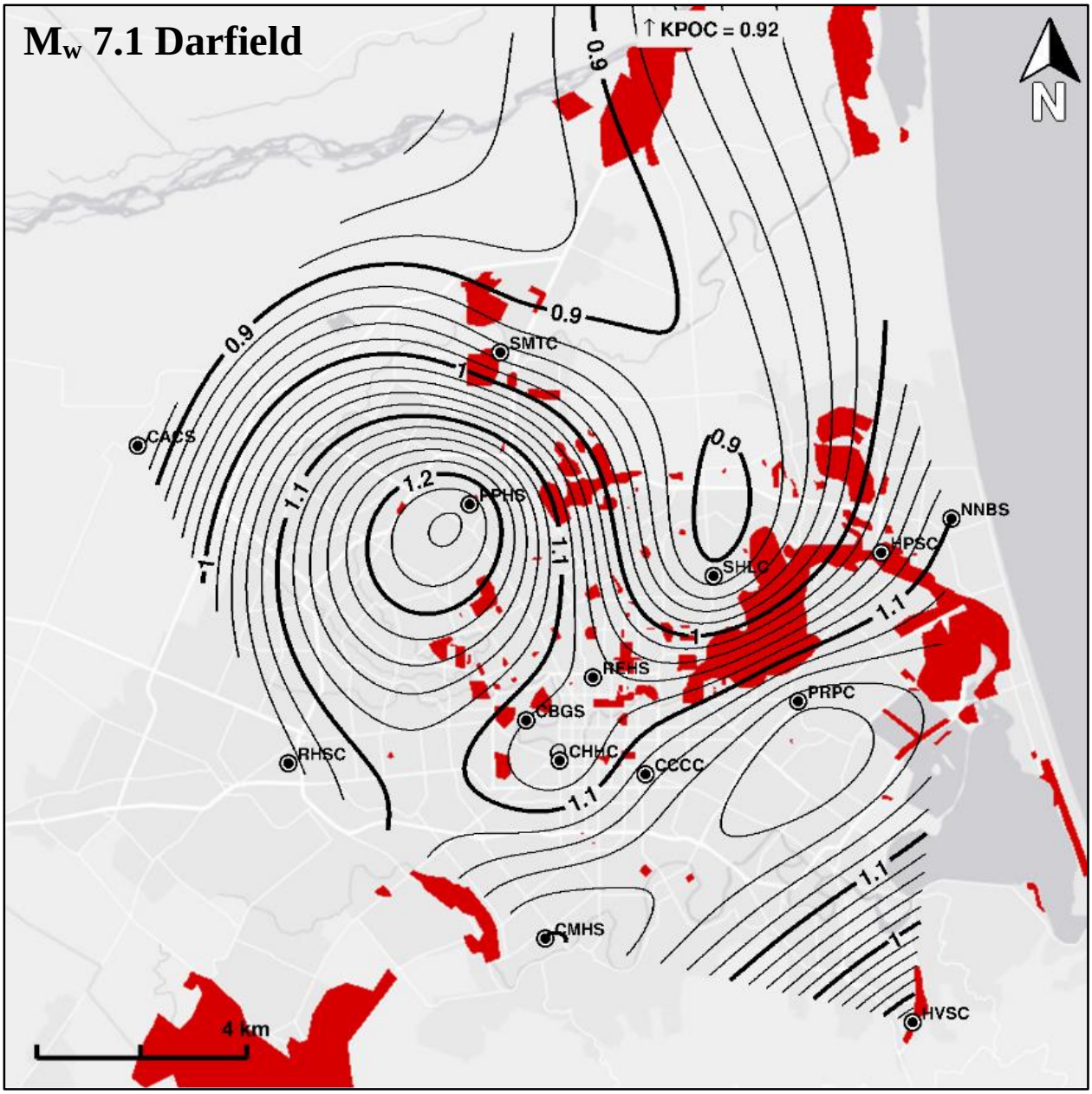

Figure D.5 Contour plots of MSF computed using n_{eqM} from the Green and Terri (2005) approach at the reference depth for the M_w 7.1 Darfield earthquake.

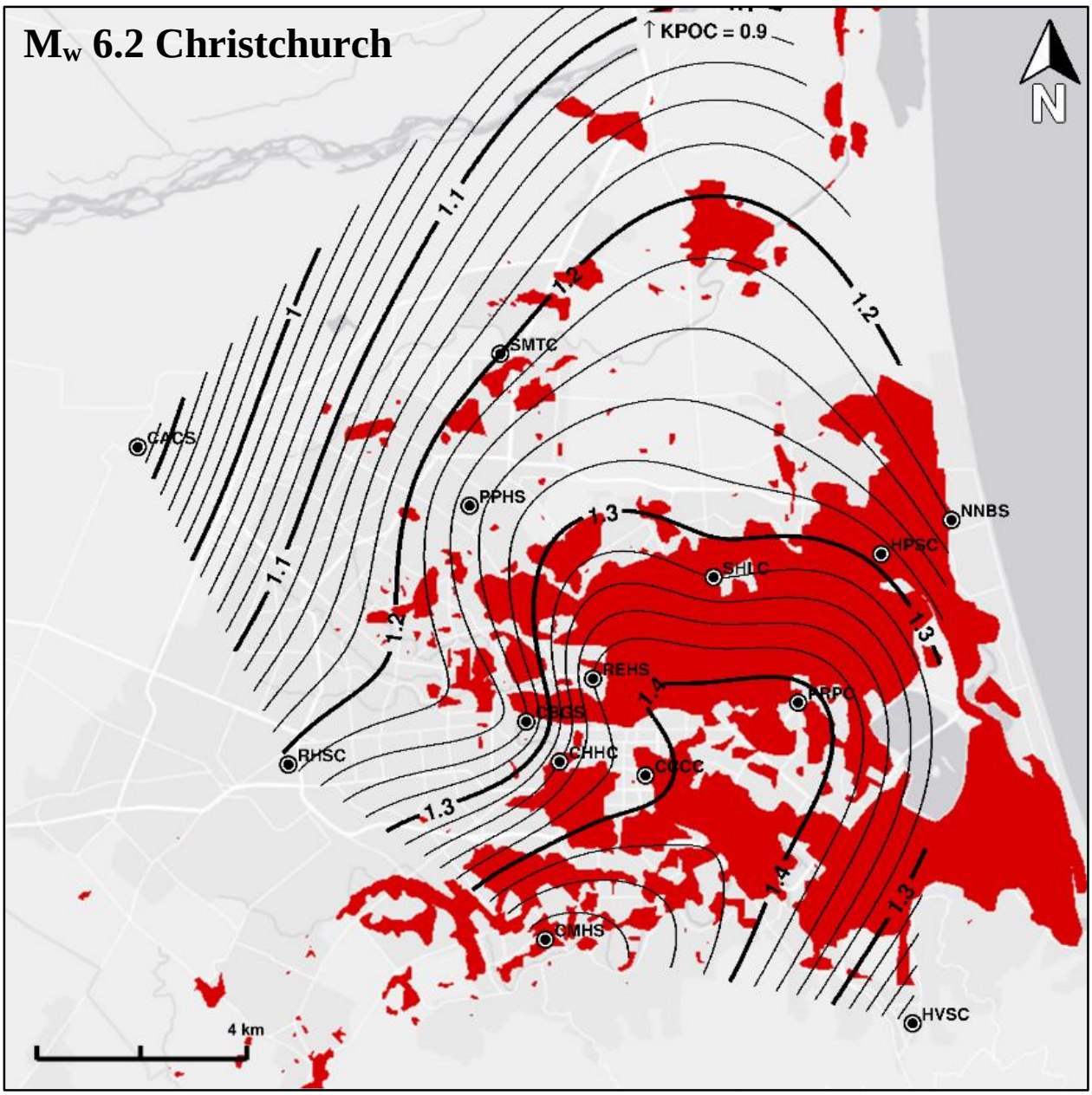

Figure D.6 Contour plots of MSF computed using n_{eqM} from the Green and Terri (2005) approach at the reference depth for the M_w 6.2 Christchurch earthquake.